Azobenzene-conjugated Propofol-derivatives for Light-control of GABA(A) Receptors in Vision Restoration

LAN YUE
B.S., University of Science and Technology of China, 2006

THESIS

Submitted as partial fulfillment of the requirements
for the degree of Doctor of Philosophy in Bioengineering
in the Graduate College of the
University of Illinois at Chicago, 2012

Chicago, Illinois

Defense Committee:

David R. Pepperberg, Chair and Advisor
Haohua Qian, National Eye Institute, NIH
Karol S. Bruzik, Medicinal Chemistry and Pharmacognosy
Richard L. Magin
John R. Hetling

Dedicated to my parents and husband, without whom this work would never have been done.

ACKNOWLEDGMENTS

I would like to thank my thesis advisor Dr. David R. Pepperberg, for his generous and patient guidance. It has been a great opportunity to work in his lab. Throughout my Ph.D study, his persistent enthusiasm in science and unwavering support has been a tremendous source of encouragement for me to accomplish my research goals. I have learned a lot from him.

I would also like to express my gratitude to our close collaborator Dr. Haohua Qian, whose insightful comments and brilliant suggestions were always great sources of inspiration for me. I am also thankful to our medicinal chemistry colleagues Dr. Michal Pawlowski and Dr. Karol S. Bruzik, who provided me with the wonderful chemical compounds. Many members of the Pepperberg lab, past and current, were extremely helpful during my thesis research, and I would like to thank them as well: Dr. An Xie, Ms. Feng Feng, Dr. Hélène Gussin, Ms. Tiffany Chen, Ms. Tara Nguyen and Dr. Niraj Muni.

ACKNOWLEDGMENTS (continued)

Finally, I would like to acknowledge my entire committee: Dr. David R. Pepperberg, Dr. Haohua Qian, Dr. Karol S. Bruzik, Dr. Richard L. Magin and Dr. John R. Hetling for valuable comments on my thesis.

LY

TABLE OF CONTENTS

TABLE OF CONTENTS (continued)

CHAPTER PAGE

TABLE OF CONTENTS (continued)

CHAPTER PAGE

TABLE OF CONTENTS (continued)

LIST OF FIGURES

LIST OF FIGURES (continued)

LIST OF FIGURES (continued)

FIGURE PAGE

LIST OF FIGURES (continued)

FIGURE PAGE

LIST OF FIGURES (continued)

FIGURE PAGE

LIST OF FIGURES (continued)

FIGURE PAGE

LIST OF ABBREVIATIONS

4D-QSAR	4-Dimentional Quantitative Structure-Activity Relationship
5Me-I4AA	5-methyl-imidazole-4-acetic acid
AMD	Age-related Macular Degeneration
ATP	Adenosine-5'-Triphosphate
BAPTA	Bis(2-aminophenoxy)ethane Tetraacetic Acid
DMSO	Dimethyl Sulfoxide
DR	Diabetic Retinopathy
ERG	Electroretinography
GABA	γ-Aminobutyric Acid
$GABA_AR$	$GABA_A$ receptor
$GABA_CR$	$GABA_C$ receptor
GLIC	Gloeobacter Ligand-gated Ion Channel
GTP	Guanosine-5'-Triphosphate

LIST OF ABBREVIATIONS (continued)

HEPES	(4-(2-Hydroxyethyl)-1-Piperazineethanesulfonic Acid
PDE	Phosphodiesterase
PNs	Purkinje Neurons
PTX	Picrotoxin
RBC	Retinal Bipolar Cell
RGC	Retinal Ganglion Cell
RP	Retinitis Pigmentosa
RPE	Retinal Pigment Epithelium
TEA	Tetraethylammonium
THIP	4,5,6,7-Tetrahydroisoxazolo(5,4-c)pyridin-3-ol
TMD	Transmembrane Domain
TPMPA	(1,2,5,6-Tetrahydropyridin-4-yl)methyl phosphinic acid
WT	Wildtype

SUMMARY

Retinal degenerative diseases are among the leading causes of permanent vision loss. In many cases, the photoreceptors of the retina are damaged, leaving the downstream retinal neurons unstimulated even though they remain functional. Re-initiating visual signaling by means of rendering photosensitivity to these inner retinal neurons could potentially restore vision in photoreceptor degenerated patients.

In this study we investigated the feasibility of building nanoscale light-regulated neuromodulators that can attach to the inner retinal neurons at the sites of postsynaptic membrane receptors to enable photo-control of neuronal activity. Specifically, we focused on $GABA_A$ receptors given their importance in visual signaling and abundance in inner retinal neurons. The background and rationale of the study are introduced in Chapter I and II. The experimental setup, protocol and procedures are described in Chapter III. Details of experimental results can be found in Chapter IV, followed by discussion in Chapter V.

The proposed nanoscale structures consist of three main components: a receptor-interactive ligand, a light-sensitive photoswitch and an anchor for attachment. The ligand employed for this study is propofol (2,6-diisopropyl phenol), a widely used anesthetic that is known to potentiate, and at high concentration to elicit $GABA_A$ receptor activity in a number of CNS neurons. Our investigation of the action of propofol on retinal bipolar cells (RBCs) reveals a marked and selective potentiation of RBC $GABA_A$ receptor activity by propofol, thus encouraging its use as the prototype modulator for inner retinal neurons. Azobenzene, a chemical compound that undergoes bi-directional photo-conversion between *trans*- and *cis*-isomers upon photon absorption, was used as the photoswitch. A number of azobenzene-conjugated propofol derivatives were synthesized and tested on recombinant $\alpha_1\beta_2\gamma_2$ $GABA_A$ receptors. These studies demonstrate the photo-control of receptor activity either by a freely diffusible agent (e.g.,

MPC088) or by a covalently tethered agent (e.g. maleimide-containing MPC100) that forms a stable carbon-sulfur bond with the cysteine substituted receptors. Further, we examined the activity of MPC088 on native $GABA_A$ receptors of retinal ganglion cells (RGCs), the output neuron of retina, and observed similar isomer-dependent regulation of membrane currents.

Overall, this thesis study demonstrates modulation of the native retinal $GABA_A$ receptors by propofol and the light-control of both recombinant and native $GABA_A$ receptors by propofol-azobenzene conjugates. Therefore it suggests the feasibility of using a propofol-based nanoscale photoswitch to present light-sensitivity to retinal neurons as a vision restoration approach.

CHAPTER 1

INTRODUCTION

1.1 Structure and function of retina

Retina is a stratified light sensitive tissue that lines the back of the eye of humans and all other vertebrate species. It is ~0.5 mm in thickness, and in humans, the diameter of the roughly hemispherical region lined by the retina is about 22 mm [1]. Neural retina consists of several layers of cell bodies and their neural processes of dendrites and axons. From outer to inner retina, the layers consist of outer nuclear layer, which contains cell bodies of photoreceptors, inner nuclear layer, which contains cells bodies of bipolar cells, horizontal cells and amacrine cells, and ganglion cell layer. In between these cell body layers are two layers of neural processes—outer and inner plexiform layers, which are the sites of synaptic interactions of the retinal cells.

Retinal pigment epithelium (RPE) cell layer lies adjacent to neural retina. RPE cells are responsible for maintaining homeostasis of retina, phagocytosis of the outer segment of photoreceptors, and are involved in the recycling of the photosensitive retinal, chromophore of the rod photoreceptor visual pigment rhodopsin. The RPE cells support this recycling specifically by enzymatically converting *all-trans* retinol (delivered from the photoreceptors upon illumination) to fresh *11-cis* retinal for delivery back to the rods. Photoreceptor layer has two cell types: rods and cones. In human eyes, rods are predominant in non-central regions of the retina whereas cones are particularly densely packed in the fovea, a small region at the center of the retina (i.e., along the visual axis). Therefore rods are responsible for peripheral vision and cones play a more important role in detail perception. Under fully dark adapted conditions (those yielding highest sensitivity of the photoreceptors), absorption of a single photon produces a response whose peak amplitude is readily measurable (several percent of the maximum saturating response). Cones, by contrast, typically exhibit much smaller response

amplitude to single photon absorption. Therefore night vision is mainly mediated by rods and cones are the primary information input in strong daylight.

Although rods and cones exhibit many physical and functional differences, they show essentially similar signal transduction pathways upon photon absorption. First, in the outer segment of both cell types there are multiple layers of membrane invaginations where abundant photopigment (a combination of protein opsin and *11-cis* retinal bound to it), G-protein transducin and phosphodiesterase (PDE) are present. In addition, the plasma membrane of the outer segment of both rods and cones contains a large quantity of cGMP-gated cation channels. Second, the axonal terminal of both cell types synapses with bipolar cells, though of different subtypes. In darkness, the cGMP gated channels are open and the photoreceptors are depolarized by ions (sodium and calcium) that flow into the cell through the channels. This depolarized, dark state produces, in turn, the release of glutamate, the photoreceptor neurotransmitter, into the synaptic cleft. When light impinges on the retina, photons are absorbed by rhodopsin and the retinal isomerizes from *11-cis*, its configuration in darkness, to *all-trans*,

triggering conformational change of opsin that subsequently activates the G-protein transducin, which, in turn, activates PDE, inducing the hydrolysis of cGMP. The reduction of cGMP results in the closure of the cation channels and the hyperpolarization of the cell, which causes a decrease in glutamate release. Glutamate receptors on post-synaptic bipolar and horizontal cells then depolarize or hyperpolarize in response to the fluctuation in the glutamate concentration at the synaptic cleft. In this way, the light signals lead to electrochemical signals in the secondary cells.

Vertically, these signals travel down, through glutamate pathway, from bipolar cells directly or indirectly to ganglion cells, where via optic nerve (the axons of the ganglion cells) the signals are transmitted to the brain. Laterally, signals were modulated by horizontal cells (mainly located pre- and post- synaptic to different photoreceptors) and amacrine cells (mainly located pre- and post- synaptic to bipolar and ganglion cells), in substantial part at inhibitory synapses that employ GABA as the neurotransmitter. Together, the vertical signal transmission and the lateral signal integration and modulation ensure the accurate coding and delivery of visual information

such as color, brightness, size, movement, etc., to the brain where this information is further processed.

1.2 Retinal degenerative diseases and treatments

Retinal degeneration is a major cause of permanent vision loss in the world and it can be found in the entire age spectrum. Epidemiologic studies have shown that the onset of retinitis pigmentosa (RP) occurs predominantly in children and young adults, while diabetic retinopathy (DR) arises typically in middle-aged adults, and age-related macular degeneration (AMD) in the elderly [2]. These diseases typically often involve progressive deterioration and loss of function of photoreceptors. For example, RP begins by primarily affecting rods (peripheral vision and night vision) and AMD mainly affects cones (central vision) [3-6]. The dysfunctional photoreceptors no longer react to light stimulation and thus fail to initiate the visual signal transduction. The loss of photoreceptoral input can lead directly or indirectly to remodeling or restructuring of post-photoreceptor inner retinal neurons [7]. However in many cases, these proximal

neurons appear to retain a capacity for signal transmission, thus raising the possibility of vision restoration by establishing a replacement mechanism of photoreceptor that can interface with the remaining healthy cells.

New treatments for retinal degeneration currently develop in two major directions. The first one focuses on photoreceptor rescue, repopulation or replacement by, for example, nutrition therapy, photoreceptor or stem cell transplantation and gene therapy [8-14]. However, nutrition therapy is only applicable at relatively early stage of the disease when a sufficient amount of photoreceptors remain. Furthermore, this therapy appears effective for only certain types of retinal degenerative disease. Specifically, it has been demonstrated that antioxidants slow photoreceptor cell death in a number of animal models of RP [15, 16]. Similarly, at present, with only a limited number of mutant genes recognized, gene therapy is only potentially applicable to a small pool of patients. In recent years, photoreceptor transplantation has received much attention for the treatment of advanced disease where all photoreceptors are dead. Particular interest has focused on stem cells as the source of photoreceptors to be

transplanted. Increased understanding of the conditions needed for stem cells to differentiate into specialized cells has led to encouraging results demonstrating some functional photoreceptor replacement in animal models (reviewed by Huang Y *et al.*, 2011 [17]). However many questions of cell function and cell connectivity by the transplanted stem cells remain to be addressed.

The second general approach for restoring retinal photosensitivity is that of a bypass of the damaged photoreceptor layer, to directly target the functional inner retinal or even cortical neurons. Work in this area to date falls into three main categories: electronic prosthestic implants [18-20], expression of non-native light-responsive ion channels ([21-23]) and presentation of photoswitchable tethered ligands to mutant ion channels [24-26].

1.2.1 Electronic prosthesis

Currently, many groups around the world are working on visual prosthetic devices, designed for sub-retinal (between RPE and damaged photoreceptor layer), epi-

retinal (on the outer surface of ganglion cell layer) or cortical (in the brain close to visual cortex) implantation. The sub-retinal design typically contains an array of light-sensitive microphotodiodes, which generate currents directly from the incident light and inject the current into the vicinity of the underlying, post-photoreceptor retinal cells. The relatively low signal level of photodiodes puts a constraint on this design therefore it always incorporates an external power supply to amplify the signal [21, 27]. Commonly, the epi-retinal and cortical designs consist of a video camera to capture images, a microprocessor to convert images to electrical signals, and a microelectrode array to deliver electrical stimulation to neurons. A cortically-based device was the earliest effort on visual prosthesis [28, 29] and basic research has demonstrated generation of phosphene (perceptions of points of light) by electrical stimulation of visual cortex [30]. Works on complex cortical implants are currently progressing and they shine light onto clinical investigation in the foreseeable future [31, 32]. However, most of the work pursuing the electronic prosthetic approach has been aimed at direct stimulation of the retina. Among most advanced of these projects are the Argus Project (epi-retinal

implant) led by Dr. M. Humayun from USC, the Retina Implant AG Project (sub-retinal) led by Dr. E. Zrenner from the University of Tuebingen, Germany [21] and the Boston Retinal Implant Project (sub-retinal) developed by teams from Harvard and MIT, led by Drs. J. Rizzo and J. Wyatt [19, 33]. The first two projects are presently in clinical trials and have demonstrated significant improvement in visual function on implanted patients [18, 34]. New designs to achieve better signal response by retina are emerging. For example the group at Stanford University led by Dr. D. Palanker employs an optoelectronic system and external control of image processing that could theoretically reach a pixel size of 25 μm, corresponding to a maximum visual acuity of 20/100, sufficient for reading with visual aids [35] and far exceeding the 20/1000 acuity level achieved by the epi- or sub-retinal design now in clinical trials.

Overall, electronic visual prostheses continue to represent a major effort within the vision restoration field, and have recently accomplished success in providing crude vision to blind patients. However, the intrinsic difference between native light-initiated visual signals and electrically stimulated signals, together with the unclear role of each

retinal neuron type in processing of the electrically initiated signals emphasize that this approach is still in its infancy.

1.2.2 Non-native light-responsive ion channels

Recent advances in opsin-based single component optogenetic tools provide an alternative engineering approach for vision restoration [36, 37]. Opsin-based light responsive proteins can be divided into two distinct superfamilies: animal opsin (visual pigments) and microbial opsin. Both of these groups of opsins are seven-transmembrane structures, but they differ in that animal opsins function as the initial stage of an intracellular phototransduction process that leads to transmembrane ion currents (e.g., human rhodopsin) whereas microbial opsins typically are themselves ion channels or pumps (e.g., channelrhdopsin). As noted above, for visual signal mediating photopigments of humans, photon absorption triggers the photoisomerization of the rhodopsin chromophore 11-*cis* retinal to all-*trans* configuration. *All-trans* retinal dissociates from opsin, and the replenishment of 11-*cis* retinal requires participation of

other cell types, for example RPE for rods and Muller cells for cones, increasing the difficulty of achieving vision restoration merely with the expression of genes that encode animal opsins. In contrast, microbial opsins typically utilize all-*trans* retinal as the active form of chromophore and after one photocycle, the bleached chromophore thermally relaxes back to the active form while remaining attached to the opsin protein [38]. In addition, in humans, the level of endogenous all-*trans* retinal is sufficient to meet the requirement of heterologously expressed microbial opsin for its chromophore [39, 40]. Therefore these light-sensitive ion channels/pumps have drawn great attention for application to vision restoration.

Optogenetics with microbial opsins began with channelrhodopsin (ChR), a blue light sensitive cation channel, introduced into hippocampal neurons in 2005 where it was found to confer milli-second precision control of neuronal spiking [41]. Currently, the most heavily studied microbial opsins also include halorhodospin (NpHR), a yellow light sensitive chloride pump and bacteriorhodopsin (BR), a green light-sensitive proton pump. Investigators from multiple groups have demonstrated selective activation and

silencing of neuronal activity with these optogenetic tools [42, 43]. For example, the study conducted by the Boyden and Horager group, which shows that the blind mice with injection of ON-bipolar cell targeting ChR genes exhibites improved visually guided behavior [21, 44], is particularly encouraging for the application of light-responsive channels in vision restoration. But before it can be used for clinical therapy, this technique must overcome hurdles that include, for example, the small single-channel conductance, the relatively low expression level of the introduced opsin, and the safety issue associated with gene expression.

1.2.3 Photoswitchable tethered ligands

Further strategy of engineering photo-control into inner retinal neurons is the tethering of photoswitchable ligands onto ion channels of inner retinal neurons to achieve regulation of the ion flow in response to light, and thereby depolarize or hyperpolarize the cell. Photoswitchability of the reported light-sensitive ligands has been rendered by the azobenzene moiety, a photoisomerizable structure composed of two

phenyl rings linked by an N=N double bond. For parent azobenzene, *trans*-to-*cis* isomerization (fast, femtosecond scale) is triggered by UV and the *cis* isomer remains stable in dark (thermal relaxation rate very slow, on the time scale of hours) until converted back to the *trans*-configuration by visible light. This bi-directional photoisomerization with light of two wavelengths affords tremendous flexibility in optical control of neuronal activity.

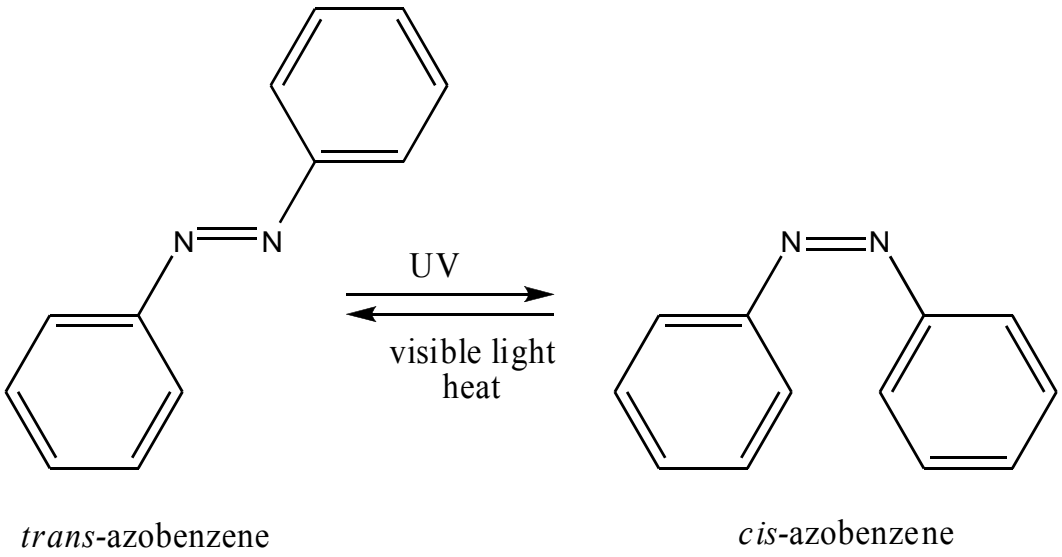

Fig. 1.2.1: Photoisomerization of azobenzene.

In actual application, ligand coupled azobenzene is attached, through a cysteine reactive group, to the native or introduced cysteine of the ion channel. Photoconversion between two isomeric states either presents or removes the ligand component from its binding site, making only one isomeric state able to exert its effect on the channel activity. The ligand of such tethered constructs reported in previous studies include agonist, antagonist and channel blocker.

Light-gated nAChR was first reported by Bartels *et al* in 1971 [45] and was studied throughout the following decade (see review by Lester et al, 1980 [46]). In this type of engineered receptor, the agonist-azobenzene-conjugate was tethered to a cysteine residue in the cys-loop of the native ACh receptor, close to the ACh binding site on the receptor, allowing the agonist to activate the receptor in *trans*-configuration. Agonist in the shortened *cis*-configuration was not able to reach the binding site. Reversible control of current flow in these conjugated channels was achieved by light of two wavelengths (320 and 420 nm). More recently, successes with light-gated K^+ channel and light-gated iGluR were demonstrated by the Berkeley group [47-50], using

azobenzene-based photoswitchable ligands tethered to a genetically introduced, cysteine engineered version of the ion channel. Light of the same wavelength produces opposite changes in membrane voltage on these two types of synthetic channels. With the K^+ channel, the tethered ligand (a quarternary ammonium compound that functions as a channel blocker) in *trans*-configuration blocks the channel pore and *cis*-generating light opens the channel, triggering membrane hyperpolarization. With the iGluR, membrane depolarization was produced by the ligand (glutamate) in *cis*-configuration. This complementary control of the neuronal activity makes possible the mimicry of the behavior of both ON and OFF retinal cells in response to light. In 2011, Caporale *et al* demonstrated consistent restoration of light sensitivity in mice with no light perception by selectively expressing the light-gated iGluR in retinal ganglion cells [26].

Presently described azobenzene-based photoswitches that are tethered to ion channels have the limitation of slow relaxation. However by comparison with the expression of opsin-based light-gated channels, the photoswitch-based counterparts have the major advantages of overall larger whole cell current due to larger single-

channel conductance, bi-directional (ON and OFF) control of neuronal activity with two wavelengths and thus a more precise control of timing, particularly in the cell's sustained response to light. In addition, the photoisomerization properties, such as stimulation wavelength and relaxation rate, can be tuned by changing the chemistry of the groups around the azobenzene moiety.

1.2.4 Our approach

As noted earlier, in retina, the visual signal that travels vertically from outer to inner layers via excitatory glutamate pathway is subject to lateral modulation by inhibitory pathways, largely mediated by GABAergic synapses. Studies by the Berkeley team on light-gated glutamate receptors potentially provides a tool to restore excitatory signal transduction, and in order to best simulate the complex visual signal processing in retina, the horizontal tuning signal also needs to be recovered. Our study focuses on presenting GABA receptors with light-sensitivity using photoswitchable tethered ligands. For ultimate application in vision restoration, we anticipate tethering of the ligand-

photoswitch conjugates onto native receptor via an antibody-like affinity reagent and therefore avoiding the creation or introduction of an engineered receptor that tethers the ligand (Schematic representation see Fig. 1.2.2). With this primary purpose in mind, the focus of the work described in this thesis is on chemical constructs that are diffusible (i.e., lacking an anchoring moiety) and that exhibit activity at native $GABA_A$ receptors. However, an important component of the present work, the rationale for which will be described below, has involved tethering chemically synthesized ligands on cysteine-introduced $GABA_A$ receptors in a recombinant expression system.

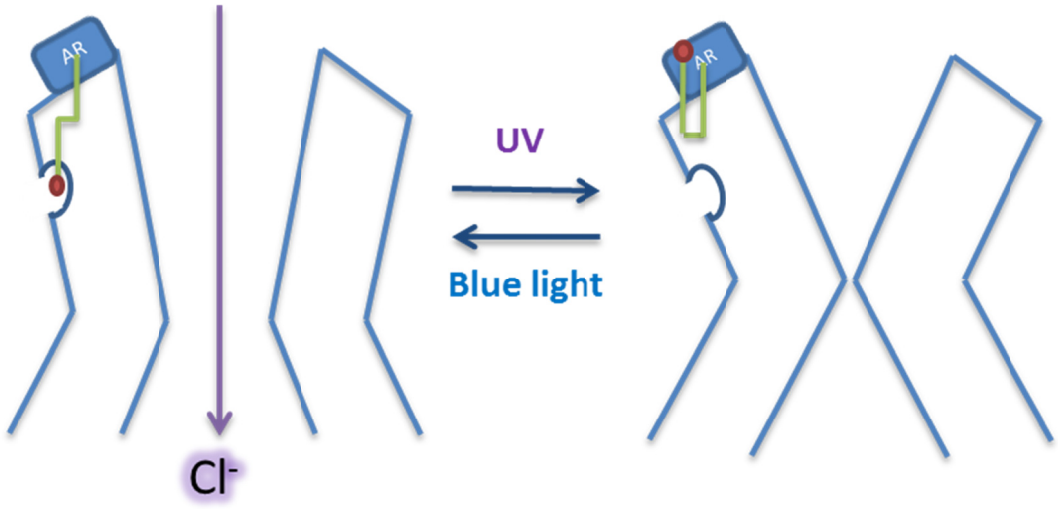

Fig. 1.2.2: Schematic representation of a photo-control model of GABA receptors. Inter-conversion of the *trans*- and *cis*-isomer of the photoswitch component (green zigzag arm) delivers the ligand (red filled dot) to or removes it from the binding site, inducing the conformational change of the receptor (cross-section shown in the figure), which results in the modulation of the ion flow through the channel pore. The structure is tethered onto the receptor via affinity reagent (abbreviated as AR).

CHAPTER 2

GABA RECEPTORS

2.1 Structure of $GABA_A$ receptors

$GABA_A$ receptors ($GABA_ARs$) are pentameric, ligand-gated ion channels activated by γ-aminobutyric acid (GABA). As membrane proteins, they consist of an extracellular domain, a transmembrane domain (TMD) composed of 4 α-helix subdomains TM1-4 and an intracellular domain. Binding of GABA to the agonist binding sites at the extracellular domain triggers a conformational change of the receptor transmembrane domain and leads to the opening of the channel pore, allowing the chloride ions to flow down their electrochemical gradient. In adult neurons, the reversal potential of chloride ions is typically lower than the resting membrane potential, and therefore drives the influx of chloride ions and produces hyperpolarization of the membrane that prevents the firing of action potentials. In $GABA_ARs$, five subunits are arranged pseudosymmetrically, where TM2 of each subunit lines the central pore.

Sixteen different classical $GABA_A$ subunit types have been identified, including six α subunit types $\alpha_{1\text{-}6}$, three β subunit types $\beta_{1\text{-}3}$, three γ subunit types $\gamma_{1\text{-}3}$, as well as a δ, an ε, a π and a θ subunit type. Yet only a limited number of combinations of these subunits have been found to yield functional receptors. The most common $GABA_AR$ composition in mammalian CNS consists of two α1 subunits, two β2 subunits and a single γ2 subunit [51]. In addition, ρ_1-ρ_3 subunits were found in the receptor type originally termed $GABA_C$ receptors and recently reclassified as $GABA_A$-ρ receptors. The ρ subunits assemble into either homo-pentamers with five identical subunit types or hetero-pentamers, usually with two subunit types. Throughout this thesis, for an easier distinction, we continue to use $GABA_C$ receptors to designate $GABA_A$-ρ receptors and $GABA_A$ receptors to designate classical $GABA_A$ receptors.

2.2 $GABA_A$ receptors on retinal bipolar cells and ganglion cells

Retinal bipolar cells (RBCs) possess $GABA_A$ and $GABA_C$ receptors, which mediate fast inhibitory signaling in bipolar cells of the retina [52-54] (for a review, see

Ref. [55]. Electrophysiological and immunocytochemical data indicate that $GABA_A$ and $GABA_C$ receptors on bipolar cells are localized primarily at the axon terminals, postsynaptic to amacrine cells [56-58]. The proportion of $GABA_A$ and $GABA_C$ mediated responses varies for different bipolar cells types and depends on GABA concentration, due to different GABA sensitivities of $GABA_A$ and $GABA_C$ receptors. At a GABA concentration of 25 μM, on rod bipolar cells, the $GABA_C$–mediated response represents ~70% of the overall response to GABA whereas for cone bipolar cells, only ~20% of the response was mediated by $GABA_C$Rs [57]. Furthermore, expression of $GABA_A$R α_1, α_3, $\beta_{2/3}$, and γ_2 subunits and $GABA_C$R ρ_1 and ρ_2 subunits in rod bipolar cells has been reported [59-62]. However, the specific subunit compositions of these receptors of bipolar cells are as yet unknown. A large number of electrophysiological and immunocytochemical data demonstrates the presence of $GABA_A$Rs on all mammalian retinal ganglion cells (RGCs). Retinae across many mammalian species, e.g., rat, rabbit and monkey express α_1, $\beta_{2/3}$ and γ_2 subunits [63-65]. In some rat RGCs, α_4 and α_6 subunits have been identified [66]. In contrast, $GABA_C$Rs are absent in mammalian

RGCs [67, 68]. A majority of the RGC $GABA_A$Rs is distributed at the cell's dendrites postsynaptic to amacrine cells, suggesting lateral inhibition on ganglion cells by amacrine cells [69, 70].

2.3 Pharmacology of $GABA_A$ receptors

In addition to GABA, $GABA_A$Rs are activated by a number of GABA analogs such as muscimol, gabapentin and gaboxadol, which similarly bind to the agonist binding sites on the receptor. Their activities are diminished by a group of antagonists, which, can be further classified into competitive and non-competitive antagonists. The former group, including bicuculline and gabazine, typically competes with agonists for the same binding sites and the latter (e.g., picrotoxin; PTX) inhibits the channel activity by blocking the extracellular side of the channel pore. Another diverse group of naturally occurring and synthetic low-molecular weight compounds are known to allosterically modulate the $GABA_A$R activity by binding to various sites distinct from the GABA binding sites. These $GABA_A$-modulating agents include benzodiazepines, barbiturates,

ethanol, neuroactive steroids, and volatile and non-volatile anesthetics [71, 72]. On $\alpha_1\beta_2\gamma_2$ $GABA_AR$s, the agonist binding sites reside at the interface of α and β subunits on the extracellular side [73] whereas the benzodiazepine modulatory site lies at the α and γ interface [74-76].

2.4 $GABA_A$ receptor allosteric modulator propofol

2.4.1 Activity of propofol on $GABA_A$ receptors

Among the extensive group of $GABA_A$ modulators is propofol (2,6-diisopropylphenol, Fig. 2.4.1), a nonvolatile general anesthetic that allosterically enhances or induces the $GABA_A$ receptor activity. The action of propofol on native and recombinant $GABA_A$ receptors of differing subunit composition has been investigated in multiple cell types [77-79]. For example, in *Xenopus* oocytes engineered to express $\alpha_1\beta_2\gamma_{2s}$ $GABA_AR$s, propofol at low concentrations (~1-100 μM) allosterically potentiates the GABA-elicited response; the compound at higher concentrations (~100-1000 μM) activates the receptor in the absence of GABA [79]. It has been shown that propofol

slows receptor deactivation and desensitization [80]; these actions could underlie the enhancement effect of this compound on the $GABA_AR$. In addition to $\alpha_1\beta_2\gamma_{2s}$, Sanna *et al.* expressed $GABA_ARs$ of 17 other different subunit compositions in *Xenopus* oocytes and detected a modulatory action of propofol on all these receptors with no specific subunit requirement, though the potency and efficacy varied among different receptor subunit constructs [81]. In contrast, the direct activation of propofol required the expression of β subunit [82], which likely suggests that the binding site of propofol underlying the modulatory effect may be distinct from that which mediates the activation effect.

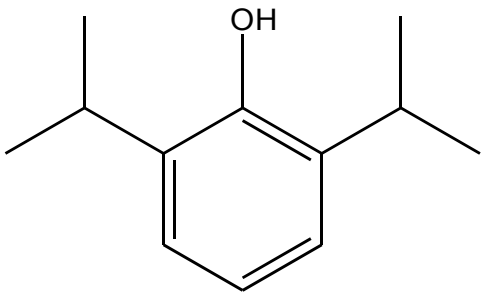

Fig. 2.4.1: Chemical structure of propofol.

2.4.2 Clinical relevance of propofol in retina

The systemic administration of propofol significantly alters electroretinographic (ERG) responses recorded from the intact eye. Kommenen *et al*. tested the effect of increasing the infusion rate of anesthetizing propofol on ERGs recorded from dogs, and observed an enhancement of the *b*-wave response with increasing propofol infusion rate [83]. In addition, Ng *et al.* found that administering propofol to the isolated perfused porcine eye reduces and delays the p1 component of the multi-focal ERG [84]. However, it remains unclear whether these effects are mediated by GABA receptors in retina.

2.4.3 Structure-activity relationships of propofol analogs

Ever since the discovery of the anesthetic effects of propofol in 1970s, researchers have investigated a wide range of propofol analogs to better understand the pharmacological activity of the ligand. Four 4-dimentional quantitative structure-activity relationship (4D-QSAR) models built upon 27 propofol analogs by Krasowski *et al.* reveal three important ligand-$GABA_A$ receptors binding interactions: the formation of

a hydrogen bond involving the ligand –OH group; a hydrophobic pocket binding interaction involving the 6-substituent of the ligand phenol ring; and a similar pocket binding interaction involving the 2-substituent [85]. Another study mainly focusing on the substitutions at the para position of the phenol ring suggests that lipophilicity and, less importantly, the steric effects of the substituents are the two main factors determining binding affinity of the ligand [71]. These and other studies [86, 87] provide a framework for the design of propofol analogs to produce improved aqueous solubility and higher anesthetic potency.

2.4.4 Propofol binding sites

Despite many studies of propofol's activity on $GABA_ARs$, the binding site of the ligand and its gating mechanism remain unclear, largely due to the unavailability of the crystal structure of $GABA_ARs$. Using site-directed mutagenesis, previous studies identified several amino acid residues on the β subunit that affect propofol activity, including β_2-M286, β_2-Y444 and $\beta_{2/3}$-N265 [88-90]. Yet it was not entirely clear whether

these residues lie in the binding pocket of propofol and directly affect the binding of the compound, or whether they are involved in allosteric coupling of the binding event to channel gating. Analogs of etomidate, another general anesthetic that is thought to bind to a site overlapping yet distinct from that of propofol, were found by Li *et al.* [91] to photo-label brain $GABA_ARs$ at residues of α_1M236 and β_3M286. Subsequently, Li *et al.* found this labeling was partially inhibited by propofol [92]. Interpretation of these data using the homology model based on nAChR structures suggests that sites in the upper region of the transmembrane domain mediate the modulatory effect of pentameric ligand-gated ion channels. A recent study by Hugues *et al.* [93] describing the X-ray structure of propofol-bound pH-gated bacterial homologue GLIC, a pentameric ligand-gated ion channel homologous to $GABA_ARs$, provides new insights into the mechanism of propofol action. On the homo-pentameric structure of GLIC, the propofol binding site was found to reside in the upper half of the transmembrane domain in a cavity that exists within each subunit. This intra-subunit cavity is accessible from the lipid bilayer through the crevice between the M1 and M4 helices. Another cavity of comparable

volume is located at the interface between subunits on the other side of M1 helix. It is not accessible from the outside but is linked to the intra-subunit cavity by a narrow tunnel. Using the GLIC crystal structure and the sequence alignment between GLIC and $GABA_AR$, α_1-M236 and β_3-M286, two $GABA_AR$ residues previously labeled by etomidate, were found to point toward the inter-subunit cavity close to the intra-subunit general anesthetic binding site. A pronounced reorganization of these cavities observed in the initial steps of channel gating, which involves a transient communication between the two cavities, may underlie propofol-mediated potentiation [93].

2.5 Goal of the present study

The functional significance of $GABA_ARs$ on bipolar and ganglion cells as well as the unsuccessful early attempts with the photo-control of $GABA_CRs$ raised our interest in engineering light-regulation in $GABA_ARs$. However, the initial attempt on conjugating a photoswitch with receptor agonists such as GABA and muscimol produced new compounds of very low activity, possibly owing to the steric constraint

imposed by the agonist binding site. This led us to adopt a different approach, which is to engineer photo-regulation by perturbing the receptor structure at a site distinct from the agonist-binding pocket. The abundance and diversity of known allosteric modulators of $GABA_AR$s, including propofol itself, suggested the feasibility of this alternative approach. Previous studies on the ligand-receptor interaction of propofol and the wide applicability of propofol on a multitude of $GABA_AR$s of different subunit composition gave rise to the candidacy of propofol as the allosteric effector in the photoswitchable membrane-tethered construct. To determine the effect of propofol on native retinal $GABA_AR$ and $GABA_CR$ respectively, we first examined the activity of propofol on retinal bipolar cells, an important cell type with both $GABA_AR$ and $GABA_CR$ expressed. The results obtained demonstrated a marked modulation of the native $GABA_AR$ activity by propofol, further suggesting the workability of propofol-based structures in retinal neurons. With the aim of developing photo-responsive propofol derivatives, we screened, on the platform of *Xenopus* oocyte-expressing $\alpha_1\beta_2\gamma_2$ $GABA_AR$s, chemically tailored azobenzene-containing structures derived from propofol. This screening led to

our discovery of a compound with particularly high potency and excellent photo-responsiveness in the oocyte system. Building on this discovery, we then investigated the action of this compound on rat retinal ganglion cells, the retinal output neuron with abundant $GABA_AR$s and found that the compound exhibits isomer state-dependent modulation as well as direct activation of the native $GABA_AR$s of these cells. Further, we tested the tetherability of the light-sensitive structure by incubating a maleimide-terminated propofol-photoswitch conjugate with oocytes that expressed a cysteine-substituted $GABA_AR$. The results obtained with the maleimide terminated conjugate indicated, in addition to successful covalent attachment, a preservation of light-regulated activity of the tethered structure.

CHAPTER 3

MATERIALS AND METHODS

3.1 Preparative and electrophysiological recording procedures for oocyte experiments

3.1.1 Oocyte removal and defolliculation

Xenopus laevis females were purchased from Xenopus 1 (Dexter, MI) and maintained at the UIC Biologic Resource Laboratory (BRL) in tanks with circulating water. All animal procedures for the experiments using *Xenopus laevis* were conducted in accordance with institutional policies of the University of Illinois at Chicago and with the Statement for the Use of Animals in Ophthalmic and Vision Research adopted by the Association for Research in Vision and Ophthalmology (ARVO). The standard saline solution (Ringer solution) used for oocyte experiments contained 100 mM NaCl, 2 mM KCl, 2 mM $CaCl_2$, 1 mM $MgCl_2$, 5 mM HEPES, and 10 mM glucose, at pH 7.4. Animals

were anesthetized with MS222 (3-amino benzoic acid ethyl ester; Sigma–Aldrich, St. Louis, MO, USA) (1.4 g/l). Ovarian tissues were removed surgically and immediately transferred to a petri dish filled with Ca-free Ringer. The tissue was divided by forceps into smaller clumps, which were subsequently immersed in Ca-free Ringer containing 2 mg/ml collagenase (Sigma–Aldrich). Oocytes were isolated and defolliculated by shaking for 1 h at room temperature on a multi-purpose rotator (Thermo Scientific, Asheville, NC) and by mechanical trituration (repeated passage through a glass pipette). Oocytes were washed, selected and then incubated in standard Ringer at 16 ˚C.

3.1.2 RNA injection

For the functional expression of $GABA_A$ receptors, each oocyte was injected (Drummond Nanoject II; Drummond Scientific Co., Broomall, PA, USA) with ~50 nL cRNA mixture (~0.5 µg/µL) that coded for wildtype (WT) or mutant $\alpha_1\beta_2\gamma_2$ $GABA_A$ receptors. The cRNAs encoding rat α_1, rat β_2 and human γ_{2S} subunit were mixed at the ratio of 1:1:8; the 8-fold mass excess of γ subunit facilitated expression of a

homogeneous (i.e., γ-containing) $\alpha_1\beta_2\gamma_2$ receptor population. Mutant clones were produced by site-directed mutagenesis, in which an endogenous residue of a WT clone was replaced by an introduced cysteine residue. The cDNA source of the cRNA was obtained from Dr. David Weiss. The oocyte was then incubated at 16 °C in Ringer solution containing 0.1 mg/ml of gentamicin (Sigma–Aldrich) for 24-48 hours to allow adequate receptor expression before electrophysiological experiments.

3.1.3 Oocyte electrophysiology

Membrane currents passing through the ion channels were measured by the two-electrode voltage clamp technique [94] (amplifier: GeneClamp500B; Axon Instruments, Foster City, CA, USA), and low-pass filtered at 10 Hz.

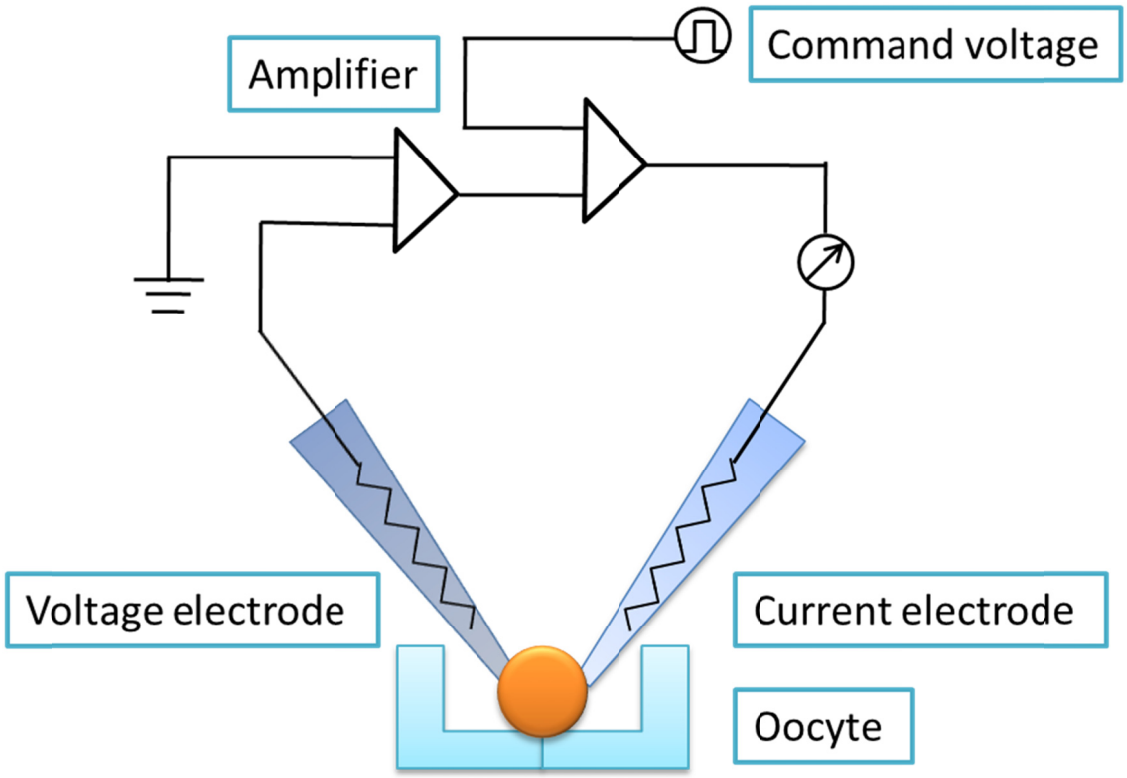

Fig. 3.1.1: Schematic representation of two-electrode voltage-clamp recording of the membrane current response. Measurements are carried out by inserting two glass pipette electrodes into the cell membrane. Both electrodes contain current conducting chlorided silver wires inside. One electrode measures transmembrane voltage, and the other pumps current into the cell to maintain the membrane voltage at the command/holding potential (-70 mV in the present experiments). When the channels open in response to pharmacological stimuli, ions cross the channels, causing the deviation of membrane potential from the holding potential. The deviation is detected by the amplifier, which delivers the compensation current to the current electrode.

Glass micropipettes for oocyte recording were prepared using a programmable puller (Sutter Instruments, Novato, CA). When filled with 3 M KCl, the electrode had a resistance of 1-10 MΩ. The voltage-clamp procedure was controlled by a computer running Clampex 8.2 (Axon Instruments) interfaced with the apparatus. Electrophysiological data were obtained in response to the presentation, to the oocyte, of Ringer solution containing pharmacological agents. The investigated compounds were either commercially available (e.g., GABA (Sigma-Aldrich) and propofol (SAFC Supply Solutions, St. Louis, MO), or synthesized by our chemistry colleagues (propofol derivatives). Test solutions were delivered via multiple channels from separate reservoirs by a gravity flow system (Automate Scientific, Berkeley, CA) operated under computer command. Unless otherwise indicated, oocytes were superfused with test solution at a rate of ~1mL/min. Experiments with UV illumination involved periods of static bathing, i.e., halted superfusion, after total turnover in the recording chamber (~15 µL) from regular Ringer to test solution. Membrane current data were obtained using Clampex 8.2 and analyzed using Clampfit 10.0 (Axon Instruments) and OriginPro7.5

(OriginLab Corporation, Northampton, MA). Unless otherwise indicated, all data are shown as mean ± S.D., and all statistical analysis employed a two-sample *t*-test.

3.1.4 Illumination conditions

Oocyte electrophysiological experiments were carried out in room light. A UV light-emitting diode with peak wavelength at 365 nm (Hamamatsu Photonics, Japan) and a white light microscope illuminator (Schott Fostec, Auburn, NY) provided UV and visible stimulating light, respectively. The UV LED was programmed to emit light at intensities ranging from 5% to 100% of its maximal capacity and was positioned 2-3 cm above the recording chamber at a ~30 degree angle from the normal plane. As measured at the position of the oocyte, the maximal (100%) intensity of the UV light at 365 nm was 220 μW/mm^2. Unless otherwise indicated, the UV LED was operated at its maximal intensity. At 440 nm, the nominal strength of the visible (white) light (referred to as high-intensity visible light) was 28 μW/mm^2, and that of the ambient illumination was 0.045 μW/mm^2. In all experiments, low-intensity visible light from the microscope

illuminator (3 μW/mm^2 at 440 nm) was present at all times except those involving high-intensity visible illumination.

3.2 Preparative and electrophysiological recording procedures for retinal neuron experiments

3.2.1 Isolation of retinal bipolar cells

All animal procedures with rats were conducted in accordance with institutional policies and with the ARVO Statement for the Use of Animals in Ophthalmic and Vision Research. The electrophysiological experiments were conducted on isolated, enzymatically dissociated bipolar cells obtained from adult Sprague-Dawley and Long-Evans rats (male and female) (Charles River Laboratories, Wilmington, MA). Procedures for animal euthanization, isolation of the retina, and dissociation of retinal cells were similar to those described by Ramsey *et al*. [95]. Rats were euthanized by CO_2 and eyes were enucleated and hemisected. The retina detached from the posterior eyecup was cut into three pieces and immersed in a modified Ames media

(supplemented with 0.88 g/l NaCl, 2.36 g/l HEPES, and 10,000 units/l penicillin/streptomycin, pH 7.4) containing 2 mg/ml papain (EMD Biosciences, San Diego, CA) and 1 mg/ml of L-cysteine (Sigma, St. Louis, MO). After about 40 minutes of gentle shaking, the tissue was washed 4 times with papain-free Ames medium and then was triturated using a sterile pipette. The dispersed tissue was allowed to settle for 1 minute to the bottom of the tube. Aliquots of the supernatant containing dissociated cells were then placed in petri dishes containing mammalian Ringer that consisted of 135 mM NaCl, 5 mM KCl, 2 mM $CaCl_2$, 2 mM $MgCl_2$, 10 mM glucose, and 5 mM HEPES, pH 7.4. Isolated bipolar cells, likely rod bipolar cells, were identified on the basis of their characteristic morphology: a small soma, with dendrites and a long axon extending from opposite sides of the soma.

3.2.2 Isolation of retinal ganglion cells

Enzymatically dissociated ganglion cells were obtained from adult Sprague-Dawley rats (male and female, 6-16 weeks of age) (Charles River Laboratories).

Procedures were similar to those described for retinal bipolar cells, except that retinal cell dissociation in papain-supplemented Ames medium involved a shorter duration (20 min rather than 40 min) accompanied with somewhat more vigorous shaking. Isolated ganglion cells were identified by their large size, spherical shape, and the presence of large voltage-gated sodium current.

3.2.3 Whole-cell patch-clamp recording

Whole-cell patch-clamp techniques similar to those described [95, 96] were used to record membrane current responses of solitary retinal cells to test agents. Isolated bipolar/ganglion cells were maintained at room temperature for 1-2 hrs prior to recording. The patch pipette with a resistance of 8-12 MΩ was pulled in two stages using a micro-electrode puller (Model PP830, Narishige Group, Tokyo, Japan). The pipette was filled with an intracellular solution containing 95 mM $CsCH_3SO_3$, 20 mM TEA-Cl (tetraethylammonium chloride), 10 mM glutamic acid, 1 mM BAPTA (bis(2-aminophenoxy)ethane tetraacetic acid), 10 mM HEPES (4-(2-hydroxyethyl)-1-

piperazineethanesulfonic acid), 8 mM phosphocreatine di(tris), 1 mM MgATP (magnesium adenosine-5'-triphosphate) and 0.2 mM Na_2GTP (sodium guanosine-5'-triphosphate); pH adjusted to 7.2 with CsOH. Cesium was employed to block potassium current. Unlike the two-electrode configuration used for oocyte experiments, the single electrode was brought into contact with the cell by a motor-driven three-dimensional manipulator (Newport, Fountain, CA) and was not inserted into the cell membrane. By applying light suction to the pipette, a high resistance seal (giga-seal) was formed between the pipette and the cell membrane. Further suction ruptured the patch of membrane under the tip of the micropipette, yielding a whole-cell recording configuration and providing access for the electrode to the interior of the cell. The chlorided silver wire inside the electrode conducted currents to the amplifier. Cells were clamped at −60 mV for bipolar cells and at 0 mV for ganglion cells (Axopatch 200B amplifier; Axon Instruments), and experimental runs were controlled by pClamp system software (Axon Instruments). Electrophysiological data were obtained in response to defined concentrations of test compounds dissolved in mammalian Ringer.

Supplementation of aqueous solutions with propofol and its derivatives was carried out by adding an aliquot of a stock solution containing the compound dissolved in DMSO (dimethyl sulfoxide). In all experiments, the amount of carrier DMSO present in the applied test solution was <1% (v/v). Test solutions were delivered from separate reservoirs by a gravity-driven multi-channel perfusion system operated under computer command. As in the oocyte experiments, data were collected by pClamp software and analyzed with Clampfit 10.0 and Origin 7.5.

3.2.4 UV illumination apparatus

The UV-LED used in the oocyte experiments was used for pre-treatment of the test compound with UV. For preparation of *cis*-dominant MPC088 and related compounds, the test solution of initially *trans*-dominant configuration underwent a 5-min UV illumination prior to its placement in the perfusion reservoir. All preparative procedures were performed in the dark, and the reservoirs and perfusion lines were light-protected with aluminum foil. The same UV-LED was also adopted for real-time UV

illumination during patch clamp recording. Here, the LED head was placed ~2 cm above the recording cell by a one-dimensional positioner such that light emitted by the LED was reflected by a mirror to illuminate an area covering the clamped cell (Fig. 3.2.1).

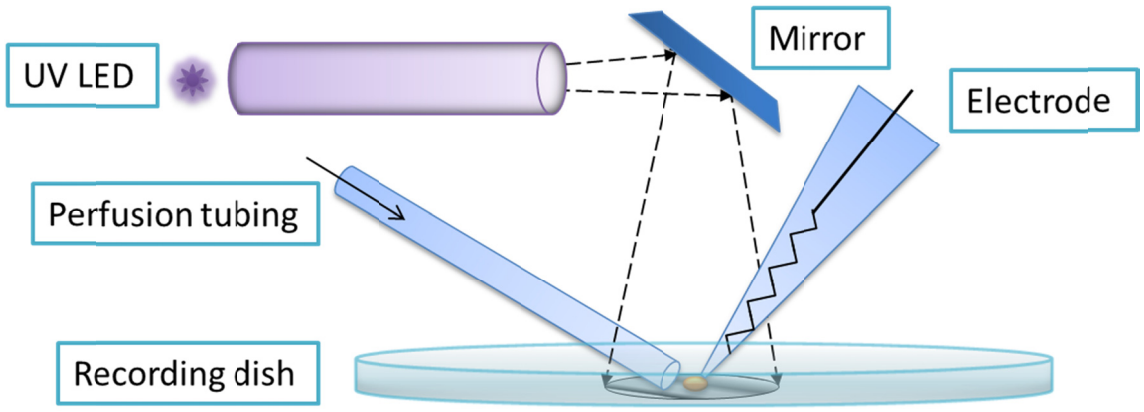

Fig. 3.2.1: Schematic representation of the UV apparatus for the real-time illumination in patch-clamp recording. The total distance traveled by light, from the LED head to the cell, was similar to that used in the oocyte experiments.

3.3 Analysis of electrophysiological data

3.3.1 Dose-response fitting to Hill Equation

To quantitatively describe the effect of a test agent, dose-response data derived from membrane current responses elicited by GABA or other ligands in electrophysiological experiments were analyzed in relation to the Hill Equation:

$$\frac{I}{I_{max}} = \frac{[C]^n}{[C]^n + {EC_{50}}^n}$$

In this equation, I is the membrane current peak amplitude elicited by a ligand at concentration $[C]$, I_{max} is the maximum peak amplitude achievable by the ligand and EC_{50} is the concentration of the ligand producing a half-maximal response. The Hill coefficient n is an index of the sharpness of the rise of the response function and often is interpreted as a measure of the cooperativity of ligand binding. That is, a unit value of n suggests that only one binding site of the ligand is involved in the activation of the receptor. Values of n > 1 may result from multiple ligand binding and may indicate a positive cooperativity of the ligand binding: that is, the case in which binding of one

ligand to the receptor increases the binding affinity of the ligand for one or more additional sites of the receptor. In such a case of multiple-site binding, the highest possible experimentally determined Hill coefficient is equal to or smaller than the number of binding sites involved in facilitating that response [97]. Generally, for a given ligand, I_{max} describes the efficacy of the ligand, and EC_{50} is an indication of its potency. For example, with $GABA_A$Rs, when co-applied with a given concentration of competitive antagonist such as bicuculline, the dose-response curve of GABA shifts to the right (larger EC_{50}), with typically no change in I_{max}, whereas co-application of GABA and a non-competitive antagonist such as picrotoxin may yield an unchanged EC_{50} but a reduced I_{max}.

Similarly, the dose-response data obtained with a channel inhibitor in the presence of a fixed concentration of an agonist can be fitted by the Hill equation of the following form:

$$\frac{I}{I_{max}} = \frac{{IC_{50}}^n}{[C]^n + {IC_{50}}^n}$$

where I_{max} is the response in the absence of the inhibitor and IC_{50} is the concentration that gives rise to half-maximal inhibition. Unitary and > 1 values of the Hill coefficient are often interpreted as in the relation described above for agonist binding.

3.3.2 Noise analysis

Noise analysis is a useful method to calculate the single-channel property from current fluctuations in a membrane containing many channels [98]. In the case of a membrane with N independent channels of the same kind, the mean membrane current $\langle I \rangle$ and variance σ^2 are given by the following expressions:

$$\langle I \rangle = Nip$$

$$\sigma^2 = Ni^2p(1-p)$$

where i is the single channel current, p is the channel open probability, and the closing probability is $1-p$. Combining these two expressions reveals the relationship of the variance and the mean current:

$$\sigma^2 = i\langle I\rangle - \frac{\langle I\rangle^2}{N}$$

When plotted as σ^2 versus $\langle I\rangle$, this equation is a parabola, and within the limit of very small $\langle I\rangle$, the single-channel current i can be obtained as the slope of the parabola.

Noise analysis of representative waveforms obtained from retinal bipolar cells in the absence and presence of propofol followed procedures similar to those described [53, 95]. Responses were recorded at a sampling rate of 2.5 kHz and were segmented into 200-ms intervals. $\langle I\rangle$ and σ^2 (calculated after passing a 5-Hz high-pass filter) were determined for each 200-ms segment of the responses. For each investigated cell, data obtained under a given experimental condition were analyzed by linear regression to derive the slope $\sigma^2/\langle I\rangle$, and the single-channel conductance was obtained by dividing this ratio by the driving force for chloride ion (60 mV).

3.4 UV-Vis spectrophotometry

Absorption spectra of the azobenzene-containing propofol-derivatives were obtained on a UV-vis spectrophotometer (Cary 300Bio, Varian Inc, Palo Alto, CA). The instrument was controlled by a computer running Cary WinUV software, which was set to scan with the wavelength from 280-600 nm at the rate of 600 nm/min. The sample prepared in DMSO was contained in the sample cuvette and unsupplemented DMSO in the reference cuvette. The photo-isomerizing UV and visible light sources used in spectrophotometric experiments were the same as those used in oocyte experiments. Absorption spectra were obtained before and after 5 min UV illumination, and subsequently after exposure to visible light.

As indicated in previous studies [99] and validated by our own data, the *trans*- and *cis*- isomers of parent (i.e., unmodified) azobenzene exhibited distinct absorption characteristics. The sample containing predominantly *trans*-isomer exhibited a major absorption peak at ~320 nm and a minor peak at ~430 nm. The *cis*-generating UV irradiation diminished the major but enhanced the minor peak. However, due to a much

lower extinction coefficient of the *cis*-isomer, the absorption enhancement at ~430 nm was not as pronounced as the reduction at ~320 nm (Fig.3.4.1). In this thesis study, the progress and extent of photoisomerization of azobenzene-containing derivatives were determined by analyzing absorption spectra.

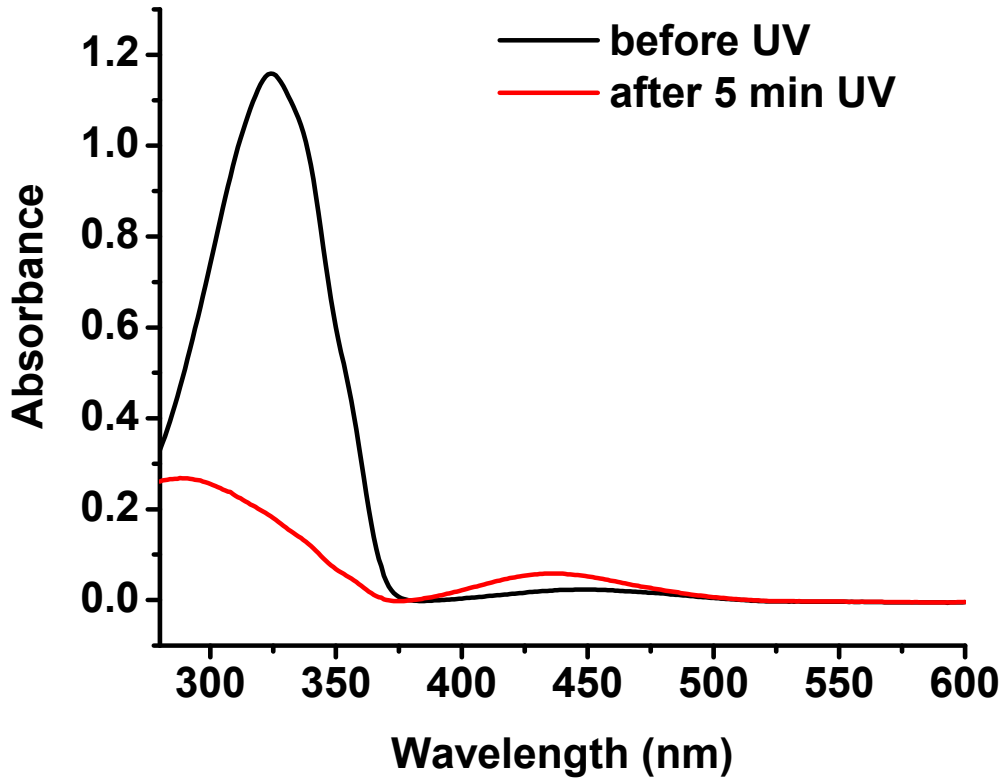

Fig. 3.4.1: Absorption spectra of 100 μM azobenzene obtained in DMSO before (black) and after (red) 5 min UV irradiation.

CHAPTER 4

RESULTS

4.1 Activity of propofol on native and recombinant $GABA_A$ receptors

To examine the workability of using propofol as the effector component of the light sensitive neuromodulating structure, we first needed to determine the activity of parent propofol on native retinal neurons. To this end we tested propofol on retinal bipolar cells and found a robust potentiating effect, specifically, on $GABA_A$ receptors of this cell type, whose subunit compositions are not yet entirely clear. Due to its wide distribution and functional significance in CNS, the $GABA_A$ receptor subtype of subunit composition $\alpha_1\beta_2\gamma_2$ was chosen, in our study, as the testing platform for screening propofol derivatives. Hereby, we also tested propofol on this receptor subtype and used the results obtained as the standard for later comparison with activities exhibited by newly synthesized propofol compounds.

4.1.1 Activity on native retinal bipolar cells

First, the effect of propofol was examined on GABA-induced response contributed by both $GABA_A$ and $GABA_C$ receptors. Then we pharmacologically isolated $GABA_A$ or $GABA_C$ components and thereby obtained the specific action of propofol on each receptor subtype.

4.1.1.1 Effect on GABA-elicited response

Fig. 4.1.1, which illustrates responses recorded from a bipolar cell in response to GABA alone and to co-applied GABA and propofol, shows that propofol markedly increased the GABA-elicited response. Shown are responses recorded from a single cell (Fig. 4.1.1A), with the application of either 10 μM GABA alone (black trace) or with co-applied 150 μM propofol (red trace). Similarly, Fig. 4.1.1B shows data from a second cell that received 10 μM GABA in the absence and presence of 500 μM propofol (black and red traces, respectively). In both experiments, the inclusion of propofol produced a substantial increase in the response (Fig. 4.1.1A, 1.8-fold; Fig. 4.1.1B, 1.6-fold).

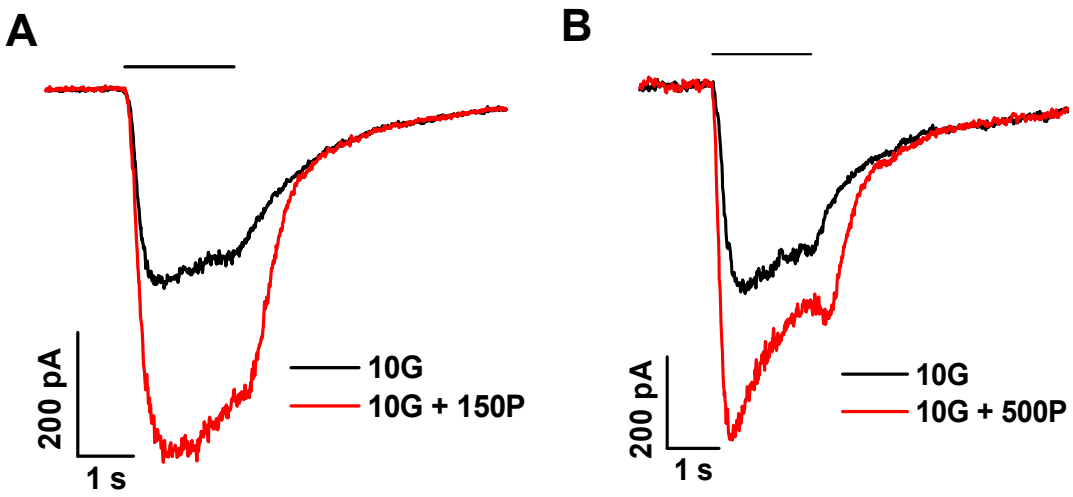

Fig. 4.1.1: Enhancement effect of propofol on GABA-elicited response of RBCs. (A) Responses elicited by 10 μM GABA in the absence (*black trace*) and presence (*red trace*) of 150 μM propofol. (B) Effect of co-applied 500 μM propofol on the response to 10 μM GABA.

Given that both $GABA_A$ and $GABA_C$ receptors are present on retinal bipolar cells, we then examined the effect of propofol on pharmacologically isolated responses mediated by each receptor type.

4.1.1.2 Absence of activity on $GABA_C$ receptors

To activate $GABA_C$ receptors only, we applied 5Me-I4AA, a recently described $GABA_C$-specific activator that exhibits a micromolar EC_{50} value at ρ_1 $GABA_C$ receptor [100]. Fig. 4.2.1A shows results obtained in a representative experiment that tested the susceptibility of the 5Me-I4AA–mediated response to TPMPA, a known $GABA_C$ antagonist. By comparison with the response obtained in the absence of TPMPA (black trace), those obtained with co-applied 100 and 200 µM TPMPA exhibited a dose-dependent, marked reduction in amplitude. As shown by the red trace, 100 µM TPMPA decreased the peak amplitude of 5Me-I4AA-elicited response by approximately 50%, and the diminished response to this co-applied mixture exhibited a pronounced sag from the peak, consistent with a progressively developing inhibition by TPMPA during the period of its application.

Fig. 4.2.1B presents the effect of bicuculline (200 µM; a known $GABA_A$ antagonist) and propofol (150 µM) on the response evoked by 5Me-I4AA. Here, the choice of 100 µM as the 5Me-I4AA concentration was based on the finding of Madsen

et al. [100] that, in ρ1-$GABA_C$–expressing HEK 293 cells, the response to 100 μM 5Me-I4AA is below saturation of the 5Me-I4AA response function and amounts to approximately 60% of the response to 10 μM GABA. Consistently, in our test on bipolar cells, the peak amplitude of the response to 100 μ M 5Me-I4AA represented approximately 50% of the response to 10 μM GABA (black and purple traces). Co-application of 200 μM bicuculline did not substantially alter the 5M-I4AA response (red trace), and aggregate data obtained from 8 cells yielded the ratio of 1.04 ± 0.01 for peak amplitudes in the presence *vs*. absence of bicuculline. The insensitivity of 5Me-I4AA-elicited response to bicuculline is consistent with an action of 5Me-I4AA specifically at $GABA_C$ receptors. To examine propofol's action on the $GABA_C$ receptors of retinal bipolar cells, we measured the effects of co-applied propofol on 5Me-I4AA–elicited responses of these cells. As shown by the black and blue traces, the co-applied 150 μM propofol had no substantial effect on the nominal 5Me-I4AA response, indicating that propofol has no effect on the $GABA_C$ receptors.

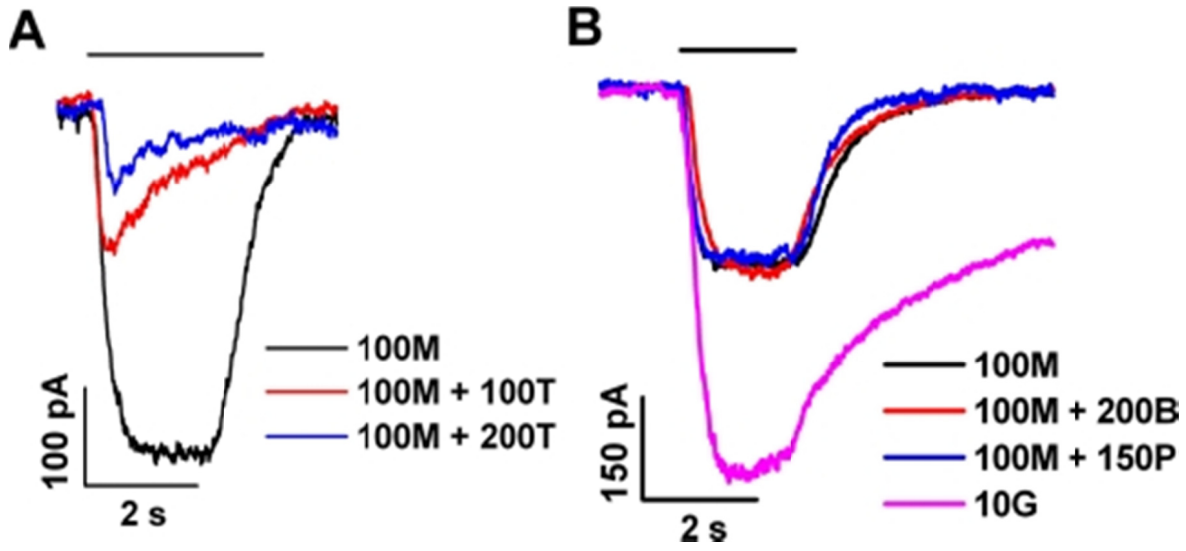

Fig. 4.1.2: Activity of propofol on $GABA_C$ receptors of RBCs. 5Me-I4AA, TPMPA, bicuculline, and propofol are abbreviated in the figure as M, T, B, and P, respectively. (A) Responses obtained from a single cell on the application of 100 µM 5Me-I4AA alone (*black trace*) and of 100 µM 5Me-I4AA with co-applied 100 or 200 µM TPMPA (*red* and *blue traces*, respectively). (B) Responses obtained from a second cell to 100 µM 5Me-I4AA alone (*black*), 100 µM 5Me-I4AA plus 200 µM bicuculline (*red*), 100 µM 5Me-I4AA plus 150 µM propofol (*blue*), and 10 µM GABA alone (*purple*).

4.1.1.3 Enhancement effect on $GABA_A$ receptors

To examine the action of propofol on bipolar cell $GABA_A$ receptors, we used TPMPA to suppress the contribution of $GABA_C$ receptors to the overall GABA-elicited response (Fig. 4.1.3). Herein all the test agents are abbreviated by first letter (GABA: G;

TPMPA: T; bicuculline: B; and propofol: P), and are accompanied by numbers that refer to the concentration in μM; for example, 10 μM GABA is denoted as 10G. In the Fig. 4.1.3 experiment, GABA was delivered at 10 μM, a concentration that exceeds the EC_{50} typically measured for $GABA_C$ receptors but below that typically measured for $GABA_A$ receptors [53]. Fig. 4.1.3A shows that TPMPA markedly reduced the GABA-elicited response (compare black and red traces); among 10 cells, the reduction produced by 100 μM TPMPA was 83% ± 2% (mean ± SD). Further, the remaining response was eliminated by 200 μM bicuculline (blue trace), indicating virtually complete suppression, by TPMPA, of $GABA_C$'s contribution. Henceforth, co-application of 10 μM GABA with 100 μM TPMPA (10G + 100T), was used as the nominal condition with which to compare the effects of propofol on bipolar cell $GABA_A$ receptors.

As shown in Fig. 4.1.3B, when co-applied with 150 μM propofol, the response evoked by (10G + 100T) was markedly increased (blue trace). Data obtained from 6 cells yielded a ratio of 5.8 ± 2.3 for the peak amplitude of $r_{10G + 100T + 150P}$ *vs.* $r_{10G + 100T}$. Henceforth, this ratio describing the propofol-induced increase in peak amplitude will be

termed the “enhancement factor” for the response. It should be noted that the propofol-dependent increase in response typically exhibited a progressive change with repeated application of the propofol. Throughout the present study, calculation of the enhancement factor was based on use of the maximum response recorded among what typically was a group of ≥3 responses obtained at a given propofol concentration. Fig. 4.1.3B shows also that the response to 150 μM propofol alone (green trace) was relatively small. Accordingly, for simplicity in the following sections, we refer to the enhancement factor described above as indicating the “potentiating” effect of propofol. In other words, we ignore the small contribution by the agonist activity of propofol.

Fig. 4.1.3C shows results obtained in another experiment that tested the effect of bicuculline on the propofol-enhanced response. Here, supplementation of the propofol-containing mixture with 500 μM bicuculline led to almost complete inhibition of the propofol-enhanced response (green trace), confirming that the potentiating action of propofol was mediated by $GABA_A$ receptors.

The enhancement of $GABA_A$ receptor activity on retinal bipolar cells is further indicated by the response elicited by THIP, a $GABA_A$-selective partial agonist [101]. As determined in the cell described in Fig. 4.1.3D and in three others, co-applied 150 μM propofol increased the response elicited by 100 μM THIP alone (100THIP) by 5.8 ± 1.1-fold (compare black and red traces). Further supplementation with 250 μM bicuculline essentially fully eliminated the enhanced response.

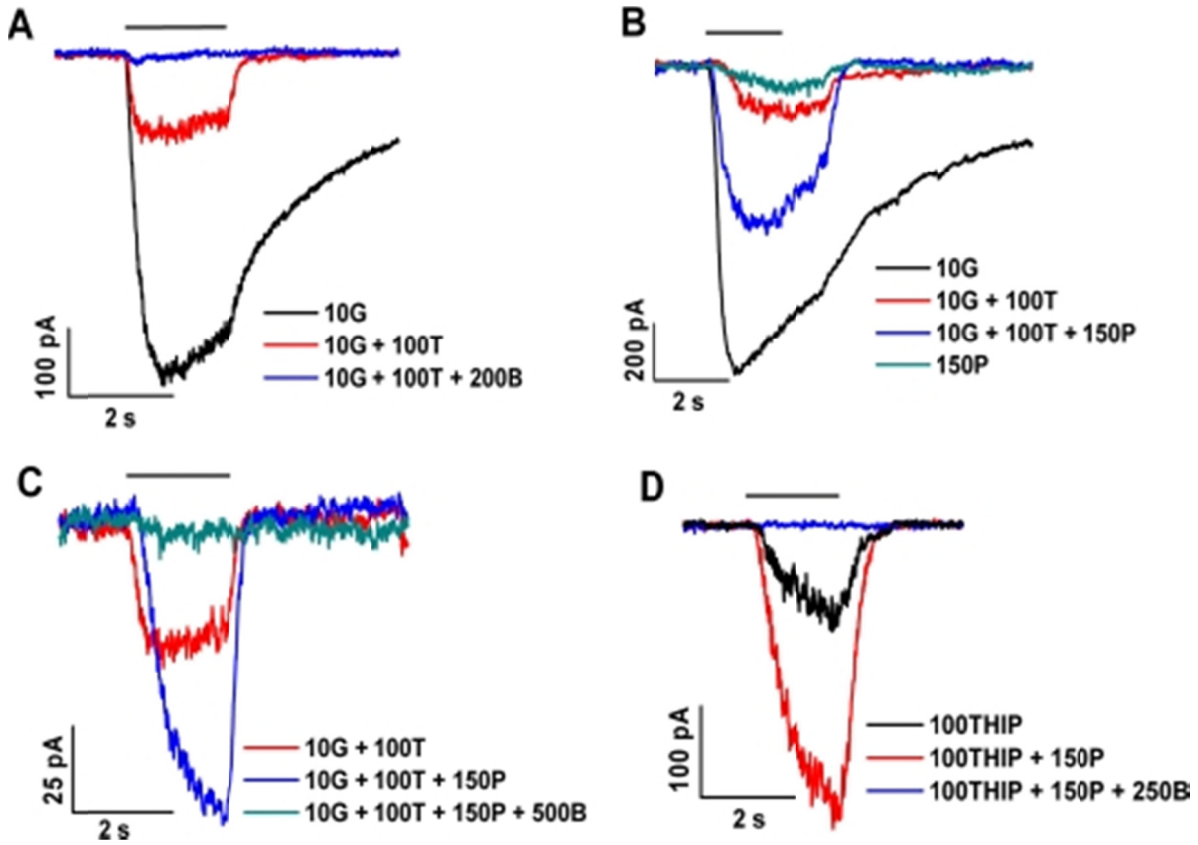

Fig. 4.1.3: Potentiating effect of propofol on $GABA_A$ receptors of RBCs. (A–D) Results obtained from four different cells. (A) 10 μM GABA (10G; *black*); 10 μM GABA plus 100 μM TPMPA (10G + 100T; *red*); 10 μM GABA plus 100 μM TPMPA plus 200 μM bicuculline (10G + 100T + 200B; *blue*). (B) 10 μM GABA (10G; *black*); 10 μM GABA plus 100 μM TPMPA (10G + 100T; *red*); 10 μM GABA plus 100 μM TPMPA plus 150 μM propofol (10G + 100T + 150P; *blue*); and 150 μM propofol (150P; *green*). (C) 10 μM GABA plus 100 μM TPMPA (10G + 100T; *red*); 10 μM GABA plus 100 μM TPMPA plus 150 μM propofol (10G + 100T + 150P, *blue*); and 10 μM GABA plus 100 μM TPMPA plus 150 μM propofol plus 500 μM bicuculline (10G + 100T + 150P + 500B; *green*). (D) 100 μM THIP (100THIP; *black*); 100 μM THIP plus 150 μM propofol (100THIP + 150P; *red*); and 100 μM THIP plus 150 μM propofol plus 250 μM bicuculline (100THIP + 150P + 250B; *blue*).

4.1.1.4 Single-channel conductance of propofol-bound $GABA_A$ receptors

The increase in response size induced by propofol (Fig. 4.1.3) could reflect an increase in single-channel conductance, an increased probability of channel opening by GABA, or some combination of these two effects. To investigate this issue, we analyzed responses from a group of cells to determine the single-channel conductance in the absence versus the presence of propofol. Fig. 4.1.4 shows the results of noise analysis of waveforms recorded from a single cell on the application of (10G + 100T) (open circles) and of (10G + 100T + 150P) (filled circles). Determinations of the mean and variance of the analyzed responses over 200-ms intervals (see 3.3.2) yielded slope values of 0.61 pA and 0.56 pA for the data obtained with (10G + 100T) and (10G + 100T + 150P), respectively. The resultant respective values for single-channel conductance were 10.2 and 9.4 pS. Among a group of nine cells, mean values of single-channel conductance determined with (10G + 100T) were 11.8 ± 3.95 pS, and those determined with (10G + 100T + 150P) were 12.8 ± 4.49 pS. The ratio of single-channel conductance obtained in the presence versus the absence of propofol—i.e., the

conductance determined with (10G + 100T + 150P) divided by that determined with (10G + 100T)—yielded 1.1 ± 0.18. Thus, 150 μM propofol had no significant effect on the single-channel conductance (P = 0.19).

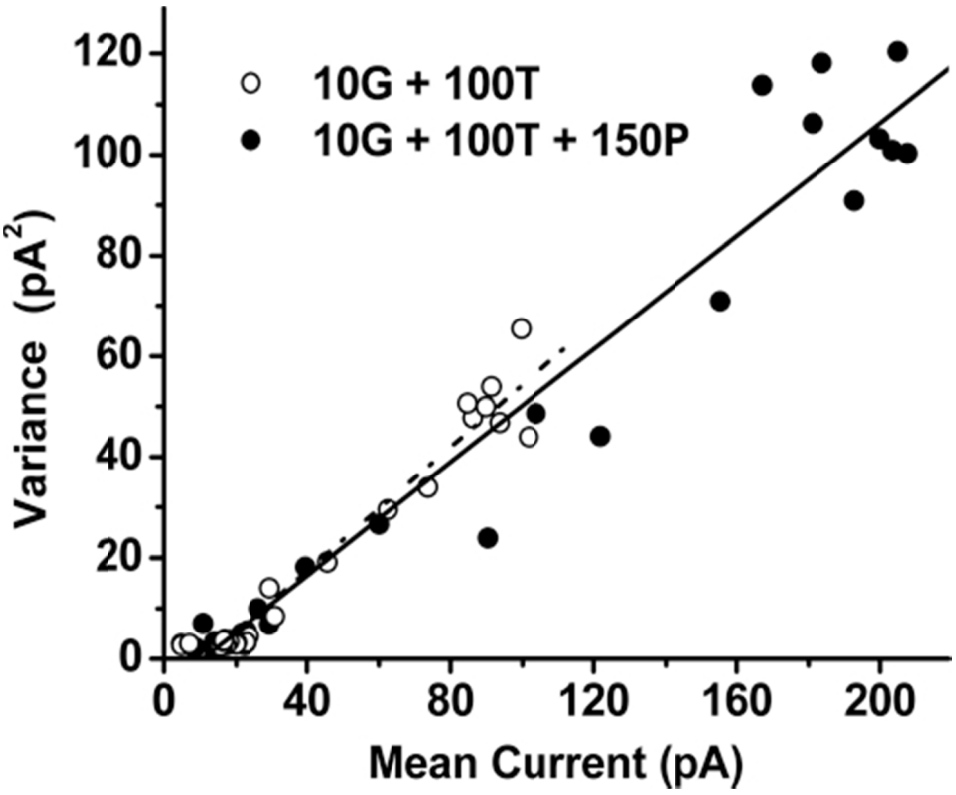

Fig. 4.1.4: Comparative noise analysis of responses to (10G + 100T) (*open circles*) *vs.* (10G + 100T + 150P) (*filled circles*). Representative data obtained from a single cell; data shown by a given symbol type represent results obtained from analysis of a single waveform.

4.1.1.5 Effect of repeated applications

The effects of propofol typically were not fully expressed on an initial brief exposure to propofol. Rather, repeated exposure of the cell to propofol led to progressive changes in the shape of the elicited current response. Fig. 4.1.5 describes these progressive changes in relation to the concentration of applied propofol. Shown are results obtained in a single representative experiment when a mixture containing varying concentration of propofol was repeatedly applied at intervals of ~15–25 seconds (A–E). At low concentrations of propofol (15 and 50 μM; A-B), initial co-application of the propofol (red trace) produced relatively little change from the nominal response to (10G + 100T) (black trace), but a large increase in peak amplitude (i.e., a response enhancement) developed with repeated presentation of the mixture (blue and purple traces, sequentially). Accompanying this change was an acceleration of the response's rising phase. By contrast, at the higher concentrations (500 and 1500 μM; D-E), the potentiating effect of propofol was essentially fully exhibited on the first presentation of propofol (red trace). Here, repeated presentations led to a progressive decrease in peak

amplitude, and to an increasingly pronounced sag from peak as well as a substantial rebound upon termination of the applied mixture (blue and purple traces). Responses obtained with an intermediate propofol concentration (150 μM; C) showed a pattern intermediate between those exhibited at the lower and higher propofol concentrations. The data shown in Fig. 4.1.5 were collected consecutively; that is, the groups of repeated exposures to single concentrations of propofol were conducted in sequential (A-to-E) order. The (10G + 100T) response was collected as a nominal response immediately before each group of propofol application. The observed similarity of these (10G + 100T) responses indicated that there was little, if any, lingering potentiating effect of propofol after ~15–25 seconds of continuous Ringer perfusion between tests.

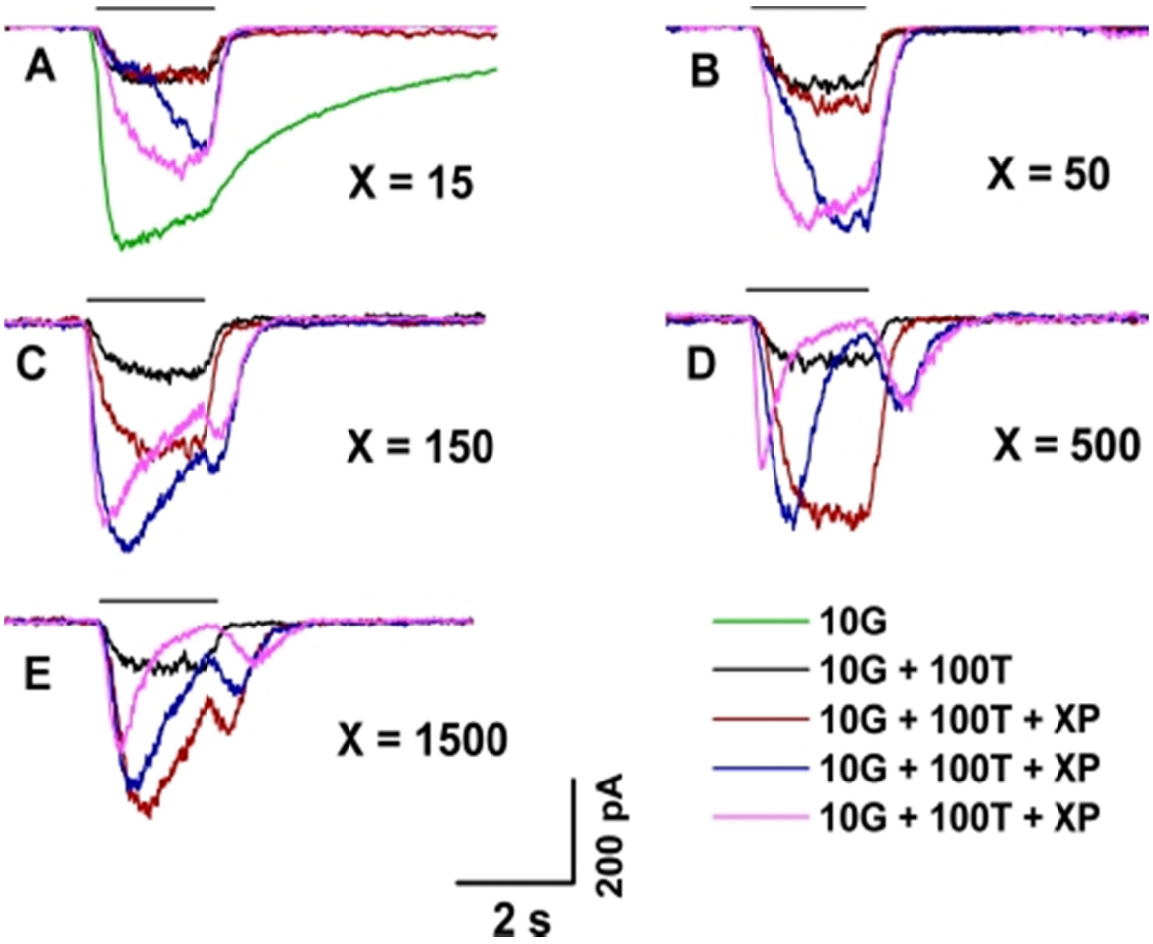

Fig. 4.1.5: Effect of repeated applications (2 seconds in duration) of propofol-containing test mixtures. Responses obtained with the use of 15, 50, 150, 500, and 1500 μM propofol (A–E, respectively). Waveforms within each panel show the nominal response to (10 μM GABA + 100 μM TPMPA) (*black*) and responses to a subsequent series of test applications in which a fixed concentration of propofol supplemented the (10 μM GABA + 100 μM TPMPA) solution (*red*, *blue*, *purple*). All data were obtained from the same cell (temporal order A–E), and waveforms within each panel were obtained in the top-to-bottom temporal order shown in the key. The response of the cell to 10 μM GABA alone is shown in (A) (*green*). Intervals between successive test applications (periods of perfusion with unsupplemented Ringer) were ~15–25 seconds.

Fig. 4.1.6 illustrates combined results obtained from four cells in experiments described in Fig. 4.1.5. Fig. 4.1.6A shows the progressive changes in the peak amplitude enhancement factor with repeated exposures to propofol of varying concentrations. At lower propofol concentrations (15–50 μM), the enhancement factor produced by the third application significantly exceeded that produced by the first application (P = 0.04 for 15 μM; P = 0.02 for 50 μM). By contrast, at higher concentrations (150–1500 μM), the enhancement factor produced by the successive applications did not significantly differ from that produced by the first application (P = 0.10 for 150 and 1500 μM; P = 0.06 for 500 μM).

Fig. 4.1.6B shows results obtained for the amplitude of the response at conclusion of the application (I_{off}), compared with the response's peak amplitude (I_{peak}). At low concentrations of propofol (15–50 μM), the peak of the response occurred at or shortly before termination of the application, and the ratio I_{off}/I_{peak} was near unity for all three applications. At 150 and 500 μM, little sag was exhibited in the initial response (I_{off}/I_{peak} near unity), but its progressive development was evident in the second and third

responses. At 1500 μM, considerable sag was present even in the first recording. The relatively large SD evident under several conditions at intermediate and high propofol concentrations indicates variation among cells in the relative extent of the sag.

Further, Fig. 4.1.6C describes the rebound component of the response seen at the intermediate and high propofol concentrations. To quantify the size of this rebound component, both the absolute peak amplitude of the response (I_{peak}) and the peak of the rebound component ($I_{rebound}$) were referenced to I_{off}, and the value of the ratio ($I_{rebound}$− I_{off})/(I_{peak}− I_{off}) was determined. At each of the three propofol concentrations for which a substantial rebound was observed, the average value of ($I_{rebound}$ − I_{off})/(I_{peak} − I_{off}) produced by the second application exceeded that produced by the first application, and at 1500 μM propofol this difference was significant (P = 0.02). At all concentrations except 1500 μM propofol, the response to the first application lacked a rebound component. In addition, the large standard deviations observed with 150 μM and 500 μM propofol indicated variation in the concentration threshold for appearance of the

rebound component. This rebound component was evident in all cells tested at 1500 μM propofol; thus, the SD at this highest concentration was relatively small.

Figs. 4.1.6D-E show determinations of the deactivation time constant of the response to the test applications described in the preceding paragraphs. Responses to the first, second, and third applications obtained under a given experimental condition were analyzed by fitting a simple exponential decay function to the recovery phase of the response (i.e., the waveform exhibited during wash-out of the test mixture). The deactivation time constants determined with 15 to 50 μM propofol did not exhibit a significant change with repeated propofol applications (P = 0.60 for 15 μM; P = 0.15 for 50 μM). Aggregate average values of these time constants (i.e., average combined results for the first, second, and third applications) obtained with 15 and 50 μM propofol applications were 184 ± 39 ms and 205 ± 51 ms, respectively. These values did not differ significantly from one another (P = 0.32; n = 12), nor did they differ significantly from the time constant determined in the absence of propofol (181 ± 31 ms; P = 0.44 for 15 μM; P = 0.10 for 50 μM; Figs. 4.1.6E). At higher propofol concentrations, there was a

progressive increase in the average time constant associated with the first application, and, at a given propofol concentration, repeated application of the propofol-containing mixture produced a further increase in the average time constant. Aggregate values of the time constants determined at 500 and 1500 μM propofol differed significantly from those determined in the absence of propofol ($P \leq 10^{-5}$); there was no significant difference between the aggregate value obtained at 150 μM and that obtained at 50 μM propofol ($P = 0.07$).

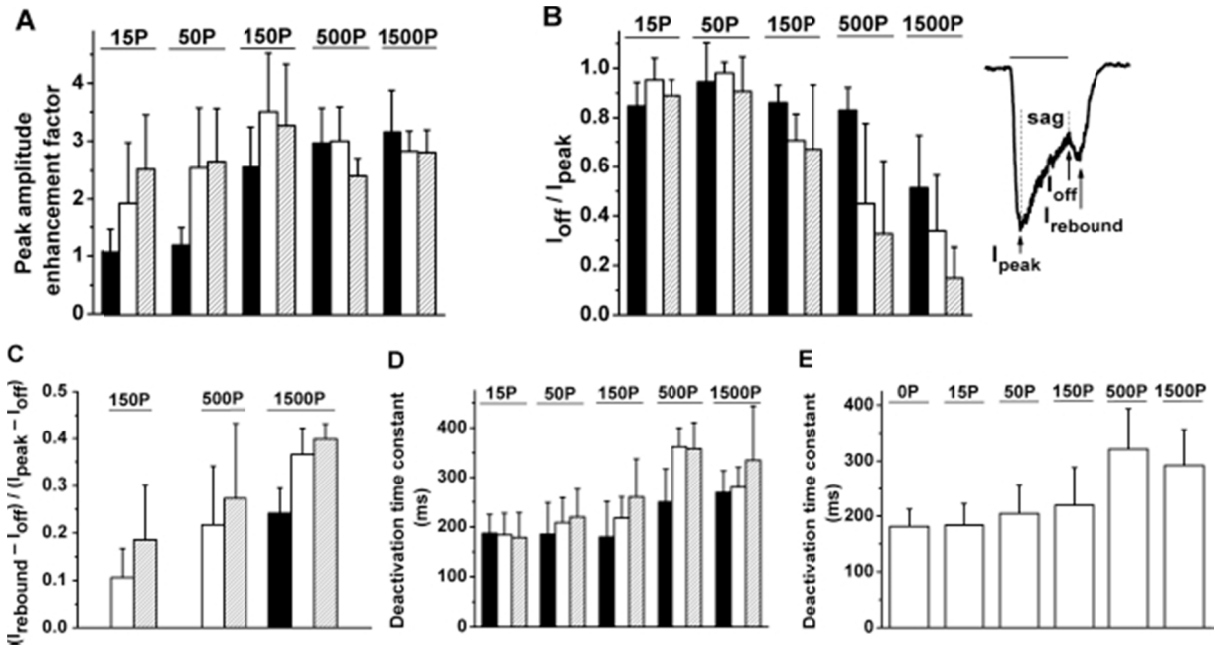

Fig. 4.1.6: Analysis of responses obtained in experiments described in Fig. 4.1.5. Each group of three histograms in (A–D) indicates the mean ± SD of a given response property determined, respectively, for the first (*filled bar*), second (*open bar*), and third (*striped bar*) application. Horizontal bar above each group of histograms: propofol concentration in μM. Data obtained from four to five cells at a given propofol concentration. (A) Propofol-induced enhancement factor (ratio of peak amplitudes). (B) I_{off}/I_{peak}, a measure of response sag. (C) $(I_{rebound} - I_{off})/(I_{peak} - I_{off})$, a measure of response rebound. I_{peak}, I_{off}, and $I_{rebound}$ for a representative single waveform (response to (10G + 100T + 150P)) are illustrated at the right in (B). (D) Deactivation time constant after test mixture application. (E) Combined results for deactivation time constant obtained from the first, second, and third applications at a given propofol concentration. Histogram 0P: data obtained with omission of propofol (i.e., responses to (10G + 100T)).

The experiments described above used 10 μM GABA (in combination with 100 μM TPMPA), the response to which was much smaller than the saturating GABA response. We used a protocol similar to that depicted in Fig.4.1.5 to determine whether propofol potentiation is exhibited at 30 μM GABA and whether the effects of propofol on the shape of the response at 30 μM GABA resemble those observed at 10 μM. Here the concentration of 30 μM was chosen based on its approximate correspondence with the EC_{50} for GABA at $\alpha_1\beta_2\gamma_2$ $GABA_A$ receptors. Under this condition, the potentiating effect of 150 μM propofol on the response to (30G + 200T) was smaller than that exhibited at 10 μM GABA, and the first of three serial responses exhibited the greatest amplitude (average enhancement factor, 1.3 ± 0.1; n = 3). The responses to later applications showed, on average, a progressively more extensive sag and a relatively more pronounced rebound current. Notably, the average I_{off}/I_{peak} obtained for the first, second, and third applications, respectively, was 0.72, 0.60, and 0.56, which were generally smaller than that obtained with 10 μM GABA, therefore suggesting a more extensive sag associated with responses that involve 30 μM GABA presentation.

4.1.1.6 Effect of propofol background perfusion

To investigate the nature of different components in the waveform of (G + T + P) response and its progressive changes described by Figs. 4.1.5 and 4.1.6, we conducted experiments in which applications of GABA and TPMPA were superimposed on a continuous background perfusion with propofol-containing medium. We also conducted a complementary type of experiment in which the background Ringer perfusion was substituted by medium containing (10G + 100T). Fig.4.1.7 shows results obtained in these experiments with altered perfusing medium.

A and B show two representative results of the same type of experiment involving determinations of the response to (10G + 100T + 150P) without *vs.* with the background perfusion of propofol. In each experiment, the response obtained with Ringer perfusion shown by the black trace was the “stabilized” response of the cell to (10G + 100T + 150P); responses to this test mixture were obtained in later runs among a series of (G + T + P) applications and showed no substantial difference from the preceding run (i.e., ≤10% change in peak amplitude between consecutive runs). In the

experiments depicted in A and B, the enhancement exerted by 150P did not differ substantially (benchmark (10G + 100T) response not illustrated). However, the nominal (10G + 100T + 150P) responses obtained in the two experiments (black traces) exhibited differences in both the rate of response onset and the relative extents of sag and rebound current: the nominal response of A exhibited a relatively fast onset and the presence of a small rebound, whereas that of B showed a relatively slow onset and no rebound current. This difference in the behavior of propofol is consistent with the finding, in the experiments depicted in Fig. 4.1.6B-C, of substantial variation (i.e., relatively large SD) in the extents of response sag and rebound component among cells with ≥150 μM propofol, and it may reflect variability among cells in the concentration of propofol required for its fully developed action. Red traces in A and B show the response to (100G + 100T + 150P) obtained with propofol perfusion. In A, the red trace closely resembled the nominal response obtained during the period of (G + T + P) application but lacked a rebound component and exhibited a prolonged deactivation phase at the conclusion of the test mixture application. In B, by comparison with the

nominal response, the red trace exhibited a faster rise to peak, a more pronounced sag as well as a prolonged deactivation phase.

Fig.4.1.7C compares the stabilized response to (10G + 100T + 150P) (black trace) with the response obtained in the perfusing medium of (10G + 100T) (blue trace). Here, the latter response departed from a level that itself reflected activation by the perfusing (10G + 100T) (compare baselines of the two illustrated traces). By comparison with the nominal response, that obtained with (G + T) perfusion showed a similar onset rate and peak amplitude (including the baseline difference), but an enhanced rebound current.

These results suggested a combination of two mechanisms underlying the development of the response sag. The first of these mechanisms is a desensitization effect of $GABA_A$Rs, as revealed by comparison of the experiments involving 10 and 30 μM GABA, respectively, in the presence of identical concentration of propofol. The results showed that higher GABA concentration yielded a more pronounced sag, consistent with the dependence of receptor desensitization on GABA concentration. The

second suggested mechanism is the blocking effect of propofol, as indicated by properties of the response rebound. On a simple hypothesis, the basis of this rebound is the result of rapid dissociation of a blocker (propofol) from GABA-bound receptors that are already in the active state. This hypothesis readily explains the experimental results obtained with propofol or (G + T) background perfusion, where in the former case, the rebound was eliminated by the maintained presence of propofol during response deactivation and in the latter case, maintained activation of $GABA_A$ receptors by a stable GABA concentration enhanced the rebound component. Previous studies have reported an inhibitory effect of high concentrations of propofol at $GABA_A$ receptors [77, 79] and have shown that etomidate, a compound whose binding site overlaps with (albeit is distinct from) the propofol binding site [102], can at high concentration exhibit channel-blocking activity [91, 103, 104].

Fig.4.1.7D analyzes the effect of background perfusion with propofol or (G + T) on the deactivation time constant of the response to (10G + 100T + 150P). As in the experiments depicted in Fig.4.1.6D, exponential time constants were determined for the

recovery phase of the (G + T + P) response. The deactivation time constant of the (G + T + P) response obtained on a continuous propofol perfusion, which represents the washout rate of GABA in the presence of propofol, is significantly slower than the washout rate of GABA in Ringer perfusion, as illustrated by the deactivation time constant of (G + T) response in Fig 4.1.6D (P= 0.00003). Similarly, the deactivation time constant obtained with (G + T) perfusion roughly represents the washout rate of propofol in the presence of GABA. Therefore the deactivation kinetics of the (G + T + P) response in Ringer perfusion reflects the combined effects of the two washout processes. The slowed washout of GABA in the propofol perfusion is consistent with a propofol-dependent stabilization of the GABA-bound state, an effect noted by Bai *et al.* in their studies of propofol on hippocampal neurons [97].

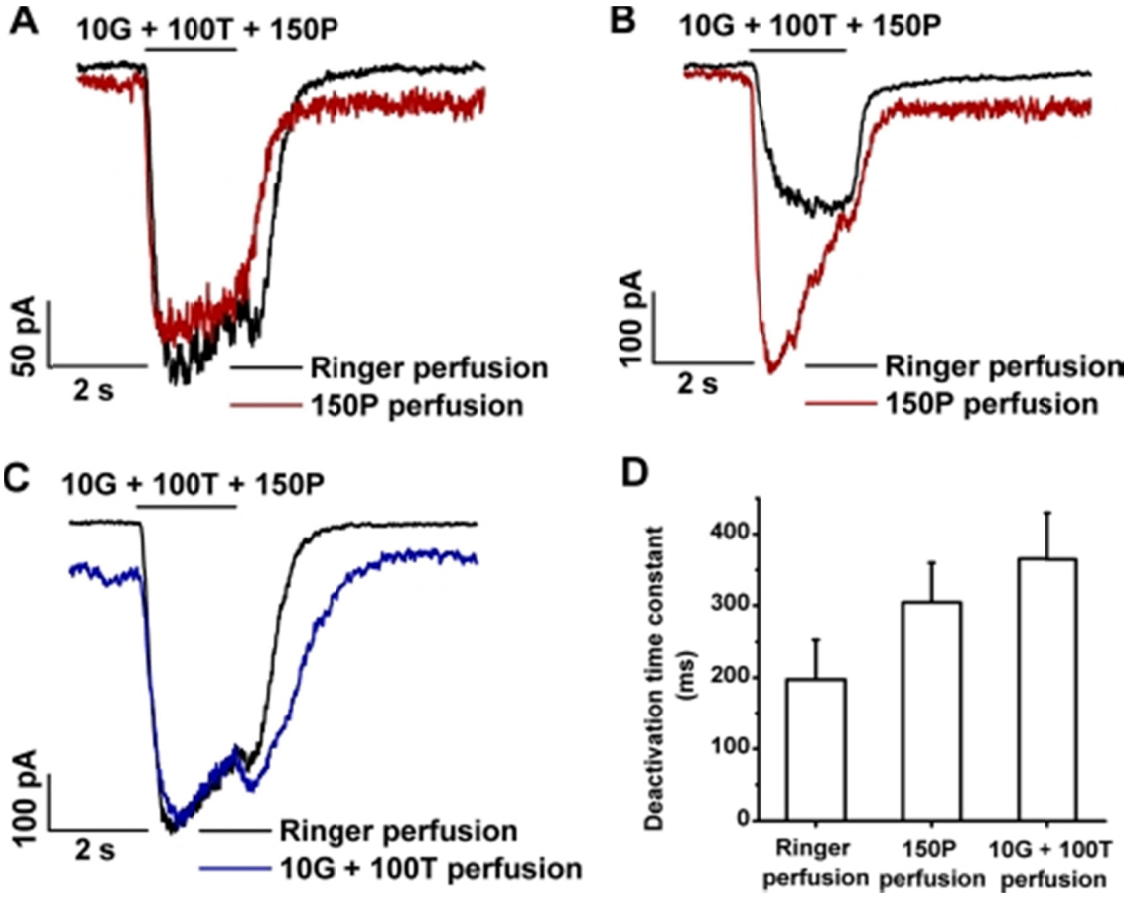

Fig. 4.1.7: Dependence of the response to (GABA + TPMPA + propofol) on perfusion with propofol or (GABA + TPMPA). (A) Responses obtained in a single representative experiment before (black) and during (red) the perfusion with medium that contained 150 µM propofol. (B) Responses obtained from another cell before (black) and during (red) propofol perfusion. In the experiments of (A) and (B), the switch to propofol-containing medium occurred at the beginning of the recording of the red trace. (C) Responses obtained from a cell before (black) and during (blue) perfusion with 10 µM GABA plus 100 µM TPMPA (10G + 100T). The switch to (10G + 100T)-containing medium occurred at the beginning of the recording of the blue trace. (D) Deactivation time constants determined for perfusion with Ringer, propofol, and (G + T). Histograms show the mean ± SD for data obtained from five cells.

4.1.1.7 Effect of including propofol in the patch pipette solution

For the progressive development of propofol activity, we considered the possibility that the effect of propofol depends on an action of the compound at or near the intracellular side of the cell membrane. For example, the gradual development of the changes seen with repeated applications of propofol might reflect the time required for diffusion of the lipophilic, externally applied propofol across the membrane. To test this possibility, we asked whether the inclusion of propofol in the solution contained within the patch pipette, a condition expected to facilitate the passage of propofol to the interior of the cell, alters the response to either the nominal (10G + 100T) test solution or to a propofol-supplemented test solution (10G + 100T + 150 P). Fig.4.1.8 shows results obtained in a single representative experiment that used supplementation of the standard pipette solution (see 3.2.1) with 200μM propofol. As illustrated by the black trace recorded immediately after breakage of the patch membrane and by the purple trace recorded ~1.5 minutes after membrane breakage, there was no substantial change in the (10G + 100T) response. (These traces are comparable to those recorded

without propofol in the pipette, for example, the black traces in Fig. 4.1.5) Furthermore, successive applications of (10G + 100T + 150 P) produced changes in response size and kinetics similar to those observed in the Fig. 4.1.5 experiment (compare the red, blue, and green traces in Fig. 4.1.8 with, respectively, the red, blue, and purple traces in Fig. 4.1.5C). In addition, as determined in the Figure 4.1.8 experiment and in four others of identical design, the enhancement factor resulting from application of the (10G + 100T + 150P) test solution was 5.6 ± 2.9, which did not differ significantly from the factor determined with use of the standard pipette solution (P = 0.92). Therefore, inclusion of propofol in the pipette solution does not have a significant influence on the activity of externally applied GABA and propofol.

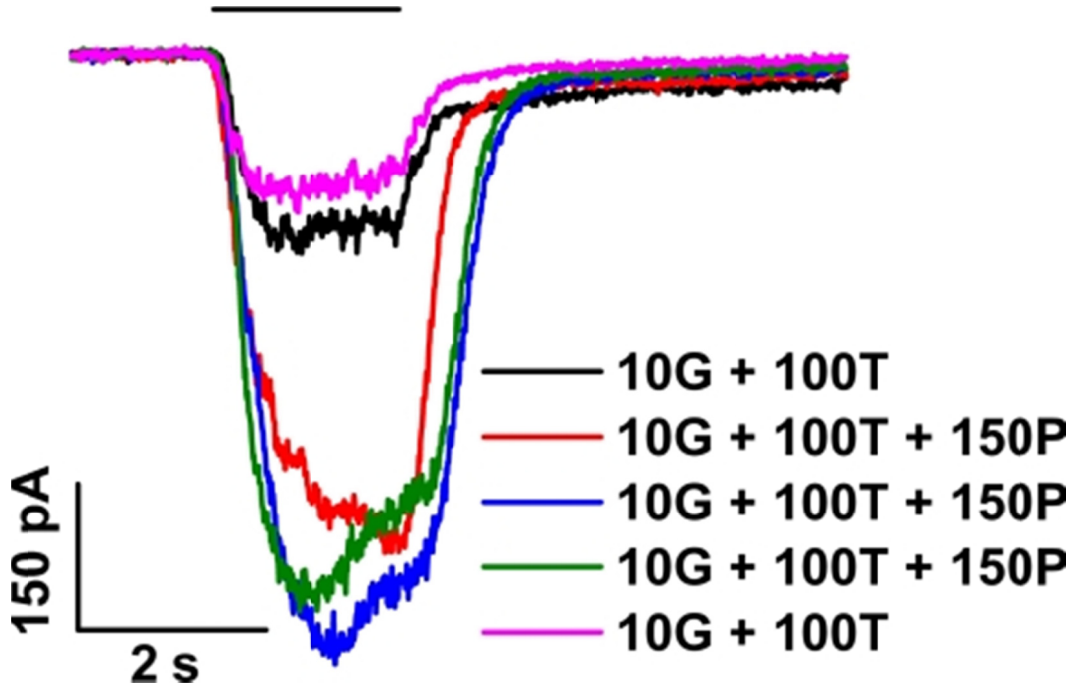

Fig. 4.1.8: Responses obtained with the inclusion of propofol in the solution filling the patch pipette. Data obtained from a single cell. Test applications consisted of (10G + 100T) (black, purple) and (10G + 100T + 150P) (red, blue and green).

4.1.2 Activity on recombinant $\alpha_1\beta_2\gamma_2$ $GABA_A$ receptors

We examined both potentiating and activating/agonist actions of propofol on oocytes expressing recombinant wildtype $\alpha_1\beta_2\gamma_2$ $GABA_A$Rs. To test for a potentiating effect, we co-applied propofol of varying concentrations (1-300 μM) with 3 μM GABA, a

concentration far below saturation of the GABA dose response function. Responses obtained were normalized to the amplitude of the near-saturating response elicited by 100 μM GABA (r_{100G}). As presented in Fig. 4.1.9 (black filled squares), propofol showed a concentration-dependent enhancement effect. At 300 μM, propofol exhibited a ~17-fold enhancement on the 3 μM GABA response, i.e., increased the response from ~5% to ~85% of r_{100G}. The direct activating effect was examined in the absence of GABA co-application. Fig. 4.1.9 (red open circles) shows that substantial agonist activity of propofol was exhibited at higher concentrations, and that the maximal activity approximated to 40% of r_{100G}. The observations are presented in Fig 4.1.9.

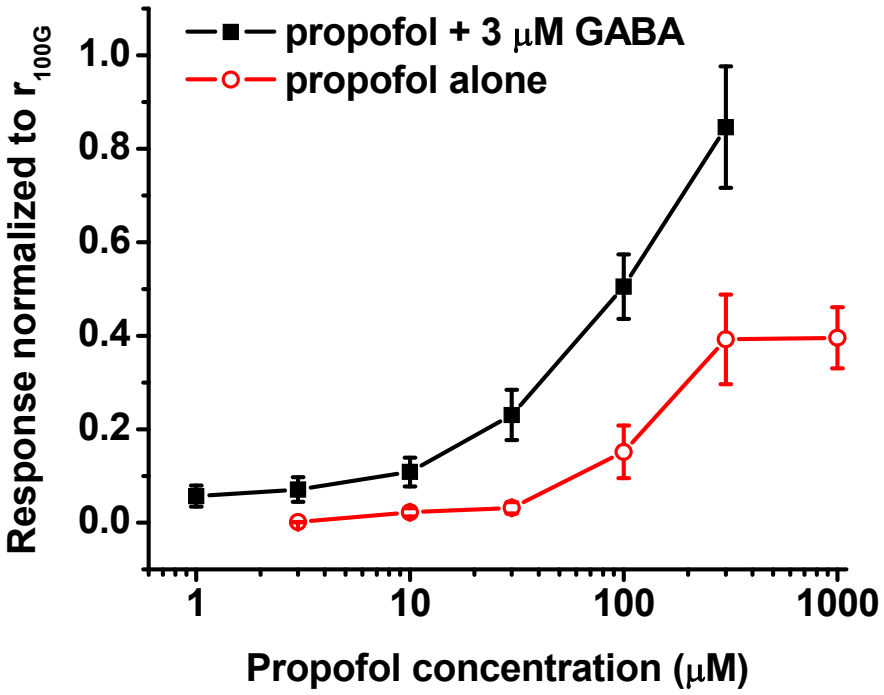

Fig. 4.1.9: Activity of propofol on oocyte expressing wildtype $\alpha_1\beta_2\gamma_2$ $GABA_A$Rs. Aggregate concentration-response data (mean ± SD) obtained in experiments that involved treatment with propofol in the presence (black filled squares; 7 oocytes) and absence (red open circles; 6 ootyes) of 3 μM GABA.

In summary, the findings presented in this section demonstrate a marked and selective potentiation by propofol on $GABA_A$ receptors of retinal bipolar cells, thus encouraging the use of propofol as the prototype effector of the photo-regulated neural modulator. In addition, the results obtained with propofol employed on oocytes expressing $\alpha_1\beta_2\gamma_2$ $GABA_ARs$ were treated as a standard for later comparison with the activity of newly synthesized propofol derivatives.

4.2 Structural modification of propofol

In order to achieve photo-regulated modulation of native $GABA_ARs$ in retina, a series of structurally modified propofol derivatives was progressively synthesized by our chemistry colleagues. In the previous sections, we have shown that propofol exhibits similar potentiating effects on both oocyte-expressed and native retinal $GABA_ARs$. Due to the technical ease and high throughput of the oocyte expression system, we screened the compounds by testing their potentiating ability on the GABA-elicited response of recombinant α1β2γ2 $GABA_ARs$. Unless otherwise indicated, the

potentiating ability is quantified by normalizing the test agent enhanced 3 μM GABA response (benchmark concentration, ~EC_2-EC_6) to the near-saturating response elicited by 100 μM GABA. Among the tested compounds, a propofol derivative termed MPC088 exhibited the most potent activity that is highly sensitive to UV and subsequent visible light illumination. Other compounds, though showing less prominent activity, are of significant value. They guided the modification direction that led to the synthesis of MPC088. In addition, their properties provide valuable structure-activity comparisons with those of MPC088. In this section, some of these compounds are discussed in chronological order of their preparation and investigation, to present the rationale behind the most important modification steps. The following account begins with the initially tested analogs of propofol from the basic propofol, explains the rationale leading to MPC088, and includes development of MPC100, a maleimide-containing tetherable form of MPC088.

4.2.1 *p*-(phenylazo)propofol derivatives

Establishing light-sensitivity for propofol analog involves incorporating the photo-isomerizable azobenzene group into the modified propofol structure. Ideally, the new compound should exhibit a significant neuromodulating effect that can be regulated by light, which triggers the inter-conversion of the *trans* and *cis* isoforms at the corresponding illumination wavelengths. The conformational change of azo group upon photo-isomerization is largely reflected by the shortening or stretching of the distance between the two azobenzene ends. In order to establish a high correlation between the activity and conformational state of the compound, it is assumed that for the N=N (azo) group, the rotation axis at the occurrence of photo-isomerization must reside close enough to the propofol moiety. Under this assumption, if the azo group were located far from the propofol terminal, owing to the enhanced flexibility of the lengthened linker chain between ligand and the azo group, the conformational change of azo moiety would be less likely to significantly affect the binding of the compound at the ligand binding site. The chemical structure of propofol contains phenol, and an azobenzene

molecule is comprised of two phenyl rings joined by an N=N double bond. It naturally occurred to us that utilizing the phenol ring of propofol as one of azobenzene phenyl rings could minimize the distance between the propofol moiety and the N=N bond. Therefore a series of arylazopropofols were synthesized, including *p*-(phenylazo)propofol unsubstituted and substituted with carboxylate and/or sulfonate group at meta- or para- position of the lower phenyl ring.

4.2.1.1 Unsubstituted *p*-(phenylazo)propofol

In this compound, the phenol ring of propofol substitutes for the upper ring of the azobenzene moiety and no substitution groups were attached to the lower ring (Fig. 4.2.1). The activity of the compound was examined at three concentrations: 15 μM, 50 μM and 150 μM. At all three concentrations, the compound presented no significant agonist activity, whereas a potentiating activity comparable to that of propofol was exhibited (Fig 4.2.2). This result encouraged the synthesis of similar compounds but with substitution at the lower ring that could be attached with linker groups for ultimate

tethering onto the receptors. Our chemistry colleagues synthesized two groups of phenylazo propofol, carrying the polar group in the meta- or para- position of the non-propofol phenyl ring.

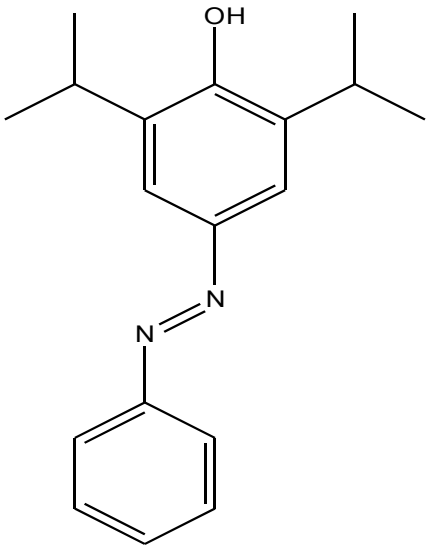

Fig. 4.2.1: Chemical structure of unsubstituted *p*-(phenylazo)propofol.

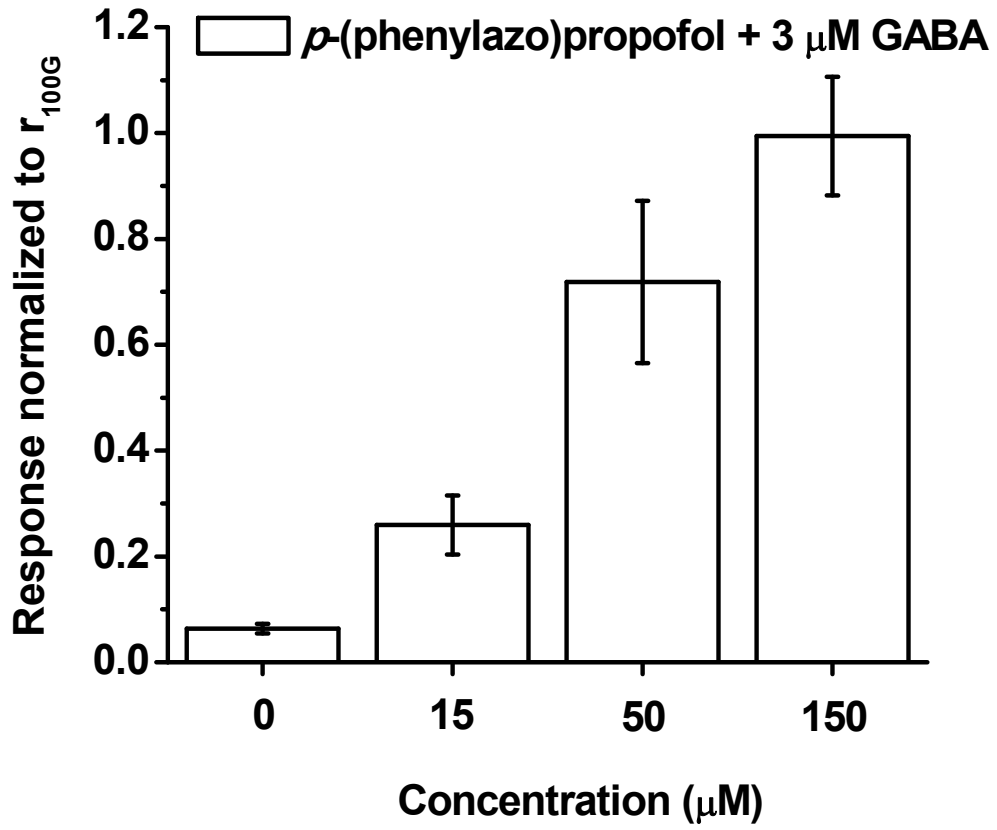

Fig. 4.2.2: Potentiating effect of *p*-(phenylazo)propofol. Columns left to right: normalized response to 3 μM GABA co-applied with 0, 15, 50, 150 μM of *p*-(phenylazo)propofol. Response amplitudes normalized to that elicited by 100 μM GABA (r_{100G}). Aggregate data obtained from 4 oocytes.

4.2.1.2 *p*-(Sulfonylphenylazo)propofol group

Two compounds fall into this category, one with the side chain of sulfonic acid at meta, the other, para position of the lower phenyl ring (Fig. 4.2.3).

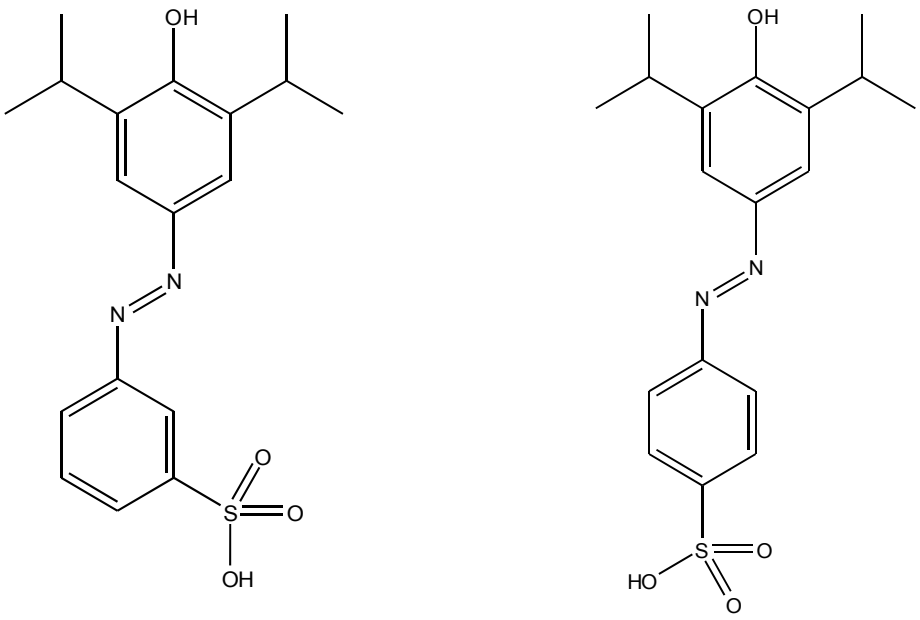

Fig. 4.2.3: Chemical structures of *p*-(*m*- and *p*-sulfonylphenylazo)propofol, respectively (left to right).

By contrast with unsubstituted *p*-(phenylazo)propofol, both meta and para substituted derivatives exhibited only a modest potentiating effect on $GABA_ARs$. The maximum enhancement amounts approximately to 6% of r_{100G} for meta and 4% for para

derivative, whereas for unsubstituted compound, the enhanced response could reach the amplitudes comparable to r_{100G}. At high concentrations, both derivatives exhibited an inhibitory effect, evident as a decline in response amplitude at these concentrations (Fig. 4.2.4A-B). In some cases, an even more extreme example occurred at 500 μM with the meta compound, where the response polarity was reversed, illustrated by the negative part of deviation bar below red dotted line (Fig. 4.2.4A).

As suggested by the following observations, the decreased response at high concentrations of both derivatives was likely due to their non-specific channel blocking effect: 1. Immediately after the resumption of the Ringer perfusion following test agent application, there was a huge upswing of the GABA response, consistent with the fast washout of the blocking compound from the outer part of the ion channel and the slower removal of the potentiating compound, presumably from the propofol binding site that is buried deeper in the cell membrane; 2. Similar response-reducing effects were also exhibited by oocytes expressing ρ_1 $GABA_C$Rs, indicating that the blocking is not specific to $GABA_A$Rs. On the hypothesis of a channel blocking effect, the change in the

response polarity on some oocytes in the presence of 500 µM meta derivative can be interpreted as an inhibition of spontaneous channel opening activity by this blocking agent. Therefore, with only a small response enhancement and a nonspecific blocking effect, neither compound in the *p*-(sulfonylphenylazo)propofol group seemed a promising candidate for further development.

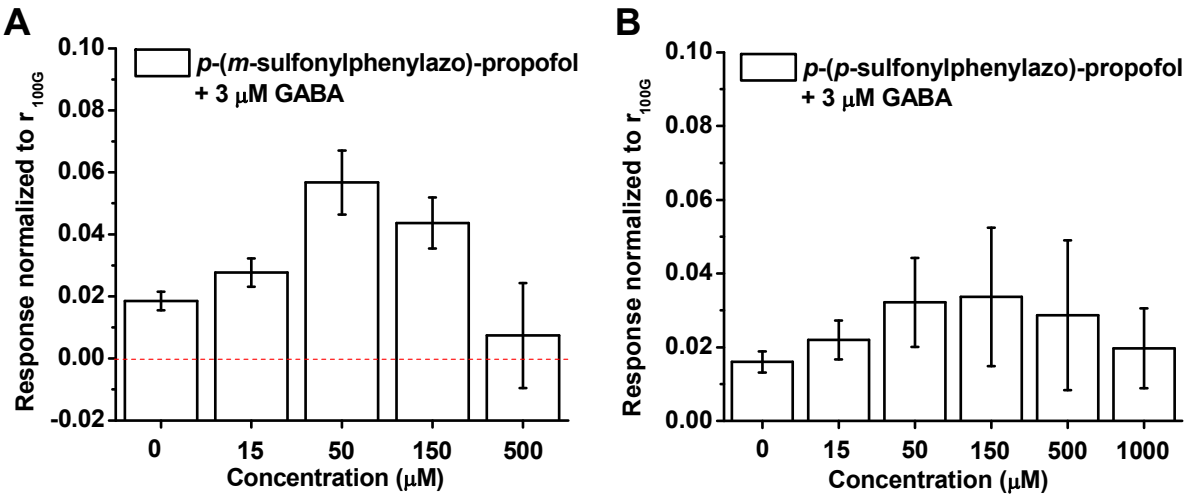

Fig. 4.2.4: Potentiating effect of propofol *p*-(*m*-sulfonylphenylazo)propofol (A) and *p*-(*p*-sulfonylphenylazo)propofol (B). (A) Columns left to right: normalized response to 3 µM GABA co-applied with 0, 15, 50, 150 and 500 µM of *p*-(*m*- sulfonylphenylazo)propofol. Aggregate data obtained from 4 oocytes. (B) Columns left to right: normalized response to 3 µ M GABA co-applied with 0, 15, 50, 150, 500 and 1000 µ M of *p*-(*p*-sulfonylphenylazo)propofol. Aggregate data obtained from 3 oocytes.

4.2.1.3 *p*-(Carboxylphenylazo)propofol group

In this group of two compounds, the substituent is changed from sulfonic to carboxylic acid, yet similarly at meta and para positions of the lower phenyl ring, respectively (Fig. 4.2.5).

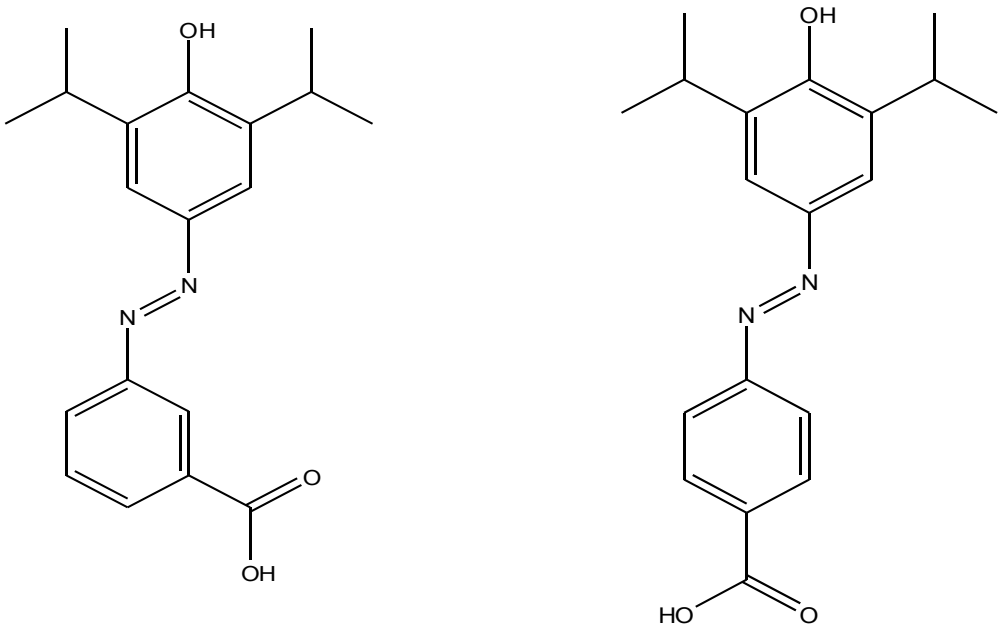

Fig. 4.2.5: Chemical structures of *p*-(*m*- and *p*-carboxylphenylazo)propofol, respectively (left to right).

By comparison with the two sulfonate-substituted compounds discussed in the previous section, *p*-(*m*-carboxylphenylazo)propofol exhibited a slightly more prominent

enhancement effect, where at 150 μM, it produced a ~4 fold enhancement of the 3 μM GABA response from approximately 4% to 16% of r_{100G} (Fig. 4.2.6). However, at this and higher concentrations, the compound elicited a non-saturable response from the recorded oocytes in the absence of GABA. This non-specific activity was observed not only on $GABA_A$-expressing oocytes, but also on oocytes that did not receive RNA injection (i.e., non-expressing oocytes), making this meta-substituted compound an unlikely candidate for further development. A similar yet more severe problem was associated with the para derivative, where the nonspecific activity started to display at lower concentrations and persisted even after the resumption of Ringer perfusion.

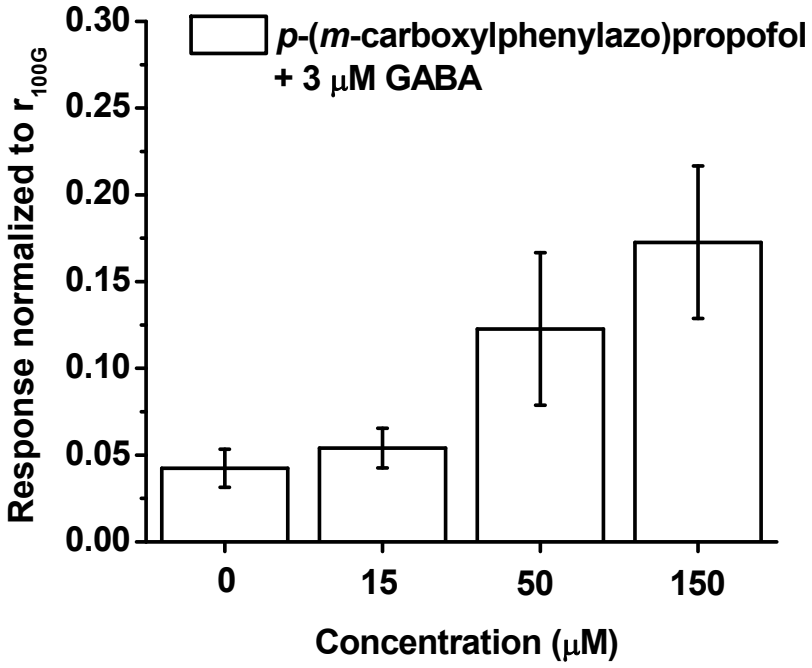

Fig. 4.2.6: Potentiating effect of *p*-(*m*-carboxylphenylazo)propofol. Columns left to right: normalized response to 3 μM GABA co-applied with 0, 15, 50 and 150 and 500 μM of *p*-(*m*-carboxylphenylazo)propofol. Aggregate data obtained from 4 oocytes.

In summary, all four arylazopropofols with substituents at meta or para positions of the non-propofol ring failed to deliver encouraging results at $GABA_ARs$, in terms of potentiating ability and target specificity. These findings suggest that side chain attachment onto the compact structure of diazenyl propofol, even at the most distant para position of the lower phenyl ring may significantly perturb the activity of the

propofol moiety. Therefore, to remedy this problem, we attempted to separate the propofol moiety from a full (biphenyl) azobenzene moiety by inserting a spacer between the two components.

4.2.2 Separation of propofol and azobenzene components

Benzophenone is a structure of two phenyl rings bonded by a carbonyl group (C=O). Here, to separate the propofol and azobenzene components, we tried using benzophenone as the basic building block, where one phenyl ring belongs to propofol moiety and the other acts as the upper azobenzene ring. In the initial study, for ease of synthesis, the first two compounds produced and examined do not possess the lower phenyl ring of azobenzene and they differ at the spacer, one with regular carbonyl group and the other reduced to alcohol (CH-OH). The comparison of these two compounds showed that the carbonyl compound exhibited higher activity and, based on this finding, a third compound containing the complete azobenzene moiety was synthesized and studied.

4.2.2.1 *p*-benzoylpropofol and *p*-(1-hydroxybenzyl)propofol

In this group of two compounds, the propofol moiety is linked, at the para position, to a phenyl ring by a carbonyl group, yielding *p*-benzoylpropofol, or by a reduced (alcohol) group, yielding *p*-(1-hydroxybenzyl)propofol (Fig. 4.2.7).

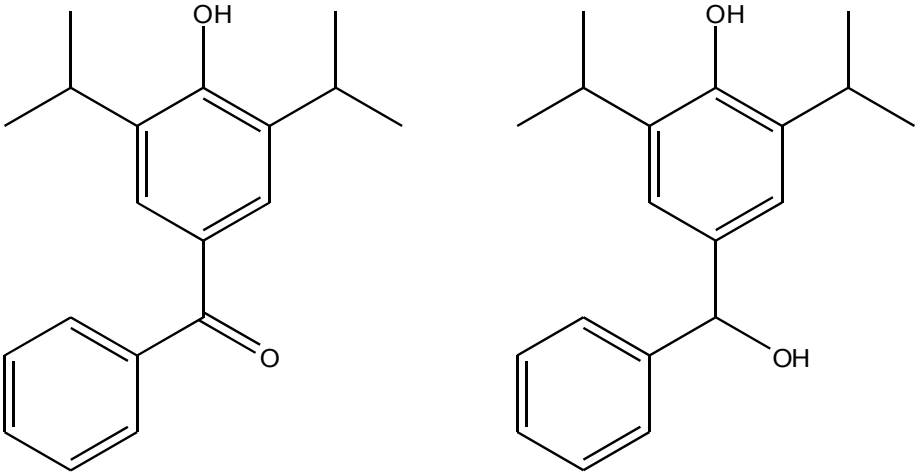

Fig. 4.2.7: Chemical structures of *p*-benzoylpropofol (left) and *p*-(1-hydroxybenzyl)propofol (right).

To determine which linker group better preserves the potentiating activity of propofol, we examined both compounds at the same concentrations (10 and 100 μM). For a paired comparison of the potentiating effect of these two compounds at each concentration, responses normalized to r_{100G} are illustrated histographically (Fig. 4.2.8).

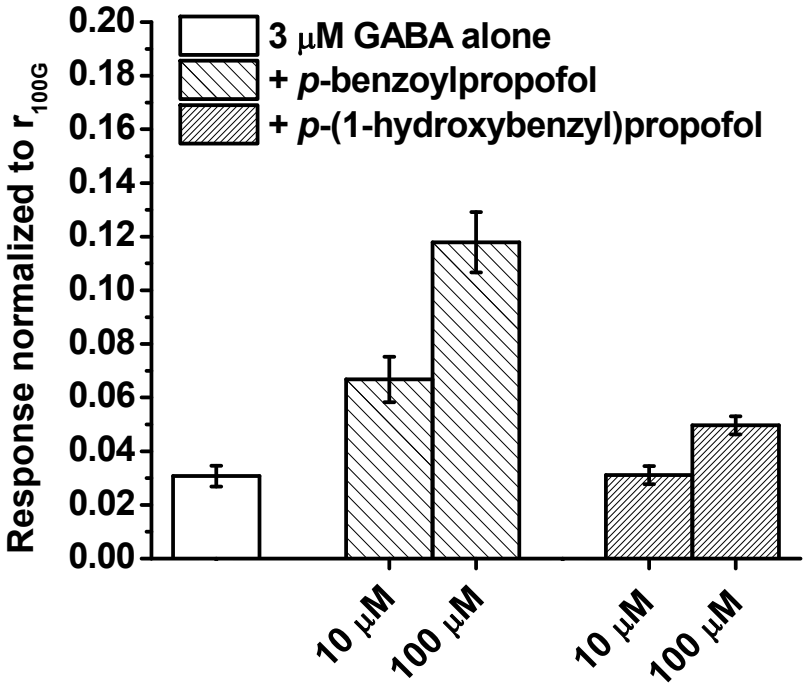

Fig. 4.2.8: Potentiating effects of *p*-benzoylpropofol and *p*-(1-hydroxybenzyl)propofol. Columns left to right: normalized response elicited by 3 μM GABA alone (left open column), co-applied with 10 or 100 μM *p*-benzoylpropofol (middle lightly shaded columns) and co-applied with 10 or 100 μM of *p*-(1-hydroxybenzyl)propofol (right heavily shaded columns). Aggregate data obtained from 3 oocytes.

As shown in Fig. 3.2.8, at both lower and higher test concentrations, the reduced compound exhibited a markedly decreased potentiating effect, indicating that by comparison with the alcohol, the carbonyl group is a more favorable linker structure between propofol and the second phenyl ring for the preservation of the physiological activity of propofol. Encouraged by this observation, we investigated a compound containing a carbonyl linker group but with a complete azobenzene moiety attached to propofol, termed *p*-(*p*-phenylazobenzoyl)propofol.

4.2.2.2 *p*-(*p*-Phenylazobenzoyl)propofol

In this compound, propofol terminal is linked, at the para position, to azobenzene via a carbonyl group (Fig. 4.2.9).

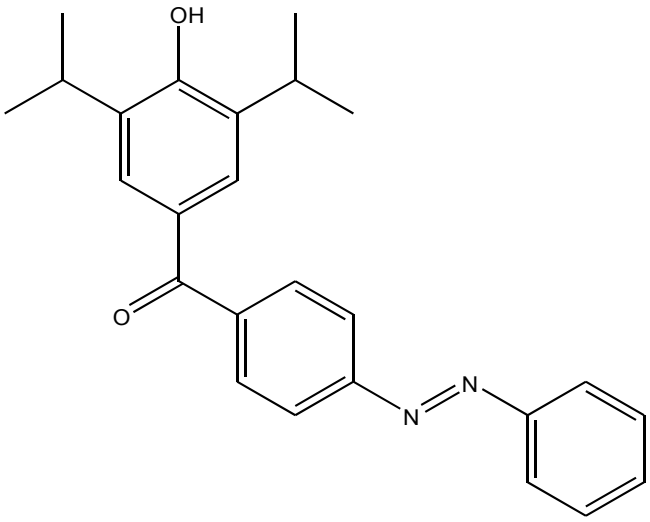

Fig. 4.2.9: Chemical structure of *p*-(*p*-phenylazobenzoyl)propofol.

By comparison with the photo-spectrum of azobenzene, *p*-(*p*-phenylazobenzoyl)propofol exhibited relatively small differences in the spectra obtained before and after UV illumination, suggesting limited photoisomerization at UV exposure. Nevertheless, its electrophysiological activity was still of interest to us, particularly in

determining the effect of the added phenyl ring (compare Figs. 4.2.7 and 4.2.9), where we compared the activity of this compound with that of *p*-benzoylpropofol. For a more direct comparison, the potentiating effect of the new compound was also obtained at 10 and 100 μM. The experimental results showed that at 10 μM, the azobenzene-containing compound exhibited a 5-fold enhancement of the 3 μM GABA elicited response, from ~4% to ~20% of r_{100G}. At 100 μM, this enhancement amounted to a 9-fold increase, to ~36% of r_{100G} (Fig. 4.2.10). This activity of *p*-(*p*-phenylazobenzoyl)propofol considerably exceeded that of *p*-benzoylpropofol at 10 and 100 μM (compare Figs. 4.2.10 and 4.2.9).

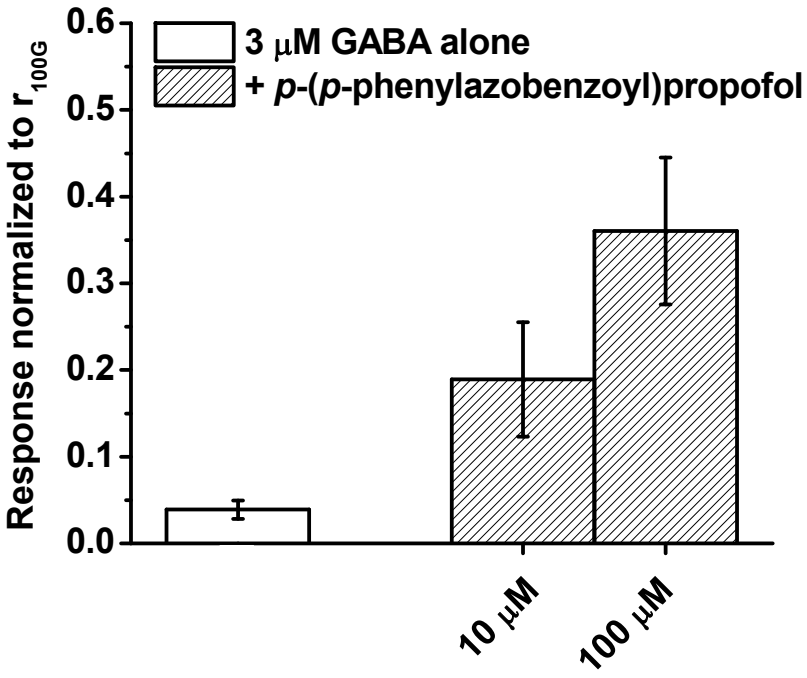

Fig. 4.2.10: Potentiating effect of *p*-(*p*-phenylazobenzoyl)propofol. Columns left to right: normalized response elicited by 3 μM GABA alone (left open column) and co-applied with 10 or 100 μM *p*-(*p*-phenylazobenzoyl)propofol (right densely filled columns). Aggregate data obtained from 5 oocytes.

The more prominent activity of *p*-(*p*-phenylazobenzoyl)propofol suggested that the incorporation of a full azobenzene group may play a favorable role in delivering the potentiating effect of the benzophenone-based propofol derivatives. However, this increased level of activity was still much lower than that of parent propofol, which potentiates the 3 μM GABA response to extents comparable to r_{100G}. To further

optimize the compound structure, we altered the spacer length between propofol and azobenzene groups and produced a series of compounds, including MPC088, the most potent compound developed in the present study.

4.2.3 Manipulation of spacer groups between propofol and azobenzene

Based on the structure of *p*-benzoylpropofol, we first tried to insert a carbon spacer of varying length between propofol and the carbonyl group. For ease of chemical synthesis, the first investigated series of such compounds does not contain the azobenzene component (Fig. 4.2.11). The most potent compounds of this series were selected and thereafter conjugated to azobenzene via different linkage groups between the carbonyl group and the upper (i.e., proximal) ring of azobenzene.

4.2.3.1 Aliphatic carboxylic acid propofol derivatives

The compounds of this series have different aliphatic carboxylic acid groups (acetic, propionic and butyric acid) added at the para position of propofol phenyl ring.

That is, they contain varying numbers of methylene groups (1, 2 and 3, respectively) between propofol and the carboxyl group. The terminating carboxyl serves for future conjugation to amine-terminated azobenzene-containing structures.

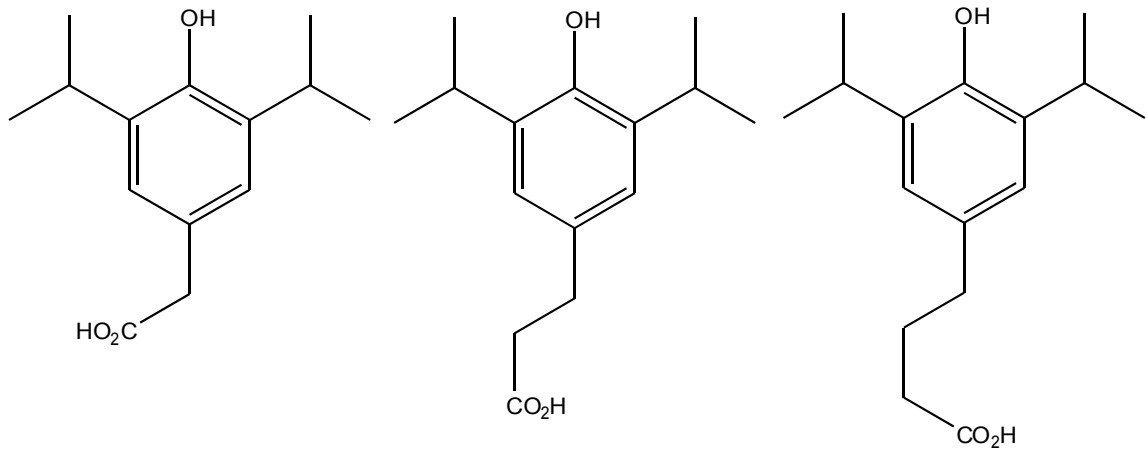

Fig. 4.2.11: Chemical structures of propofol acetic acid (left), propofol propionic acid (middle) and propofol butyric acid (right).

The activity of these carboxylic acid derivatives were tested at 50 and 500 μM, in the presence of 3 μM GABA. As shown in Fig 4.2.12, at 50 μM, all three compounds exhibited a modest enhancement of the GABA response and the 2-fold enhancement by propofol butyric acid was relatively greater than that by the other two compounds.

However, at 500 μM, propofol acetic acid displayed a marked increase in the potentiation of the GABA response, to almost 40% of r_{100G}, whereas the other two exhibited only a small further enhancement of the response. Due to the marked difference in relative potentiation strengths of propofol acetic acid and butyric acid at the lower *vs.* higher concentration, we selected both compounds as candidates for azobenzene conjugation. In this reaction, by forming an amide linkage, the aliphatic carboxylic acid propofol derivatives were coupled to the amine-terminated azobenzene analogs. Two immediate compounds, MPC066 and MPC069, were synthesized under this route. Due to the chemical complexity of these and similar investigated azobenzene-containing structures, they will for simplicity be named using a numerical index rather than a structure-based terminology.

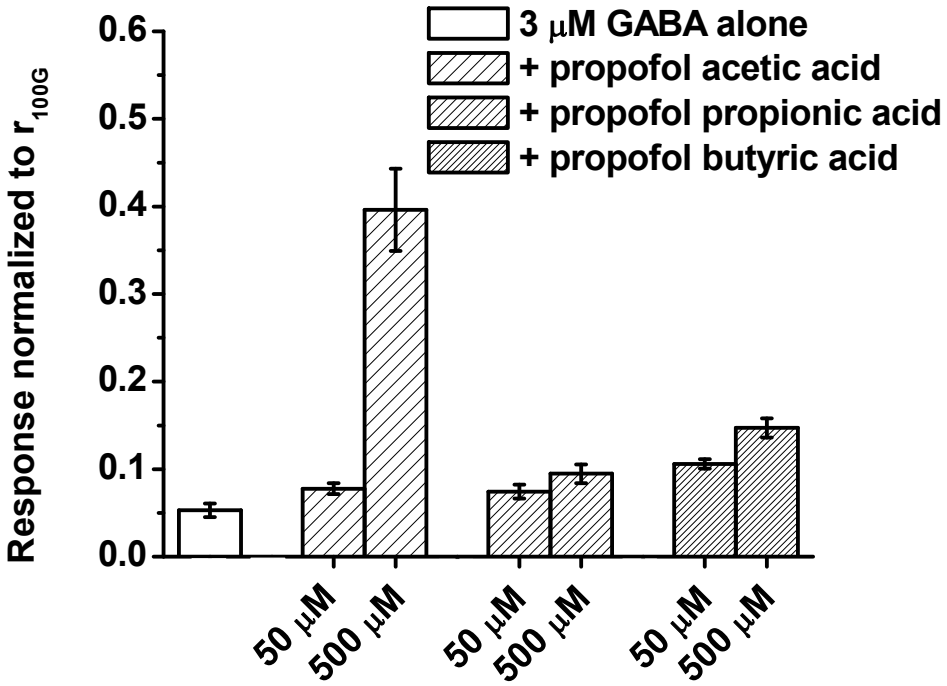

Fig. 4.2.12: Potentiating effect of aliphatic carboxylic acid propofol derivatives. Columns left to right: normalized response elicited by 3 μM GABA alone (open column; left), co-applied with 50 or 500 μM propofol acetic acid (lightly shaded columns; middle left), co-applied with 50 or 500 μM propofol propionic acid (medium shaded columns; middle right) and co-applied with 50 or 500 μM propofol butyric acid (heavily shaded columns; right). Aggregate data obtained from 5 oocytes.

4.2.3.2 Azobenzene-conjugated ligands: MPC066 and MPC069

MPC066 was synthesized on the basis of the structure of propofol butyric acid and MPC069 on propofol acetic acid. As shown in Fig. 4.2.13, both compounds have a methylene group inserted between the amide of the spacer and the proximal ring of

azobenzene, as well as a carboxyl group substituted at the para position of the distal azobenzene ring. This terminating carboxyl group served for future attachment of other functional groups, for example, maleimide-containing tethering groups.

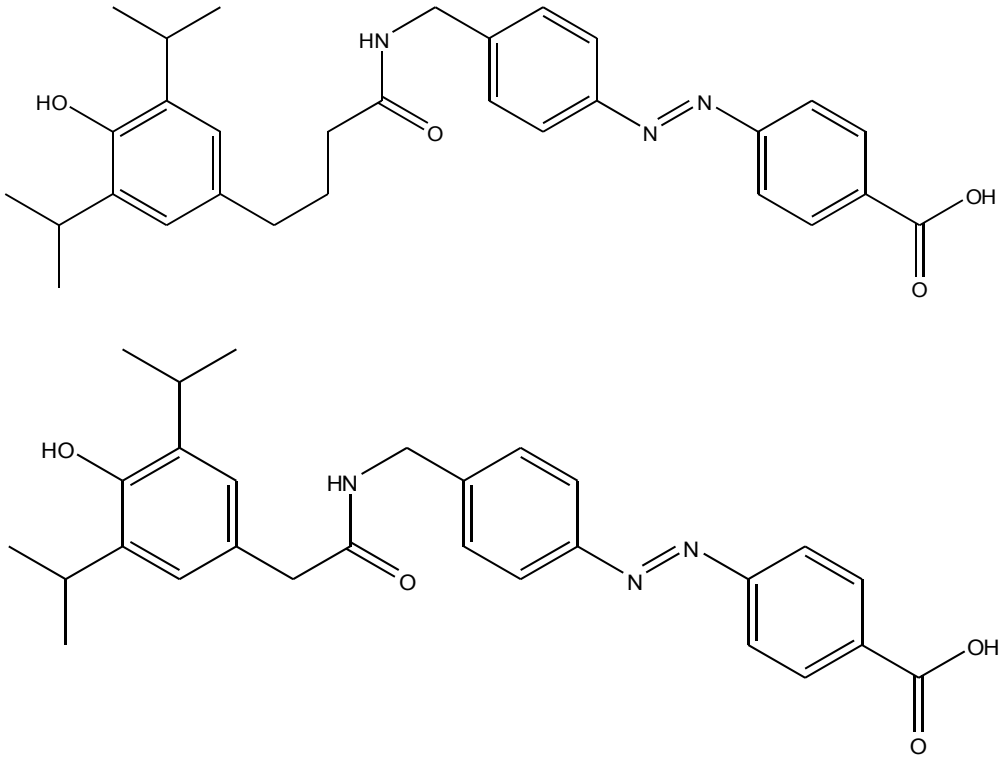

Fig. 4.2.13: Chemical structures of MPC066 (upper) and MPC069 (lower).

The potentiating effect of both compounds was tested at varying concentrations in the presence of 3 μM GABA, as in previous experiments. Fig. 4.2.14 shows the activity of MPC066 and MPC069, each at a lower concentration of 1 μM and a higher concentration, 10 μM for MPC066 and 15 μM for MPC069, respectively. Here, at 1 μM, MPC066 exhibited a nearly 4-fold enhancement of the 3 μM GABA response, from ~5% to ~18% of r_{100G}, and was almost twice as potent as MPC069 (~2 fold enhancement to 10% of r_{100G}). At higher concentrations, 10 μM MPC066 exhibited a ~12 fold enhancement to ~60% of r_{100G}, whereas 15 μM MPC069 presented a ~7 fold enhancement to ~35% of r_{100G}. Thus, by comparison with MPC069, MPC066 exhibited greater potentiation, and therefore the subsequent chemical structures investigated mainly adopted a four-carbon spacer between propofol and the amide group.

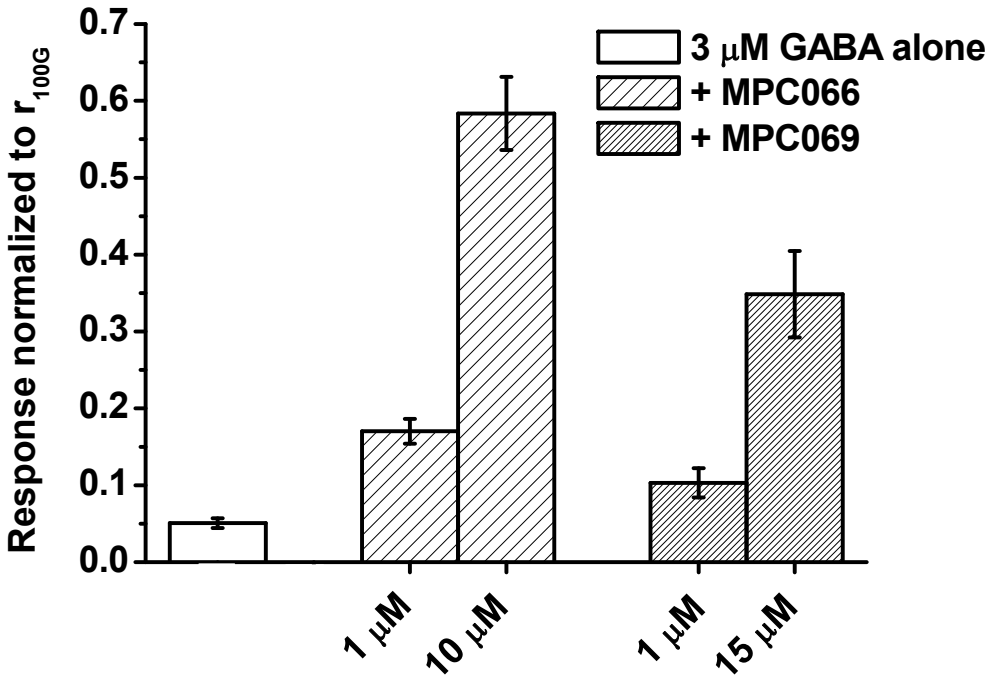

Fig. 4.2.14: Potentiating effect of MPC066 and MPC069. Columns left to right: normalized response elicited by 3 μM GABA alone (open column; left), co-applied with 1 or 10 μM MPC066 (lightly shaded columns; middle) and co-applied with 1 or 15 μM MPC069 (heavily shaded columns; right). Aggregate data obtained from 5 oocytes for the MPC066 results and 3 oocytes for MPC069 results, respectively. Results for GABA alone obtained from the combined 8 oocytes.

The results obtained in spectrophotometric experiments (Fig. 4.2.15) show that, similar to azobenzene, UV illumination decreased the major absorption peak at 338 nm and produced a minor peak at 438 nm for both MPC066 and MPC069. Subsequent white light illumination significantly recovered the major peak, though not

fully to the original level, likely due to the difference in the photostationary state of the compound under room light and white light illumination (similar experiments discussed in detail in 4.3.1). This bi-directional spectral shift, triggered by *cis*-generating UV and *trans*-generating white light, respectively, reflects the photo-isomerization of the azobenzene components of both compounds, and encouraged their electrophysiological testing in the presence of UV illumination.

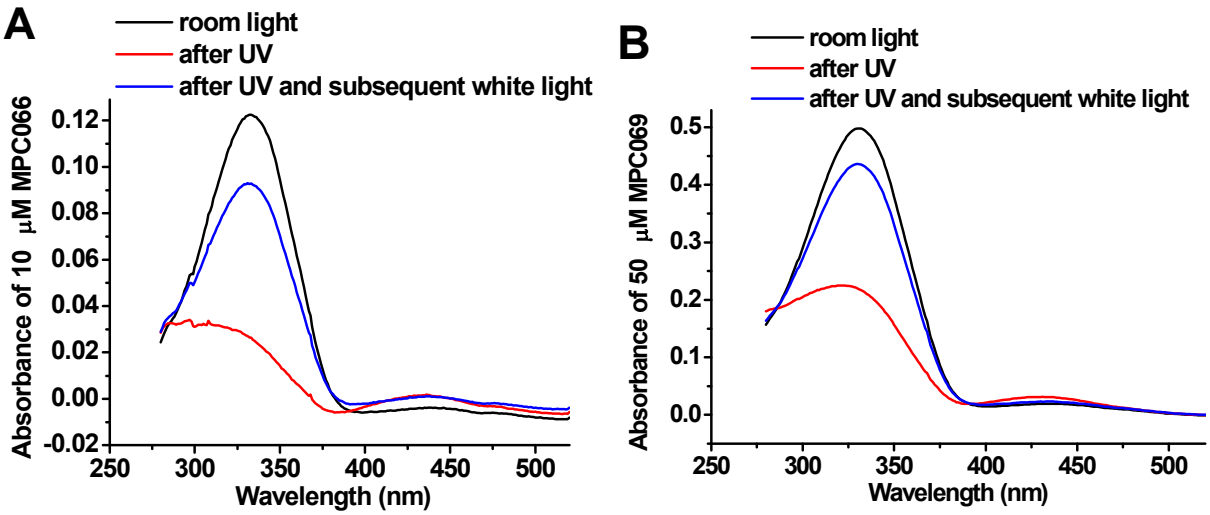

Fig. 4.2.15: Absorbance spectra of 15 µM MPC066 (A) and 50 µM MPC069 (B) under room light, after UV illumination and after subsequent white light illumination. The spectra exhibiting the 338 and 438 nm peaks resemble, respectively, those exhibited by the *trans* and *cis* isomers of unmodified azobenzene.

As indicated in 3.1.4, our UV light source is a 365 nm LED and the white light source is the microscope illuminator tuned to the highest intensity (labeled Vis-High in Fig.4.2.16 and other figures involving white light illumination). Room light combined with the white light of the microscope illuminator at low intensity level represented the ambient illumination present throughout the experiment (labeled as Vis-Low). $GABA_A$-expressing oocytes were first exposed to alternating UV and High-Vis light during static bathing of the oocytes in GABA-supplemented MPC066 or MPC069 solution, and subsequently perfused with un-illuminated fresh test solution. To better evaluate the influence of different illumination conditions on the potentiating effect of test agents, here we normalized the response amplitudes to the unpotentiated level, i.e., to the response amplitude elicited by 3 μM GABA alone.

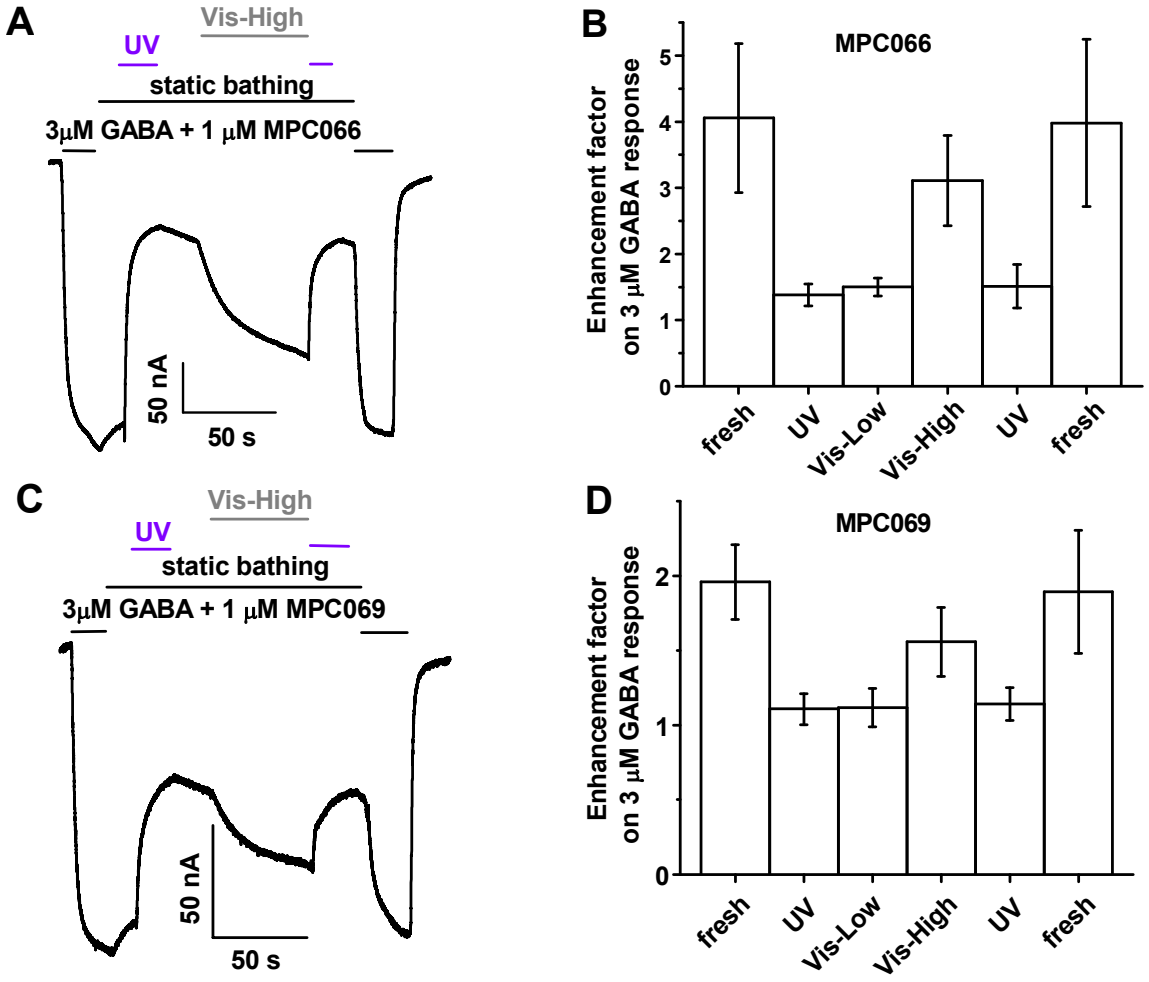

Fig. 4.2.16: Light regulation of the activities of MPC066 (A-B) and MPC069 (C-D). (A) Representative waveform obtained with UV illumination, and with low and high intensities of white light (Vis-Low and Vis-High, respectively) during static bathing of the oocyte with 3 μM GABA + 1 μM MPC066. (B) Quantified modulation of response enhancement by MPC066 under the illumination conditions noted in Panel A experiment. Aggregate results obtained from 4 oocytes. (C) Representative waveform obtained in an experiment similar to A, but with 3 μM GABA + 1 μM MPC069. (D) Quantified modulation of response enhancement by MPC069 under the illumination conditions noted in Panel C experiment. Aggregate results obtained from 4 oocytes.

As shown in Fig.4.2.16 A-B, the MPC066-potentiated GABA response was sensitive to UV and subsequent white light illumination. Exposure to UV light reduced the enhancement factor of the un-illuminated solution (i.e., fresh solution not previously exposed to UV) from ~4 fold to ~1.4 fold. This reduced current level persisted under ambient light (Vis-Low), and the subsequent Vis-High illumination reversed the effect of UV light. A subsequent second round of UV illumination produced a decreasing effect similar to that of the first round. The resumption of perfusion with fresh solution recovered the response to the level (~4-fold enhancement) determined prior to any UV illumination, indicating that UV modulation of the response was not due to permanent damage to the cell. Similar results were obtained with MPC069, where UV and Vis-High illuminations also produced opposite effects on the potentiated response. Based on the resemblance of the pre- and post-UV spectra of MPC066 and MPC069 (Fig. 4.2.15) to the *trans*-dominant and *cis*-dominant spectra of azobenzene, the present results suggest that potentiation by MPC066 and MPC069 largely or entirely reflects an activity of the *trans* isomer, i.e., UV-generated *cis*-isomer exhibits a significantly reduced, if any,

potentiating effect. Therefore, MPC066 and MPC069 represented two milestone compounds for the project, in being the first to exhibit a potent activity in one isoform, but not the other. Due to its relatively higher potency, we chose MPC066, which contains the 4-carbon spacer, as the structure for further modification.

4.2.3.3 Further optimization of the linkage group: MPC070 and MPC057

Similar to MPC066, both MPC070 and MPC057 have a 4-carbon spacer attached to the propofol terminal, however, MPC070 has the amide group connected to the azobenzene moiety (no extra methylene group inserted) and MPC057 contains an ester group, instead of amide, immediately next to the proximal phenyl ring (Fig. 4.2.17).

By comparison with MPC066, these two compounds with modifications of the linkage connecting the carbonyl and the azobenzene group exhibited substantially decreased activity (Fig. 4.2.18). At 5 μM, they each exhibited only a ~1.5 fold potentiation of GABA response; even at 50 μM concentration, the potentiation was less than ~3 fold (from ~5% to ~12% of r_{100G}). Therefore, for future structural optimization,

we kept the amide-methylene linkage structure between the 4-carbon spacer and the azobenzene moiety.

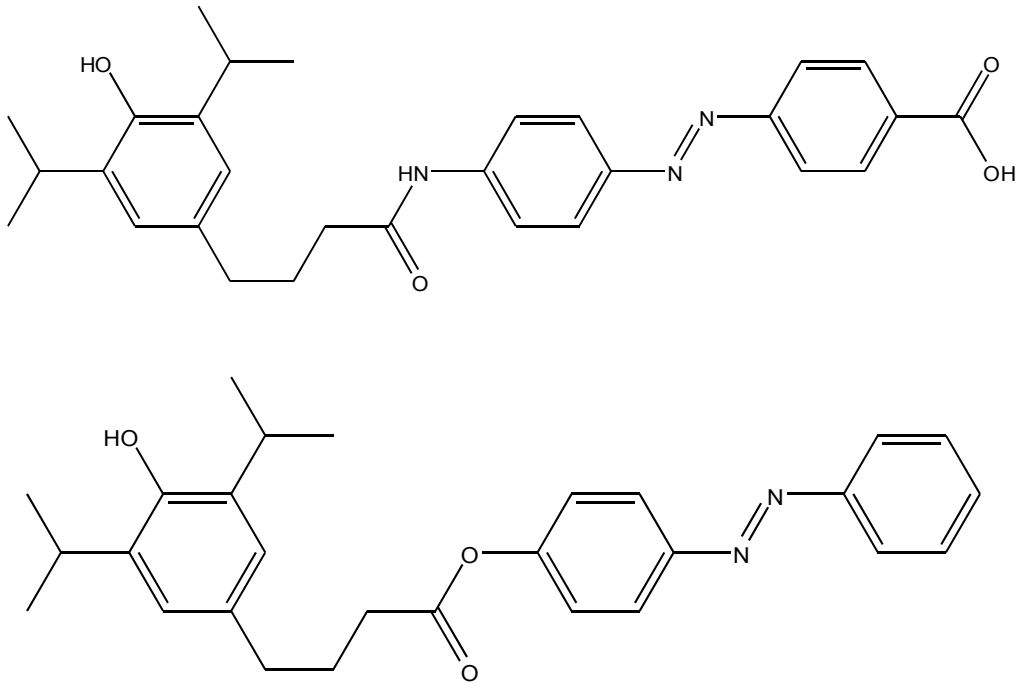

Fig. 4.2.17: Chemical structures of MPC070 (upper) and MPC057 (lower).

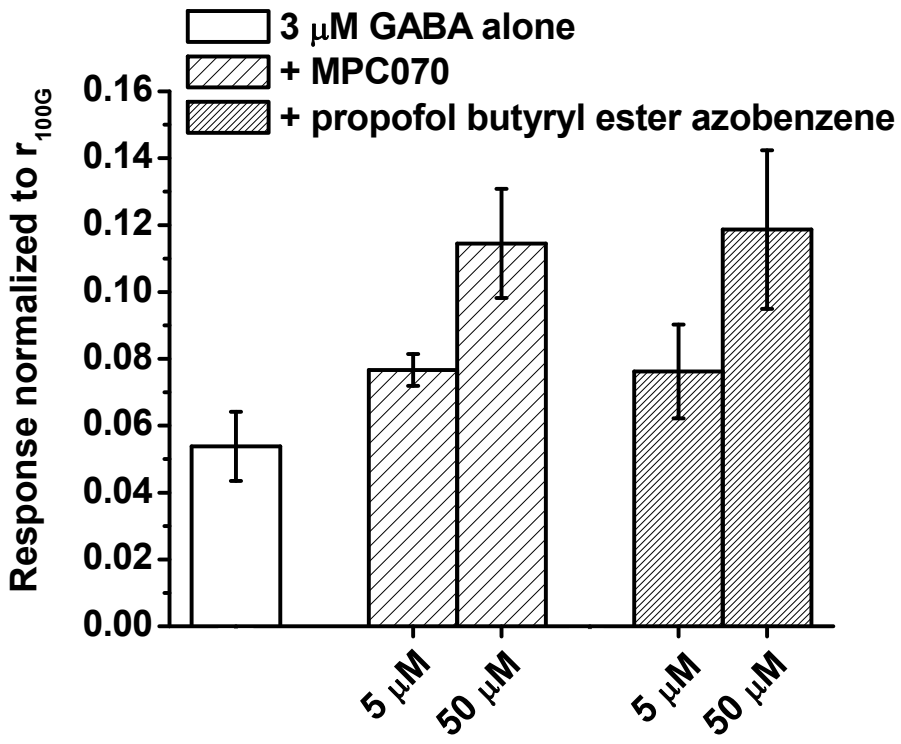

Fig. 4.2.18: Potentiating effect of MPC070 and MPC057. Columns left to right: normalized response elicited by 3 μM GABA alone (open column; left), co-applied with 5 or 50 μM MPC070 (lightly shaded columns; middle) and co-applied with 5 or 50 μM MPC057 (heavily shaded columns; right). Aggregate data obtained from 4 oocytes each for MPC070 and MPC057. Results for GABA alone obtained from the combined 8 oocytes.

4.2.3.4 Elaboration of the distal phenyl ring of azobenzene: MPC088

To test the effect of the negative charge at the carboxylate group of compound MPC066, we converted this group into a corresponding 2-aminoethylamide (Fig. 4.2.19). This structural change results in replacement of the negative charge of the ionized

carboxyl function by a positive charge in the protonated primary amine function. This terminal amino group can also be used for further functionalization.

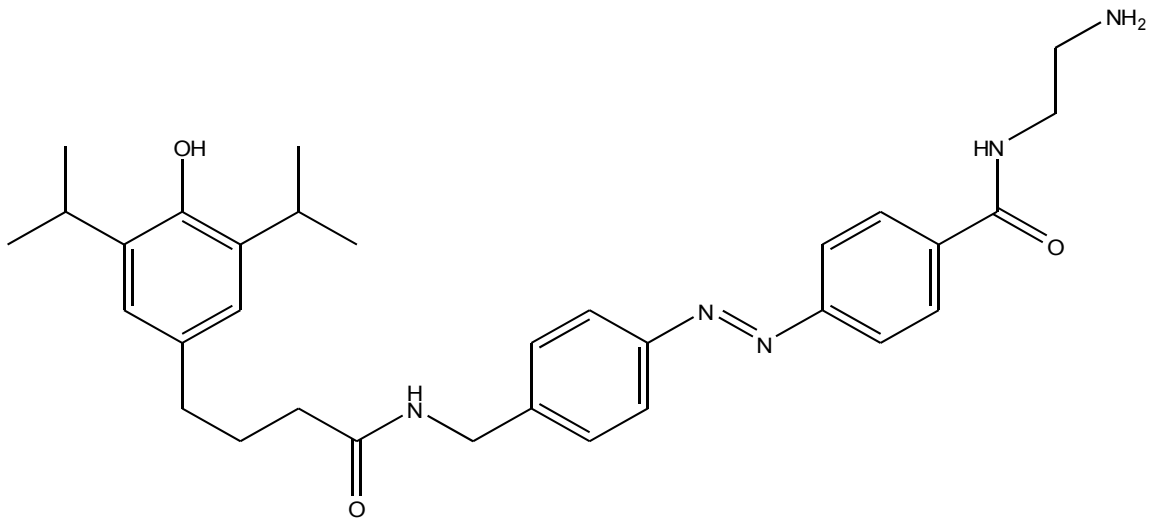

Fig. 4.2.19: Chemical structure of MPC088.

MPC088 exhibited the most potent activity among all the propofol derivatives we have investigated, even exceeding that of parent propofol. This compound not only potentiates the GABA-elicited response but also directly activates $GABA_ARs$, and both effects are strongly regulated by light. The activity of MPC088 on oocytes expressing recombinant $\alpha_1\beta_2\gamma_2$ $GABA_ARs$, and on native retinal ganglion cells, are further discussed in Sections 4.3 and 4.5, respectively.

4.2.4 Maleimide-containing tetherable MPC088: MPC100

Although our ultimate goal is to anchor a photosensitive neural modulator at native receptors, we viewed it important to test whether a tetherable MPC088 analog, when covalently attached to a modified $GABA_AR$, exhibits activity similar to that of MPC088. We therefore synthesized and tested MPC100, a tetherable derivative of MPC088, which contains a terminating maleimide linked by a 24-mer PEG chain to the amino group of MPC088 (Fig. 4.2.20).

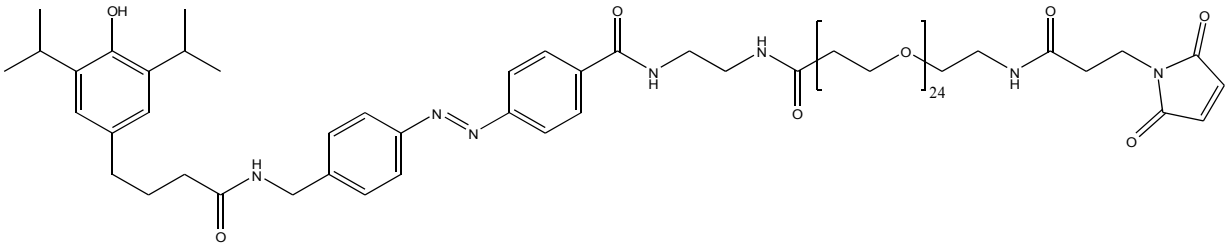

Fig. 4.2.20: Chemical structure of MPC100

The maleimide terminal was incorporated to enable reactivity with a substituted cysteine site on the target $GABA_AR$, thus forming a covalent attachment. The activity of tethered MPC100 is discussed in detail in Section 4.4.

4.3 Activity of MPC088 on recombinant $\alpha_1\beta_2\gamma_2$ $GABA_A$ receptors

As in the case of MPC066 described in 4.2.3.2, photoisomerization of MPC088 was studied in both spectrophotometric and electrophysiological experiments. In addition, as a further quantitative test of the relationship between MPC088's physiological activity and its photostationary mixture composition, the proportions of *trans* and *cis* isomer generated under different illumination conditions were determined through NMR analysis.

4.3.1 Spectrophotometric and NMR analysis of photoisomerization

UV and visible light sources of the electrophysiological apparatus were used for the spectrophotometric and NMR experiments. When prepared and maintained in ambient light, *trans*-dominant MPC088 exhibited an absorbance peak at 338 nm (Fig. 4.3.1 Panel A; spectrum 1). UV illumination (wavelengths near 365 nm) for 5 min eliminated this peak and generated a minor peak at 438 nm (spectrum 2). Exposure (10 min) to high-intensity visible light largely reversed the UV-induced change (spectrum

3) but did not fully re-establish the initial spectrum 1, and a second round of UV and visible illumination yielded spectra 4 and 5, which were virtually identical to 2 and 3, respectively. This suggested that the small difference between spectra 1 and 3 reflected a difference between the photostationary mixture of the two isomers produced by room light *vs.* the visible light source of the electrophysiological apparatus, rather than, e.g., decomposition of the *trans*-isomer due to UV illumination. Support for this conclusion came from the experiment of Panel B, which showed that in the absence of UV pre-illumination, visible light exposure induced a time-dependent reduction in the 338 nm absorption peak, similar to the difference between spectra 1 and 3 of Panel A.

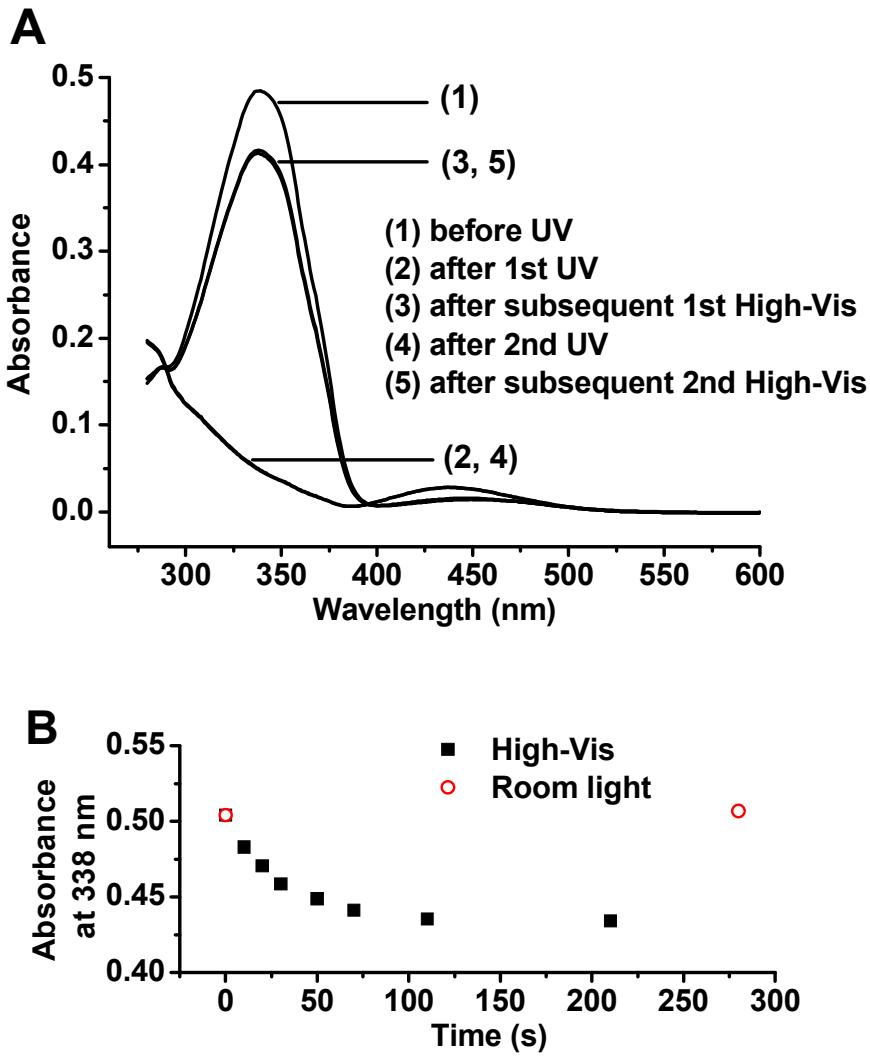

Fig. 4.3.1: Absorbance spectra of 15 μM MPC088 in DMSO. (A) Spectra obtained under room light (1), after UV (2) and subsequent visible illumination (3), and finally, after a second round of UV (4) and visible illumination (5). The spectra exhibiting the 338 and 438 nm peaks are analogous, respectively, to those exhibited by the *trans* and *cis* isomers of unmodified azobenzene. (B) Time course of absorbance change at 338 nm produced by visible illumination (filled square), by contrast with the unchanged absorbance obtained under room light (open circle).

UV and visible light also produced opposing shifts in NMR peaks associated with the benzylic methylene resonances of MPC088 (Fig. 4.3.2). Thus, the UV and visible light used in the electrophysiological experiments drove *trans*-to-*cis* and *cis*-to-*trans* isomerization, respectively. Correspondingly, the *trans*-isomer proportions under room light, after UV illumination and after subsequent visible illumination were 94%, 9% and 81%, respectively.

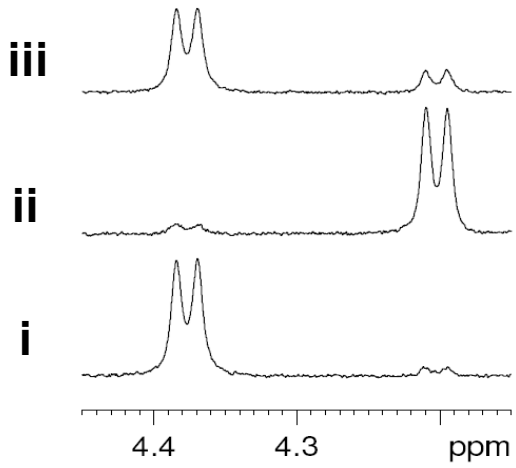

Fig. 4.3.2: Determination of *trans/cis*-isomer ratio in MPC088 by ^{1}H NMR. (i) The solution of MPC088 (2.0 mM) in DMSO-d_6 displayed two peaks for the aminomethylene group: at 4.38 ppm (for the *trans*-isomer, 94%) and 4.20 ppm (*cis*-isomer, 6%). (ii) This solution, contained in a quartz NMR tube, was subjected to UV illumination for 5 min, yielding a mixture that contained 91% *cis*- and 9% *trans*-isomer. (iii) The solution was then exposed to visible light for 10 min, yielding a mixture of 81% *trans*- and 19% *cis*-isomer.

A full cycle of spectral changes produced by UV and subsequent visible illumination indicated gradation of the changes with duration of the exposure (Fig. 4.3.3). The fitting of simple exponential functions to the data obtained with UV, reduced-intensity (10% of nominal) UV and visible light yielded time constants of 1.7 ± 0.3, 22 ± 3 and 36 ± 2 s, respectively. As revealed by their dependence on light intensity, these time constants are not governed by the kinetics of the elemental photoisomerization event [27] but rather by the photon fluxes being used.

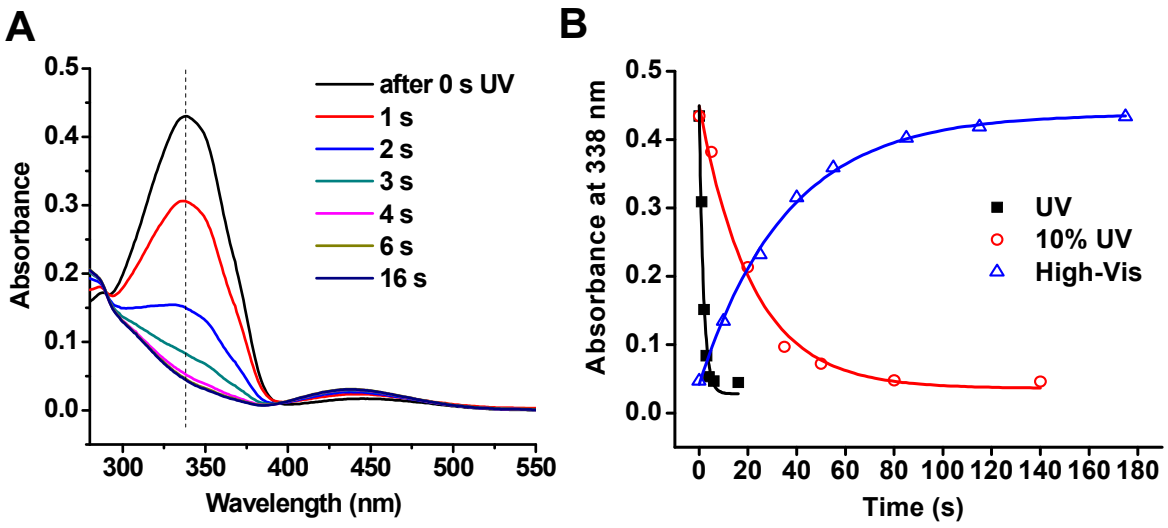

Fig. 4.3.3: Determination of the photoisomerization rate of MPC088 in DMSO. (A) Representative absorbance spectra obtained from High-Vis pre-treated 15 μM MPC088, with varying periods of UV illumination. (B) Time course of absorbance change at 338 nm (dotted line in A) produced, respectively, by nominal UV exposures (filled squares), by UV exposures of reduced intensity (10% of nominal; open circles) and by visible light illumination (open triangles).

4.3.2 Activity of *trans*-dominant MPC088

The NMR data indicate that, MPC088 is in *trans*-dominant configuration under ambient light, and that UV illumination decreases the *trans/cis* ratio. Therefore, the

electrophysiological activity of MPC088 obtained under ambient light reflects the effect of *trans*-dominant compound.

4.3.2.1 Potentiating effect

We first tested MPC088 in the presence of GABA to determine the potentiating effect of the new compound. When co-applied with 3 μM GABA, MPC088 in predominantly *trans*-isomer increased the response in a concentration-dependent fashion (Fig.4.3.4A) and exhibited a potency ~25 times that of propofol, as determined by the relationship of the MPC088 *vs*. propofol concentration for which the peak response amplitude was 50% of that elicited by 100 μM GABA alone (Fig.4.3.4B).

By analogy with the known effects of propofol, this action of MPC088 could reflect contributions from both potentiation of the GABA response and direct receptor activation (i.e., direct agonist activity). To address this question, we tested the activity of MPC088 in the absence of GABA.

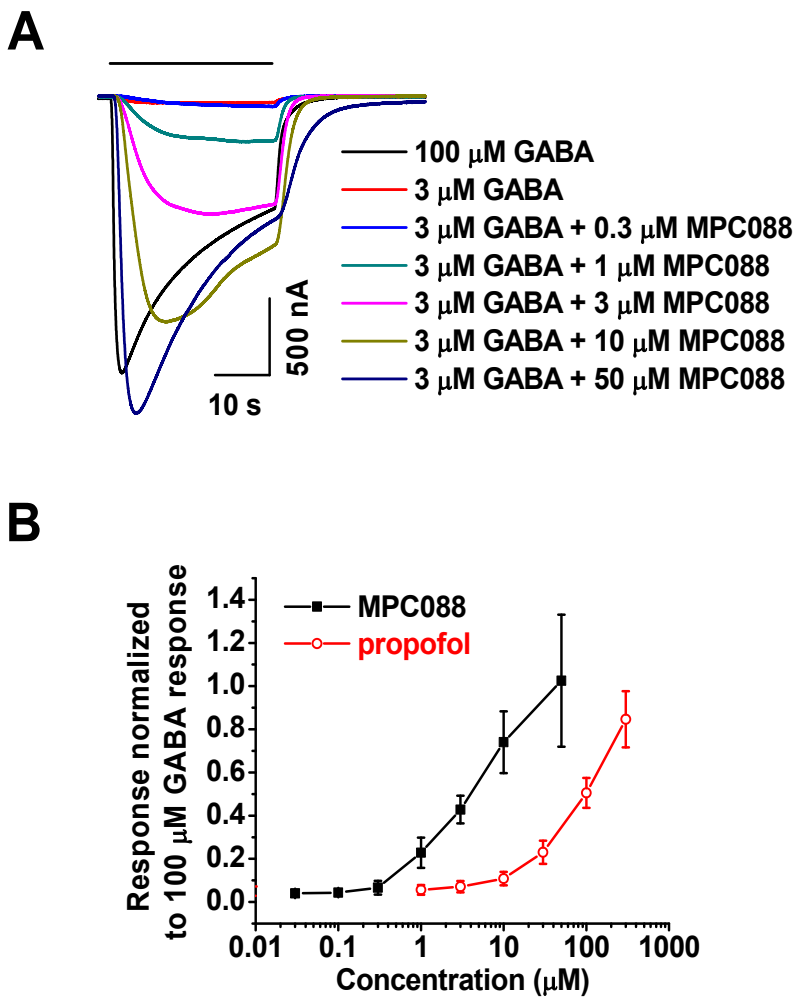

Fig. 4.3.4: Potentiating effect of *trans*-dominant MPC088 on 3 μM GABA response of $\alpha_1\beta_2\gamma_2$ $GABA_AR$-expressing oocytes. (A) Responses of a single oocyte to co-applied 3 μM GABA and varying concentrations of *trans*-dominant MPC088. Horizontal bar indicates the period of superfusion with test compound supplemented Ringer solution. (B) Aggregate dose-response data describing responses elicited by co-applied 3 μM GABA and *trans*-dominant MPC088 or propofol. Response amplitudes obtained from each oocyte normalized to that elicited by 100 μM GABA alone, a near-saturating condition that is essentially insensitive to propofol potentiation. MPC088 and propofol results (mean ± SD), each obtained from 7 oocytes. Propofol results reproduced from Fig.4.1.9.

4.3.2.2 Activating effect

In addition to potentiation, *trans*-dominant MPC088 exhibited potent activity as a direct activator/agonist of the $\alpha_1\beta_2\gamma_2$ $GABA_AR$ (Fig. 4.3.5A). The response elicited by *trans*-dominant MPC088 was clearly evident at concentrations as low as 4 μM (Fig. 4.3.5B). The maximum current generated by *trans*-dominant MPC088 was comparable with the response elicited by 100 μM GABA, while that generated by propofol represented only ~40% of the 100 μM GABA response. In addition, as determined by the concentrations of MPC088 *vs.* propofol required for a peak current equal to 40% of the 100 μM GABA-alone response, the potency of MPC088 exceeded that of propofol by ~25-fold (Fig. 4.3.5B).

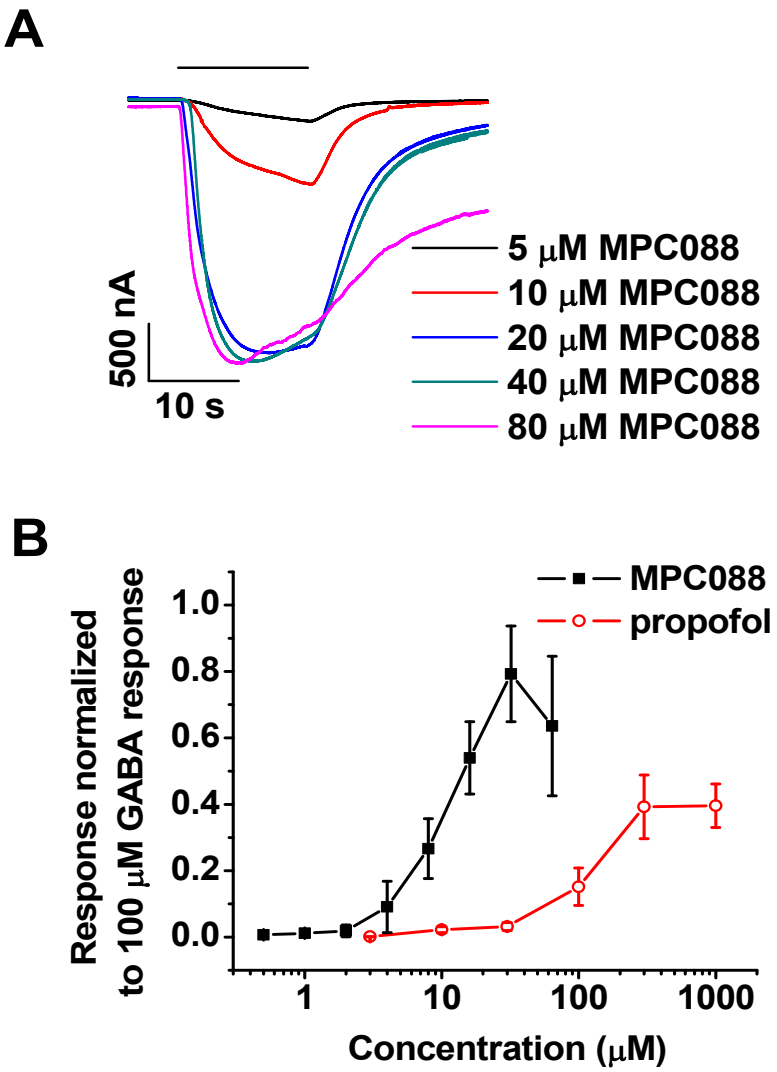

Fig. 4.3.5: Agonist activity of *trans*-dominant MPC088 on $\alpha_1\beta_2\gamma_2$ $GABA_AR$-expressing oocytes. (A) Responses of a single oocyte to varying concentration of *trans*-dominant MPC088 alone. (B) Aggregate concentration-response data describing responses activated by *trans*-dominant MPC088 or propofol. Response amplitudes obtained from each oocyte normalized to that elicited by 100 μM GABA alone. MPC088 and propofol

results (mean ± SD), each obtained from 6 oocytes. Propofol results reproduced from Fig.4.1.9.

4.3.2.3 Allosteric activator of $GABA_A$ receptors

The robust agonist activity of MPC088 prompted two questions: first, whether the activity is indeed mediated by $GABA_AR$; and second, whether the compound exerts its effect by occupying the GABA-binding site of the receptor. We addressed these questions by investigating the effects of several pharmacological agents co-applied with MPC088. The specific agents examined were the $GABA_AR$ channel blocker picrotoxin (PTX) and the competitive GABA antagonists bicuculline and gabazine (SR-95531). The MPC088-elicited response was eliminated by PTX, but was not sensitive to gabazine and was only partially antagonized by bicuculline (Fig. 4.3.6). These properties, which are shared by the known $GABA_AR$ allosteric activators alphaxalone [105, 106] and pentobarbital [73, 107], suggested that MPC088 is an allosteric activator of $GABA_AR$, i.e., it activates the receptor by binding at a site distinct from the GABA-binding site.

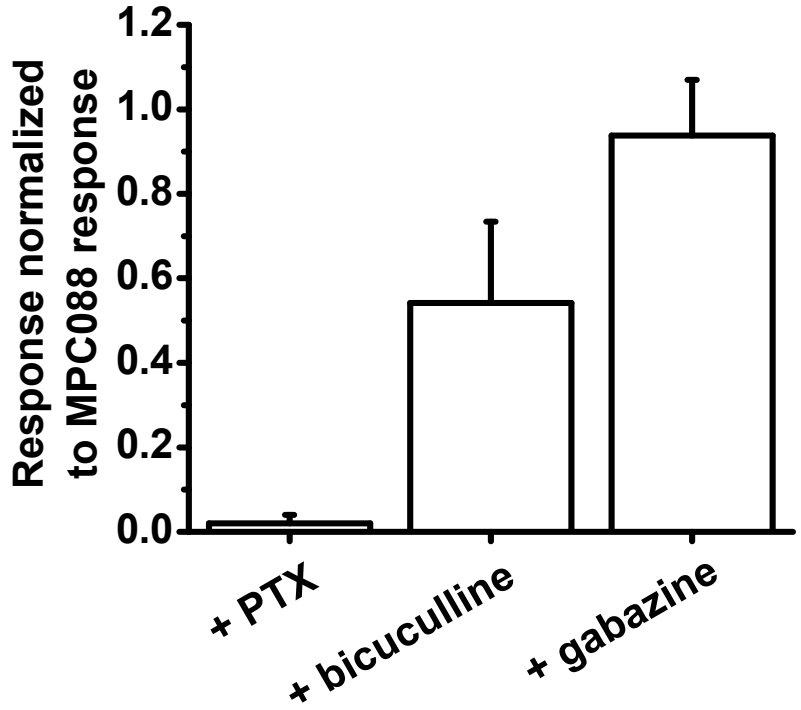

Fig. 4.3.6: Sensitivity of the MPC088 (15 μM) activated response to $GABA_AR$ inhibitors: 100 μM PTX (left column), 100 μM bicuculline (middle column) and 30 μM gabazine (right column). Response amplitudes obtained from each oocyte normalized to that elicited by 15 μM MPC088 alone. Aggregate results (mean ± SD) in each column obtained from 6 oocytes.

MPD021, a compound that lacks the propofol moiety but is otherwise identical to *trans*-MPC088, failed to exhibit any activity on $GABA_ARs$, strongly suggesting that MPC088 binds at the allosteric propofol binding site. Specifically, co-application of 3 μM GABA with 10 or 100 μM MPD021 yielded response amplitudes, relative to the 3 μM

GABA response, of 1.03 ± 0.07 ($p = 0.3$) and 1.03 ± 0.11, respectively ($p = 0.6$; $n = 6$). In addition, UV and visible light had no effect on currents induced by co-applied GABA and MPD021.

4.3.3 Influence of altered propofol binding cavity

The high potency and efficacy of MPC088 that considerably exceed those of propofol triggered our interest in studying the interaction of the compound with the $GABA_AR$ propofol-binding site. To reduce the complexity of the study, especially at higher concentrations of MPC088, where the compound's potentiating effect convolved with its direct activating effect, we focused on the agonist activity of MPC088, i.e., responses obtained in the absence of GABA. We tested *trans*-MPC088 on a group of oocyte-expressed $\alpha_1\beta_2\gamma_2$ $GABA_AR$ mutants that were previously reported to exhibit altered activity of propofol, namely, those containing the M286W, N265M, or Y444W substitution of the β-subunit [88-90]. The results showed that alteration of the propofol binding region by these site-directed mutations differentially influenced the activities of

propofol and MPC088 (Fig. 4.3.7), suggesting that the two compounds interact differently with the investigated group of substituted amino acids.

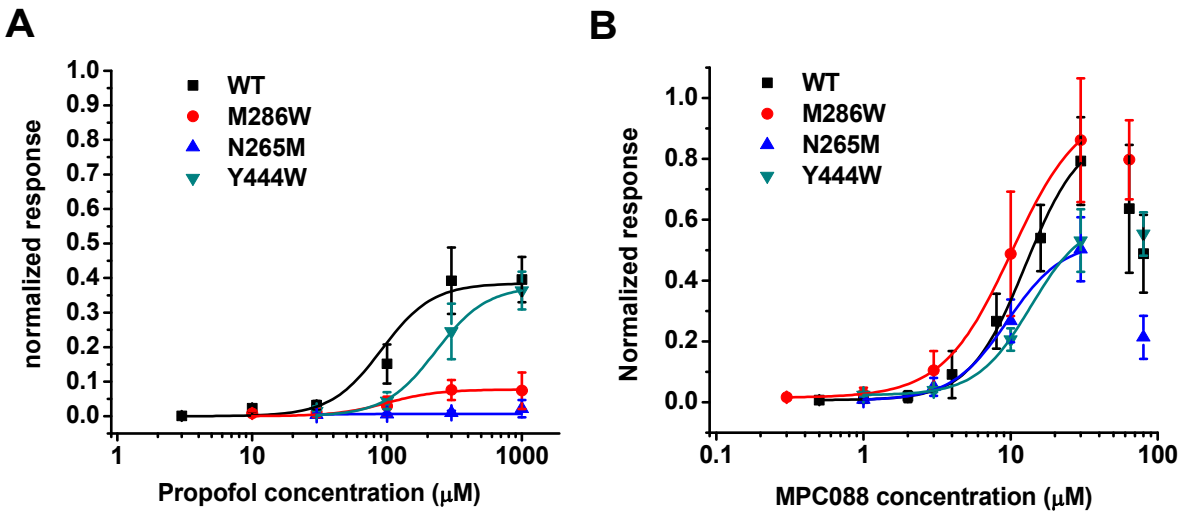

Fig. 4.3.7: Agonist activity of propofol (A) and MPC088 (B) on WT and mutant $GABA_ARs$. (A) By comparison with the WT receptors, the M286W and N265M mutants show a marked reduction (~80% and~95%, respectively) in propofol efficacy, and the Y444W mutant exhibits a ~3-fold higher propofol EC_{50}. (B) Response functions obtained for MPC088 (with points at the highest concentration ignored for the fitting) show relatively small differences in efficacy (only ~30% reduction for N265M and Y444W; no significant change for M286W) and no substantial differences in EC_{50}. Aggregate results (mean ± SD) each obtained from 4-6 oocytes.

To better understand the interaction of *trans*-MPC088 with the residues substituted in these mutant $GABA_AR$s, we also investigated how the binding of bicuculline, a competitive antagonist of GABA, affects *trans*-MPC088 activity on these receptors. First, on oocyte-expressed WT $GABA_AR$s, we fixed the concentration of *trans*-MPC088, obtained the inhibition profile of co-applied bicuculline, and compared this profile with that obtained for propofol and GABA, respectively. The results showed that, by contrast with full competitive inhibition on GABA activity, bicuculline exhibited analogous partial inhibition on propofol and MPC088 activity (Fig. 4.3.8A), suggesting that occupation of the GABA-binding site by bicuculline may similarly affect the receptor's interaction with the two allosteric activators. We then performed similar bicuculline tests on the mutant receptors. Due to the substantially compressed amplitude of the propofol-elicited response, we were able to analyze bicuculline's inhibition profile only on MPC088 activity. At WT and all three mutant receptors, bicuculline's inhibition of the MPC088 response (Fig. 4.3.8B) exhibited similar Hill coefficients (~0.7-0.8), suggesting that the mutations had little effect on bicuculline

binding. Moreover, these <1 value of the Hill coefficients suggest that the association of bicuculline with one of the two GABA-binding sites is sufficient to drive the MPC088-activated receptor into the inhibited state. Fig. 4.3.8B also shows that WT and Y444W $GABA_ARs$ exhibited a similar bicuculline inhibition profile, while M286W and N265M mutant receptors exhibited, on average, a reduced IC_{50} and greater maximum inhibition.

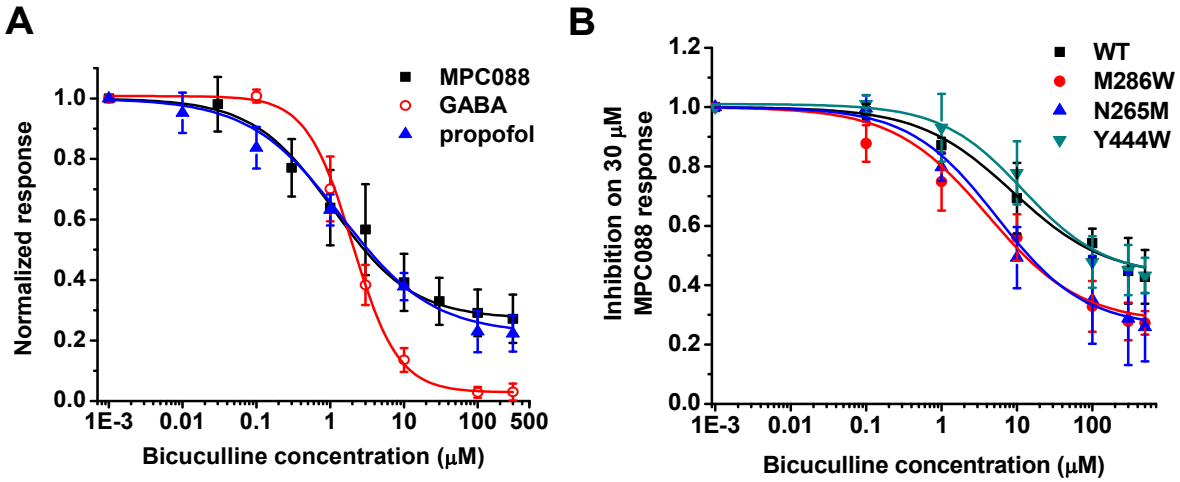

Fig. 4.3.8: Response inhibition by bicuculline at fixed concentrations of test agents. (A) Inhibition function for bicuculline at WT $GABA_ARs$, with 10 μM MPC088, 10 μM GABA and 100 μM propofol. (B) Inhibition, by bicuculline, of the 30 μM MPC088-elicited response on WT and mutant $GABA_ARs$. The IC_{50}s on WT, M286W, N265M and Y444W

are ~8.9, ~4.1, ~5.4 and ~12.0 μM, respectively; the corresponding Hill coefficients are ~0.7, ~0.7, ~0.8 and ~0.8. Aggregate results each obtained from 4-6 oocytes.

To further understand the effect of bicuculline on the activity of MPC088, we also examined the response function of *trans*-MPC088 co-applied with bicuculline at a fixed saturating concentration (Fig. 4.3.9). The results showed that, on WT and Y444W receptors, 500 μM bicuculline produced only a compressed MPC088 response function with no substantial changes in EC_{50}, whereas on M286W and N265M receptors, the co-application of bicuculline led also to a shift in MPC088 sensitivity. Because the native and introduced amino acids investigated here (methionine, tryptophan, asparagine and tyrosine) are neutral in charge, the observed changes in sensitivity are unlikely due to shifted charge in the mutants. Thus, both Fig 4.3.8B and Fig. 4.3.9 demonstrate that Y444W and WT $GABA_A$Rs behave similarly, and differ from M286W and N265M, suggesting the participation of 286 and 265 sites in sensing bicuculline's occupation of the GABA-binding site and thereby altering the allosteric activity of MPC088.

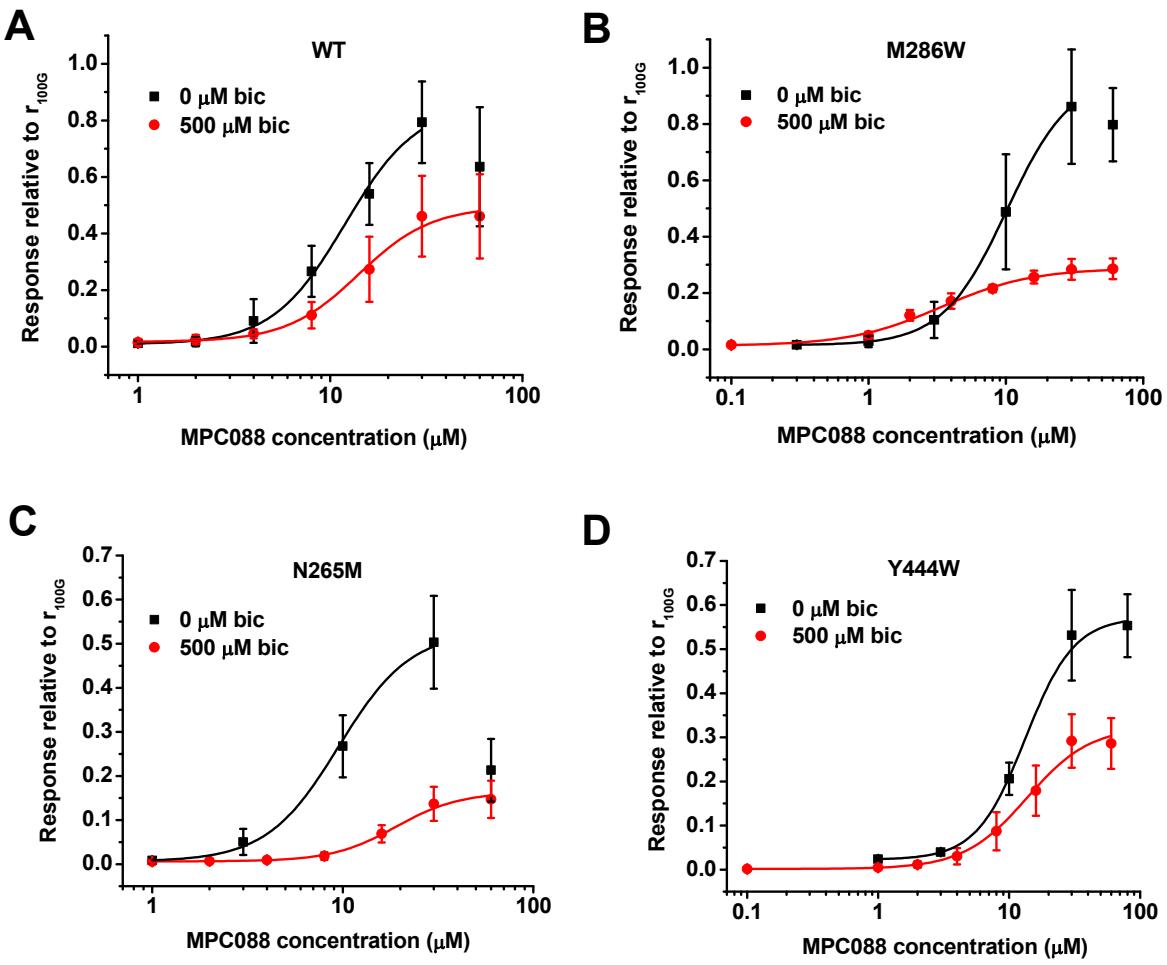

Fig. 4.3.9: MPC088 response functions on WT and mutant $GABA_AR$s in the absence (black) *vs.* presence (red) of saturating (500 μM) bicuculline. With 500 μM bicuculline, EC_{50}s for WT (A), M286W (B), N265M (C) and Y444W (D) are ~14.1, ~3.4, ~19.0 and ~13.7 μM, respectively; the corresponding Hill coefficients are ~2.3, ~1.3, ~2.6 and ~1.8. Aggregate results each obtained from 3-6 oocytes.

In summary, this set of experiments indicates that the interactions of MPC088 with the $GABA_AR$ propofol binding region differ somewhat from those of propofol. Furthermore, among three tested β-subunit mutants, we have identified two (M286W and N265M) for which bicuculline binding appears to alter the interaction of MPC088 with the binding region.

4.3.4 Light-regulation of MPC088 activity

The preceding section 4.3.1 has described spectrophotometric and NMR evidence for photoisomerization of MPC088, i.e., generation of *cis* and *trans* isomers by UV and visible light, respectively. This section presents the results of experiments in which we tested the effect of photoisomerization on the electrophysiological activity of MPC088.

4.3.4.1 Light-regulation of the potentiating effect

We tested for potentiation by MPC088 at a concentration (1 μM) associated with negligible direct activation (see Fig. 4.3.5), and specifically investigated the effect of light that isomerizes the azobenzene moiety (Fig. 4.3.10). With co-applied 3 μM GABA, 1 μM *trans*-dominant MPC088 markedly potentiated the GABA response, and brief UV illumination presented during static bathing of the oocyte decreased the membrane current to a level near that elicited by GABA alone. This level of current persisted in the ambient light (Low-Vis) after cessation of the UV illumination and, conversely, was increased by exposure to high-intensity visible light (High-Vis). The resumption of perfusion with co-applied GABA and *trans*-dominant MPC088 restored the membrane current to a level near that exhibited on the initial presentation of the compounds.

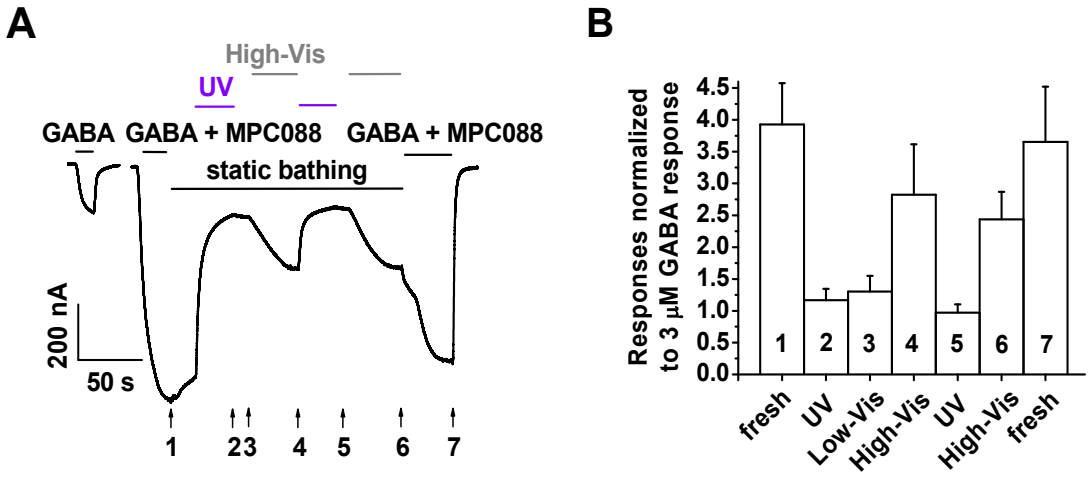

Fig. 4.3.10: Light-regulation of the potentiating effect of MPC088. (A) Light-dependent alteration of the response to 3 µM GABA by co-applied, initially *trans*-dominant, 1 µM MPC088. *Purple* and *gray* bars: period of presentation of UV light and high-intensity visible light (High-Vis), respectively. (B) Results obtained in the experiment of A and 3 others of similar design. Membrane current amplitudes (mean ± SD), normalized to the peak amplitude of the 3 µM GABA response, determined under 7 sequential conditions: (1) at the conclusion of superfusion with (3 µM GABA + 1 µM *trans*-dominant MPC088); (2) at the conclusion of UV illumination; (3) in low-intensity visible light (Low-Vis); (4) at the conclusion of high-intensity visible (High-Vis) illumination; (5) at the conclusion of a second UV illumination; (6) at the conclusion of a second high-intensity visible illumination; and (7) at the conclusion of resumed superfusion with fresh (3 µM GABA + 1 µM *trans*-dominant MPC088). These amplitude determination conditions are denoted by numbers beneath the waveform in B. Repeated-measures ANOVA conducted on the aggregate data yielded $F(6,18) = 41.975$, $p < 0.001$. Post-hoc paired-sample *t*-tests corrected for multiple comparisons indicated significant differences produced by the initial UV, the initial High-Vis, the second UV, and the second High-Vis illuminations ($p \leq 0.009$ for amplitude group 2 *vs*. group 1, for 4 *vs*. 3, for 5 *vs*. 4, and for 6 *vs*. 5, respectively); amplitude groups 7 and 1 did not differ significantly ($p = 0.075$).

4.3.4.2 Light-regulation of the activating effect

In the absence of co-applied GABA, the response elicited by MPC088 also exhibited light-dependence. UV illumination presented during static bathing strongly reduced the MPC088-elicited current. The current remained stable after cessation of UV, and visible light substantially reversed the effect of UV exposure (Fig. 4.3.11).

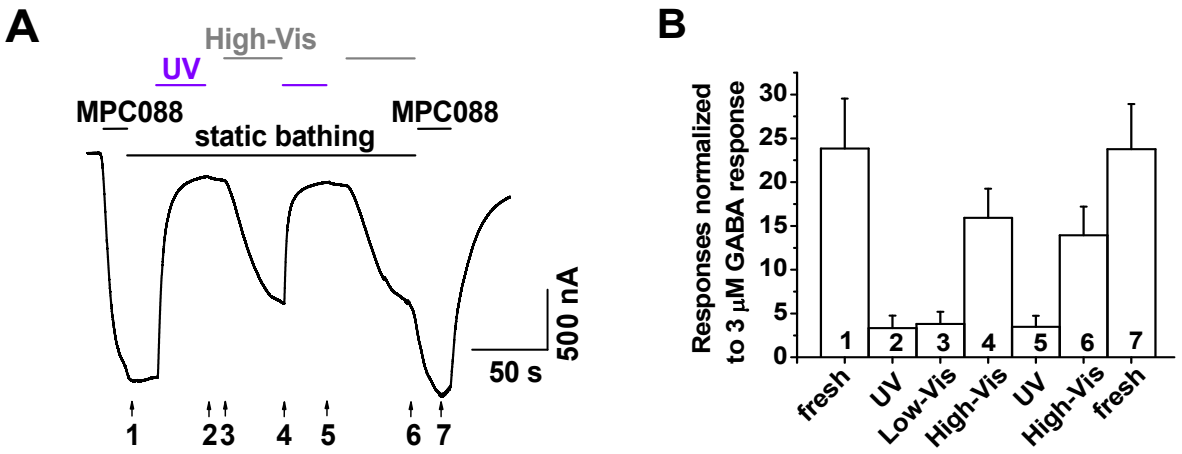

Fig. 4.3.11: Light-regulation of the activating effect of MPC088. (A) Light-dependent modulation of the response amplitude to 15 µM MPC088. (B) Normalized current amplitudes (mean ± SD) determined in the experiment of A and in 3 others of similar design. Amplitudes in each experiment normalized to that elicited by 3 µM GABA. Numbers beneath the waveform in A denote amplitude determination conditions for the experiment (see Fig. 4.3.7 legend). Repeated-measures ANOVA conducted on the

aggregate data yielded $F(6,18) = 68.988$, $p < 0.001$. Post-hoc paired-sample *t*-tests corrected for multiple comparisons indicated significant differences produced by the initial UV, the initial High-Vis, the second UV, and the second High-Vis illuminations ($p \leq 0.010$ for amplitude group 2 *vs*. group 1, for 4 *vs*. 3, for 5 *vs*. 4, and for 6 *vs.* 5, respectively); amplitude groups 7 and 1 did not differ significantly ($p = 0.96$).

Furthermore, repeated pulses of UV light presented on a background of continuous visible light during MPC088 treatment yielded cyclic changes in response amplitude (Fig. 4.3.12).

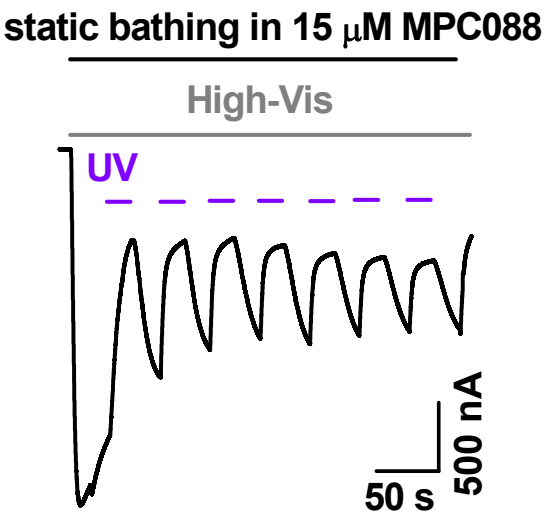

Fig. 4.3.12: Representative waveform obtained with repeated presentation of UV light during continuous High-Vis illumination.

In summary, MPC088 demonstrates a potent potentiating and agonist activity that is photo-regulated by UV and visible illumination. These results encouraged the synthesis and investigation of MPC100, a tetherable form of MPC088, which will be discussed in the next section.

4.4 Activity of MPC100 on recombinant $\alpha_1\beta_2\gamma_2$ $GABA_A$ receptors

MPC088, a freely diffusible compound, can be readily removed by superfusion of the oocyte with Ringer. We asked whether covalent tethering of a similar compound to a suitably modified receptor produces similar but persistent light-sensitive potentiation and/or activation. As a prototype approach to anchoring the photosensitive modulators to the receptor, we developed MPC100, a thiol-reactive maleimide-containing form of MPC088 (Fig. 4.2.18), and tested its activity on oocytes expressing WT as well as cysteine-substituted mutant $\alpha_1\beta_2\gamma_2$ $GABA_A$Rs.

4.4.1 Tethering MPC100 on the cysteine-substituted mutant receptor

The investigated mutant receptor has a cysteine substitution at position 79 of the single γ subunit $\alpha_1\beta_2\gamma_2$ (A79C) [108, 109], henceforth abbreviated γ-79C. The γ-79 mutation site was known to reside near the binding pocket of benzodiazepine, a different family of modulators of $GABA_AR$s. Tethering the photoswitchable structure at the γ-79 residue potentially holds two main advantages. First, previous studies [110] have shown that cysteine mutation at this site has relatively little effect on GABA activity, and the thiol group of the cysteine residue is accessible to covalent binding by externally applied methanethiosulfonate (MTS) reagents. Second, the single γ subunit of the pentameric $\alpha_1\beta_2\gamma_2$ $GABA_AR$ structure hypothetically provides one anchor site per receptor, thus reducing the system complexity for the early phase study.

We hypothesized that the thiol group of the cysteine residue in γ-79C would afford a covalent anchoring site for the maleimide-terminated MPC100, as illustrated schematically in Fig. 4.4.1.

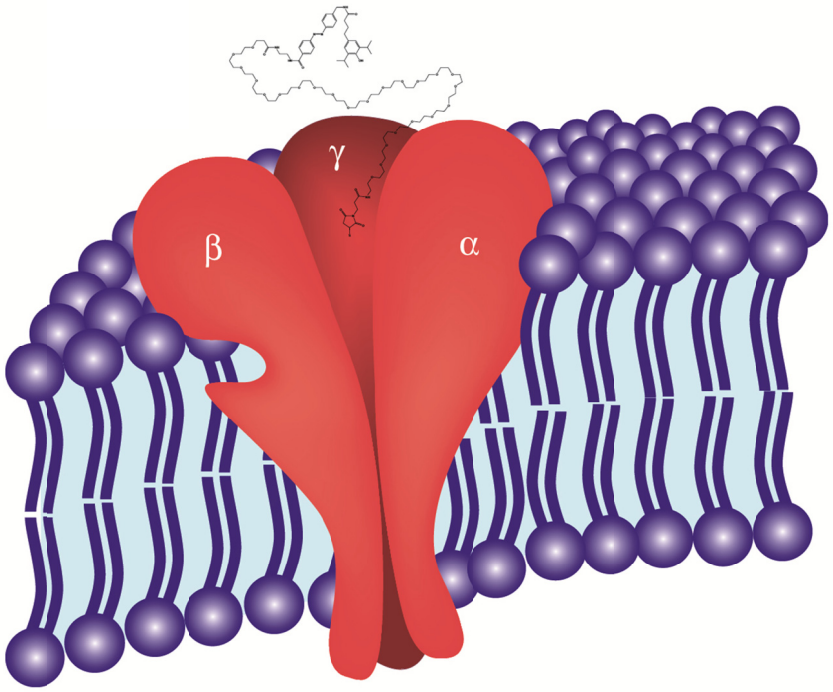

Fig. 4.4.1: Schematic diagram of MPC100 tethered to the $\alpha_1\beta_2\gamma_2$ (A79C) receptor. α, β and γ refer to subunits in this "sliced" view of the pentameric receptor; the β subunit pocket represents a propofol binding site. MPC100 and receptor subunits shown roughly to scale. The thiol anchoring site (γ-79) lies near the benzodiazepine binding cavity.

To test the tetherability of MPC100 on γ-79C $GABA_A$Rs, we first incubated the oocytes with 100 μM *trans*-dominant MPC100 for ~7 minutes and then superfused with unsupplemented Ringer for ~5 minutes to remove unbound compound. The results of the subsequent electrophysiological examination showed that covalently tethering

MPC100 to the $GABA_AR$ produced a marked, persisting potentiation of the GABA-elicited response (Fig. 4.4.2).

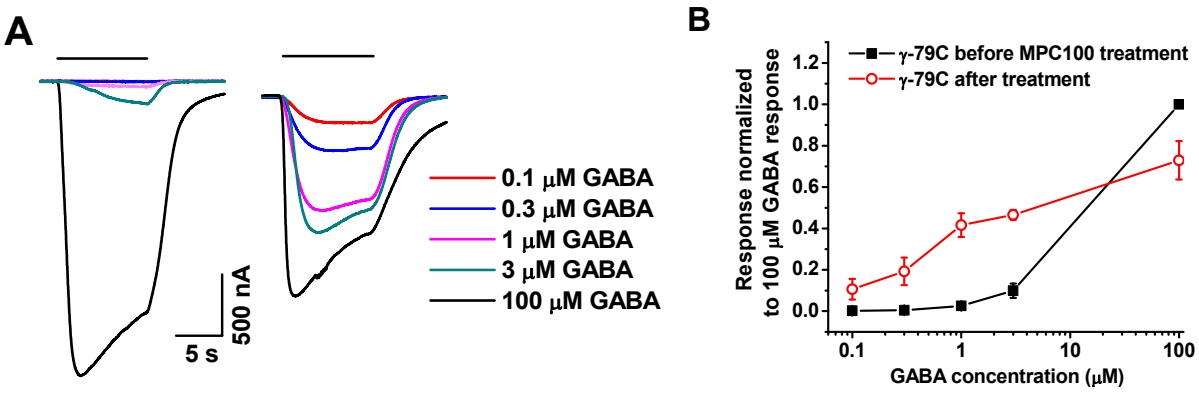

Fig. 4.4.2: Persistent potentiating effect of tethered MPC100 on $\alpha_1\beta_2\gamma_2$ (A79C) $GABA_ARs$. Responses obtained following treatment with *trans*-dominant MPC100 and subsequent Ringer perfusion. (A) Representative responses to GABA recorded from a single oocyte before (left series) and after (right series) MPC100 treatment (100 μM, ~7 min). (B) Response functions obtained before (black) and after (red) MPC100 treatment (5 oocytes). Peak amplitudes normalized to that for 100 μM GABA determined before MPC100 treatment.

Furthermore, tethered MPC100 eliminated the potentiating activity of diazepam (Fig. 4.4.3), a member of benzodiazepine family. Before MPC100 treatment,

1 μM diazepam exhibited a ~3.5-fold enhancement on the 3μM GABA response, whereas after MPC100 treatment, the same concentration of diazepam did not significantly alter the GABA response of similar amplitude. This elimination of the enhancement effect of diazepam likely reflected the blocked accessibility, to diazepam, of the benzodiazepine binding site upon occupation by MPC100. The complete removal of the diazepam effect suggests essentially complete occupancy of the available γ-79 cysteine sites on a given oocyte by MPC100.

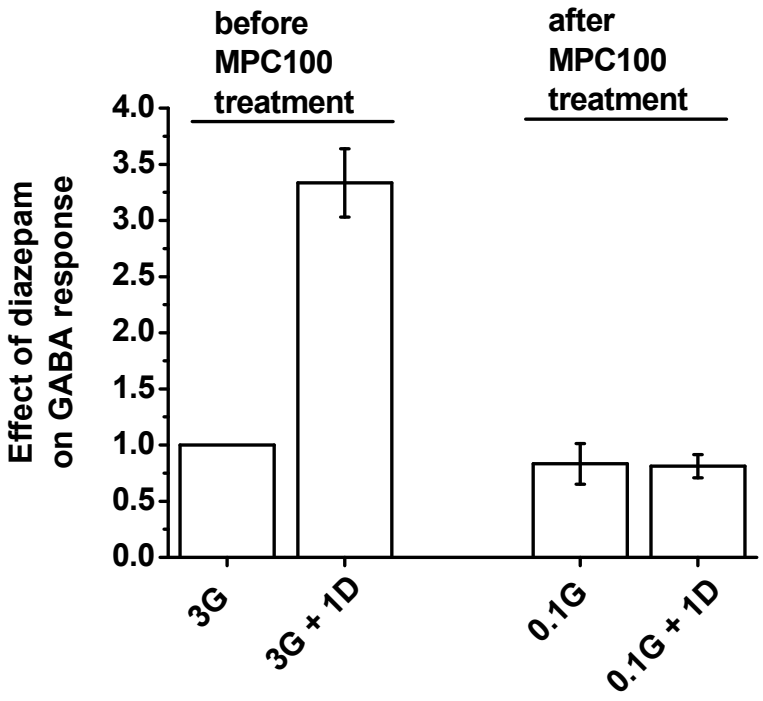

Fig. 4.4.3: Elimination, by tethered MPC100, of the potentiating effect of diazepam on GABA response. Responses to 3 μM GABA (3G) in the absence and presence of 1 μM diazepam (1D) were obtained before MPC100 treatment. After a ~7 min treatment, responses to 0.1 μM GABA (0.1G) of similar amplitude to the pre-treatment 3 μM GABA response were obtained, with and without co-applied 1 μM diazepam (1D). Amplitudes normalized to that for 3 μM GABA determined before treatment (5 oocytes).

In addition, on γ-79C-expressing oocytes, pre-treatment with a different thiol-reactive compound, methyl-$(PEG)_{11}$-maleimide, blocked tethering of the subsequently applied MPC100. Initially, 10-min treatment with 1 mM methyl-$(PEG)_{11}$-maleimide led to

a persistent increase of 71 ± 25 % (p = 0.01; n = 4) in the 3 μM GABA response. By comparison with the effect of MPC100 treatment, this increase was relatively small and insensitive to UV illumination. As benzodiazepines are potent $GABA_AR$ potentiators, the increase observed with methyl-$(PEG)_{11}$-maleimide may have arisen from occupation of the benzodiazepine binding site and the resulting sensitization of the receptor. Treatment (10 min) with 100 μM MPC100 following the treatment of methyl-$(PEG)_{11}$-maleimide did not further alter the GABA response (ratio of response amplitudes post-*vs.* pre-MPC100 treatment: 1.1 ± 0.1 (p = 0.3; n = 4). These findings, together with the non-persistent activity of MPC100 on WT $GABA_ARs$ (discussed in 4.4.4), confirms the dependence of the persistent activity of MPC100 on tethering specifically at the engineered cysteine site of the γ-79C receptor.

4.4.2 Photo-regulation of the persisting potentiation by tethered MPC100

The persistent enhancement of the GABA-elicited response by tethered MPC100 was sensitive to UV and visible light (Fig. 4.4.4); the effects of illumination

resembled those displayed by WT $GABA_AR$ in the presence of co-applied GABA and MPC088 (compare Figs. 4.4.4 and 4.3.10A). In the first phase of the experiment (black trace), the GABA response amplitude was decreased by UV illumination and conversely, increased by visible light. That is, the baseline level exhibited immediately after the second UV illumination was lower than that recorded at the beginning of the experiment (compare dotted lines i and ii). The reduced baseline remained stable during Ringer perfusion. Furthermore, in the second phase of the experiment, visible light increased the response from level iii to level iv. The similarity of current amplitudes produced by UV and visible light in the early and later phases of the experiment demonstrated that UV illumination does not irreversibly alter the activity of tethered MPC100. Furthermore, light of differing wavelength can reversibly and in a quasi-stable manner inter-convert the relatively active and inactive isomers of tethered MPC100.

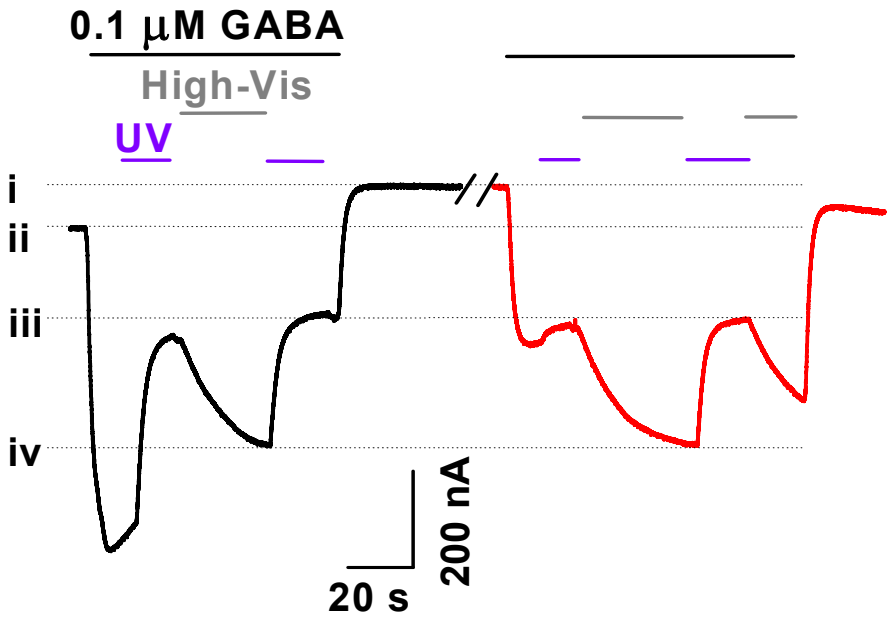

Fig. 4.4.4: Light-dependence of persistent potentiation by tethered MPC100. Black trace: response to UV and visible light in the presence of 0.1 µM GABA, following treatment with 100 µM *trans*-dominant MPC100. Dotted lines i and ii highlight the difference in baseline current between that exhibited at the beginning of the trace and that exhibited after UV illumination (line i). Dotted lines iii and iv highlight the amplitude level after UV illumination and after the subsequent visible light illumination, respectively. Red trace: later phase of the same experiment (responses obtained after a further ~1 min period of perfusion with MPC100-free Ringer). Note the similarity of current amplitudes produced by UV and visible light in the early and later phases of the experiment.

4.4.3 Photo-regulation of the persisting activation by tethered MPC100

Treatment of γ-79C-expressing oocytes with *trans*-dominant MPC100 led to a greater (i.e., more negative) baseline current (compare the baseline levels of the left and right groups of responses in Fig.4.4.2), and UV illumination produced an opposite change (Fig. 4.4.4; note the relationship of the dotted reference lines i and ii). To test the hypothesis that the baseline change reflected continuing, direct activation by the tethered MPC100, we investigated the effect of PTX presented before and after MPC100 treatment (Fig. 4.4.5). PTX application to MPC100-treated and then Ringer-washed cells reversibly reduced the baseline current by 85 ± 7% (mean ± SD; n = 5) (trace ii). UV (i.e., *cis*-generating) illumination delivered during PTX treatment did not further reduce the baseline amplitude, but inhibited baseline recovery following PTX removal, consistent with a UV-induced reduction in the amount of *trans*-MPC100 present (trace iii).

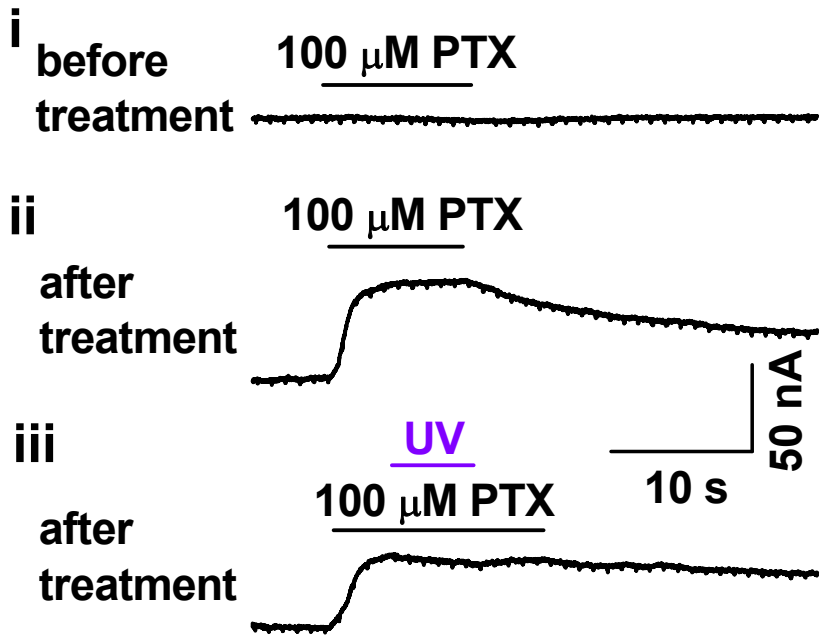

Fig. 4.4.5: Baseline currents in response to PTX obtained in a single experiment. Following the recording of trace (i), the oocyte was treated with 100 μM MPC100, then superfused with Ringer for ~5 min before the recording of trace (ii). Trace iii was recorded shortly after the recovery of trace ii to baseline.

Furthermore, as shown by Fig. 4.4.6, UV and visible light delivered to γ-79C-expressing oocytes that had previously been treated with MPC100 produced, respectively, decreases and increases in membrane current qualitatively similar to those exhibited by WT $\alpha_1\beta_2\gamma_2$ $GABA_A$Rs in the presence of *trans*-MPC088 alone (compare Figs. 4.4.6 and 4.3.11). Thus, the larger baseline current persisting after MPC100

treatment (Fig. 3c) reflected sustained, direct activation of the receptor by tethered *trans*-MPC100.

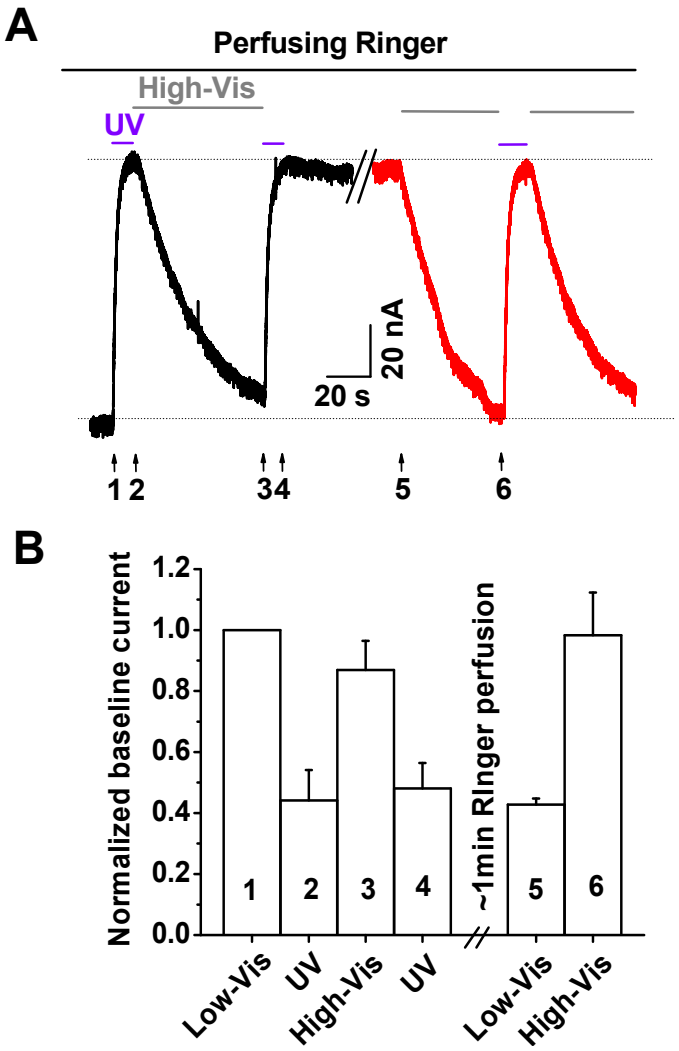

Fig. 4.4.6: Photo-regulation of the persisting agonist activity of tethered MPC100. (A) Responses to UV and visible light following exposure to *trans*-dominant MPC100 and washout of free MPC100. Data obtained from a single oocyte. A period of Ringer perfusion (~1 min) separated the initial (black trace) and later (red trace) phases of the

experiment. (B) Aggregate results obtained from the experiment of A and 3 others of similar design, each of which involved amplitude determinations under 6 sequential experimental conditions. Data (mean ± SD) normalized to the persisting shift in baseline produced by MPC100 treatment. Periods of treatment in each experiment were similar to those illustrated in A. Numbers beneath the waveforms in A denote amplitude determination conditions for the experiment. Repeated-measures ANOVA conducted on the aggregate data yielded $F(6,18) = 65.290$, $p < 0.001$. Post-hoc paired-sample *t*-tests corrected for multiple comparisons indicated significant differences produced by the initial UV, the initial High-Vis, the second UV, and the second High-Vis illuminations ($p \leq 0.007$ for amplitude group 2 *vs*. group 1, for 3 *vs*. 2, for 4 *vs*. 3, and for 6 *vs*. 5, respectively). Amplitude groups 4 and 5 did not differ significantly ($p = 0.26$), and amplitude group 6 did not differ significantly from unity (group 1) ($p = 0.96$).

4.4.4 Non-persisting activity of MPC100 on wildtype receptors

In the presence of 10 μM MPC100, wildtype $\alpha_1\beta_2\gamma_2$ receptors exhibited photo-regulatable potentiation of the GABA response (Fig. 4.4.7A), although this potentiation was smaller than that produced by equimolar *trans*-dominant MPC088 (compare data of Figs. 4.4.7A and 4.3.4). Direct activation of the WT receptors by 10 μM MPC100 was negligible (Fig. 4.4.7A). Following treatment with MPC100, the response to 0.3 μM GABA was not significantly enhanced ($p = 0.9$; $n = 4$), and neither UV nor high-intensity visible light delivered in the presence of GABA substantially affected the membrane current (Fig. 4.4.7B). The finding that Ringer perfusion eliminated the potentiating action of MPC100 at WT $\alpha_1\beta_2\gamma_2$ $GABA_A$Rs provides further evidence that the persistent effects of MPC100 required the γ-79C modification.

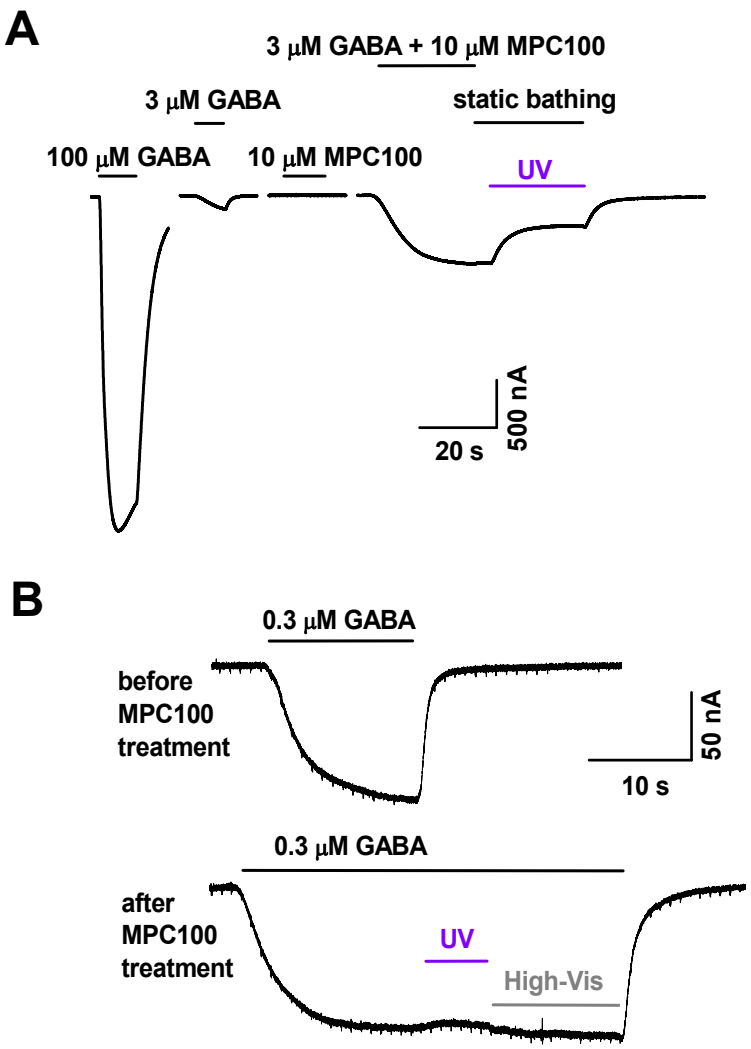

Fig. 4.4.7: Treatment of WT $\alpha_1\beta_2\gamma_2$ receptors with MPC100. (A) Membrane currents recorded from a single oocyte in response to applied MPC100. Waveforms show responses to, sequentially, (i) 100 μM GABA alone, (ii) 3 μM GABA alone, (iii) 10 μM MPC100 alone, and (iv) 10 μM MPC100 co-applied with 3 μM GABA. During phase (iv), introduction of the co-applied MPC100 and GABA was followed by a period of static bathing and UV illumination. (B) Responses of a single oocyte to 0.3 μM GABA presented before (*upper*), and after (*lower*) MPC100 treatment (100 μM, 7 min).

4.4.5 Effects of UV intensity on the rate of change in response

As shown in 4.4.2 and 4.4.4, the enhancement activity of MPC100, either as a free agent on WT receptors or as covalently anchored on γ-79C mutant receptors, was subject to photo-regulation by UV. In addition, spectrophotometric data (Fig. 4.3.3B) indicated that the change in peak absorbance of MPC088 is rate-dependent on UV intensity, i.e., higher intensity leads to an accelerated change (~1/1.7= 0.6 s^{-1} for 100% intensity; see 4.3.1) and attenuated intensity slower change. Here, we examined the influence of varying light intensity on electrophysiological behavior of MPC100, in both free and tethered form.

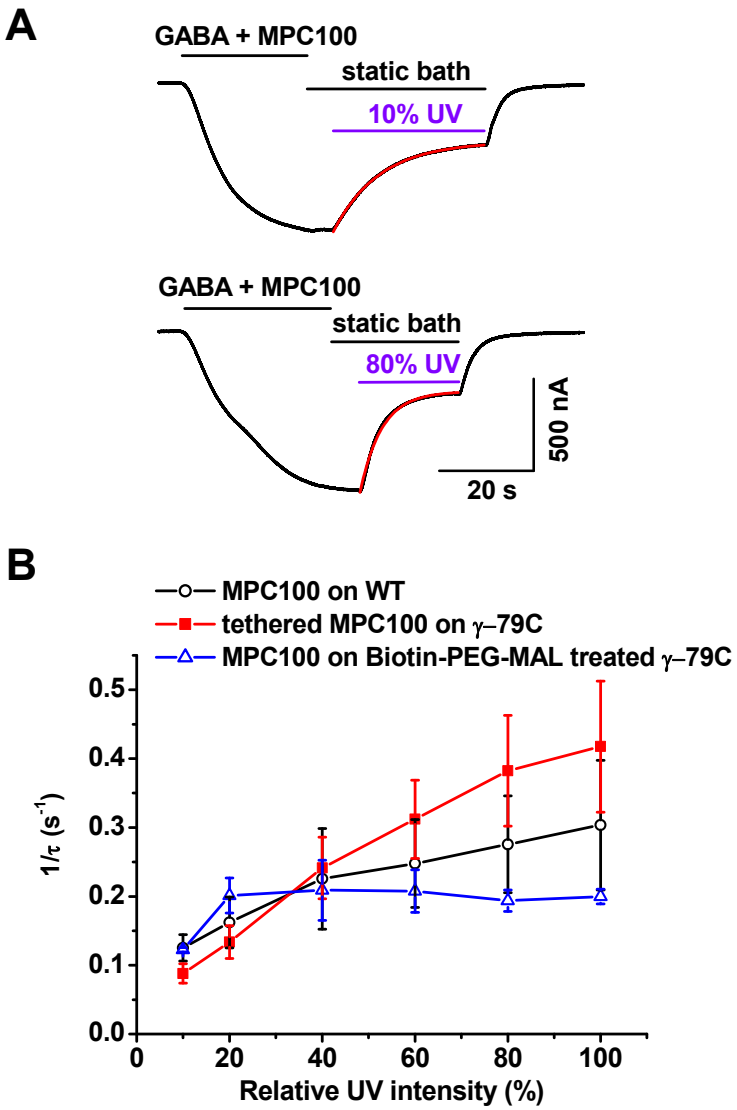

Fig. 4.4.8: Influence of light intensity on UV-induced change in MPC100 potentiated GABA response. (A) Representative waveforms obtained from single oocyte exhibit differential rate of response change induced by 10% (upper trace) and 80% (lower trace) of standard UV intensity, respectively. Black traces: data obtained from WT $\alpha_1\beta_2\gamma_2$ receptors with co-application of 3 μM GABA and 10 μM MPC100. Overlapping red curve: fitting of UV-induced response change by a simple exponential function. (B) Aggregate

response change rate (inverse of time constant) under varying UV intensity yielded by the fitting. Black open circles: data obtained from WT receptors with co-applied 3 μM GABA and 10 μM MPC100 (n=7); red filled squares: data obtained from MPC100 (100 μ M) treated γ-79C mutant receptors with 0.1 μM GABA (n=5); blue open triangles: data obtained from Biotin-PEG_{11}-Maleimide (Biotin-PEG-MAL) (1 mM) treated γ-79C mutant receptors with co-applied 3 μM GABA and 10 μM MPC100 (n=4).

We conducted the experiment of Fig. 4.4.8 by changing the light intensity of the UV LED from the 100% value that that was used in previous experiments as the standard UV illumination condition. As illustrated in Fig. 4.4.8A, at different UV intensities, namely 10% and 80% of the standard, MPC100-potentiated GABA responses obtained from WT receptors exhibited differential de-potentiation rate, consistent with a greater photon catch at higher light intensity. Fitting the current change with a simple exponential function captures well the time constant of this UV-induced de-potentiation (see black trace and its overlapping red fitting). Fig. 4.4.8B shows aggregate fitting data obtained from similar experiments with freely diffusible MPC100 on WT receptors (black open circles) and, in addition, with tethered MPC100 on γ-79C mutants (filled red squares), at varying light intensities. Here, the de-potentiation rate

was represented by 1/τ (s^{-1}, τ is the time constant of the fitting). With the increase in light intensity, average 1/τ obtained in both types of experiments increased with light intensity toward plateau levels lower than the 0.6 s^{-1} rate exhibited by the spectral change in peak absorbance at 100% UV intensity. By comparison with the diffusible form, MPC100, when tethered, exhibited a greater dynamic range in de-potentiation rate with variation of UV intensity (see the difference in 1/τ between 10% and 100% light). We considered the possibility that this difference could be caused by an allosteric influence on the propofol binding site by the occupation of benzodiazepine binding cavity. To test this possibility, we treated γ-79C mutants with Biotin-PEG_{11}-Maleimide, a cysteine-reactive compound that similarly attaches to the γ-79C of the benzodiazepine binding cavity. Responses to test mixture of GABA + MPC100 obtained from Biotin-PEG_{11}-Maleimide treated cells showed modest sensitivity to the increase in UV intensity, where a plateau of de-potentiation rate was reached at 20% UV intensity (blue open triangles in Fig. 4.4.8B). An analogous plateau was observed with diazepam-bound WT receptors (not shown), indicating that occupation of the benzodiazepine binding cavity indeed

limited the UV-induced de-potentiation rate. Compounds in benzodiazepine family, such as diazepam and flurazepam, have been shown to substantially increase the binding affinity of propofol to $GABA_AR$s [78, 111], and thus prolong the dissociation of propofol. Our finding of a slowed de-potentiation on benzodiazepine binding site-occupied receptors may reflect this prolonged dissociation of the propofol moiety of *trans*-dominant MPC100 from its binding site, which further suggests that the rate-plateau observed with UV-triggered response de-potentiation could be governed by the time constant of the dissociation of the propofol moiety. The greater dynamic range observed with the tethered MPC100, i.e., the relatively small tendency toward rate saturation, may have resulted from the constraints imposed by the linker PEG chain which may force an accelerated dissociation of the propofol moiety by pulling it away from its binding site upon photoisomerization.

In summary, the results shown in this section indicate the tetherability of MPC100 and the persisting, light-sensitive modification of $GABA_AR$ activity by the tethered compound. These results demonstrate the feasibility of anchoring an MPC088-

based structure to $GABA_A$ receptors as a retinal therapeutic device and encourage our study of MPC088 on native retinal neurons (discussed in 4.5).

4.5 Activity of MPC088 on isolated retinal ganglion cells

To test whether native $GABA_A$Rs present on retinal neurons respond to MPC088, we examined the compound on retinal ganglion cells (RGCs), the $GABA_A$R-abundant output retinal neurons that transmits signals from retina to the brain. We first compared the behavior of *trans*-dominant and UV-pre-illuminated, *cis*-dominant MPC088. We also attempted experiments in which UV illumination was delivered to initially *trans*-dominant compound in real time, i.e., during RGC recording.

4.5.1 Isomer-dependence of the potentiating effect of MPC088

When presented to single dissociated RGCs obtained from rat retina, *trans*-dominant MPC088 exhibited a concentration-dependent enhancement of the response

elicited by 2 μM GABA, a subsaturating concentration of GABA (Fig. 4.5.1A). At 1 μM, *trans*-dominant MPC088 produced only a modest (~1.5-fold) potentiation of the GABA response, whereas at 30 μM, a marked >7-fold average potentiation was exhibited. *Cis*-dominant MPC088 generated by UV pre-illumination showed a substantially reduced enhancement effect. Specifically, 10 μM *trans*-dominant MPC088 produced, on average, an approximately 5-fold potentiation of the GABA response, whereas *cis*-dominant MPC088 exhibited a much less (~2-fold) potentiation (Fig. 4.5.1B).

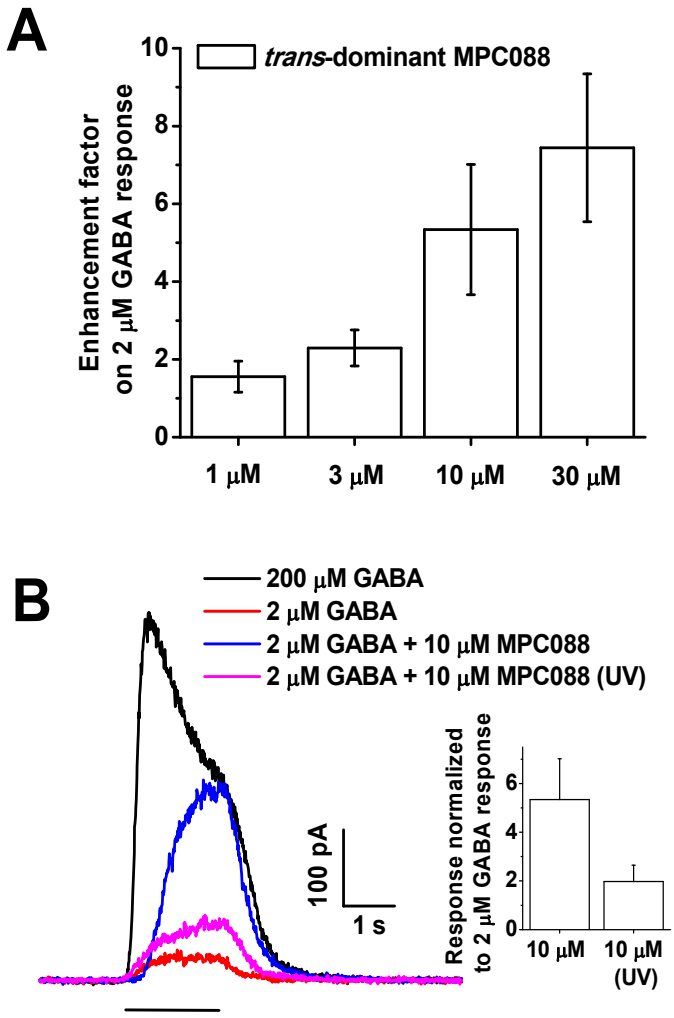

Fig. 4.5.1: Potentiating activity of *trans*- and *cis*-dominant MPC088 on RGCs. (A) Potentiation data obtained with *trans*-dominant MPC088. Columns left to right: enhancement factor at 1, 3, 10 and 30 μM. Data obtained from 3-6 cells for each column. (B) Potentiation data obtained with *trans*- and *cis*- dominant MPC088. The *cis*-dominant preparation was obtained by pre-treating *trans*-dominant MPC088 with UV light for 5 min. Representative responses were obtained from a single cell treated with 200 μM GABA (*black*), 2 μM GABA (*red*), 2 μM GABA co-applied with 10 μM of *trans*-dominant (*blue*) or *cis*-dominant (*magenta*) MPC088. *Inset*: Aggregate data for the enhancement factor determined with *trans*- and *cis*-dominant MPC088 (*left* and *right* bars, respectively) ($p = 0.003$; $n=6$).

4.5.2 Isomer-dependence of the activating effect of MPC088

In the absence of co-applied GABA, *trans*- and *cis*- dominant MPC088 also exhibited differential behavior on isolated retinal ganglion cells. At 30 μM, *trans*-dominant MPC088 alone produced a small membrane current whose peak amplitude amounted, on average, to 5% of the cell's response to 200 μM GABA (Fig. 4.5.2 Inset). However, at 60 μM, the agonist effect increased to 43 ± 9% of the response to 200 μM GABA (n = 7), and pre-treatment of *trans*-dominant MPC088 with UV light reduced this agonist activity by 88 ± 6% ($p = 0.002$; n = 4) (Fig. 4.5.2). The solubility limit of MPC088 in Ringer solution (typically, ~60 μM) made difficult the determination of activity of the compound at higher concentrations.

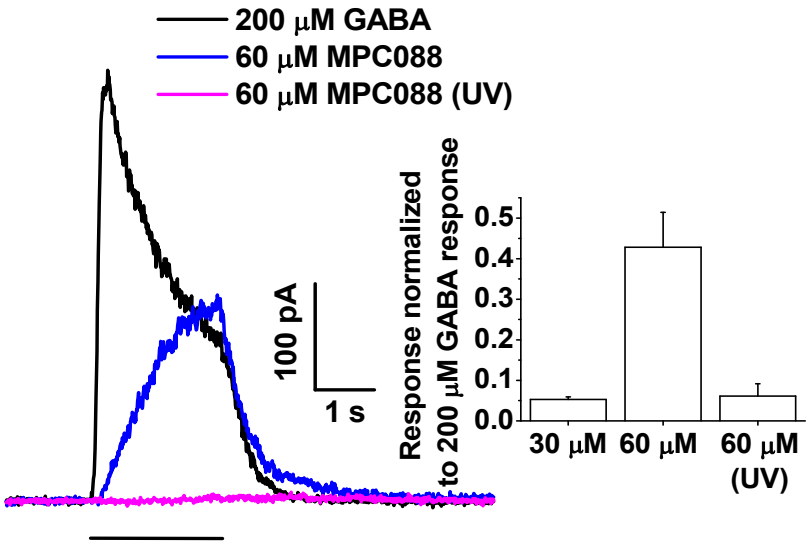

Fig. 4.5.2: Direct activation data obtained with *trans*- and *cis*-dominant MPC088 from RGCs. Representative responses obtained from a cell treated with 200 μM GABA (*black*), 60 μM of *trans*-dominant (*blue*) and 60 μM of *cis*-dominant (*magenta*) MPC088. *Inset*: Aggregate data for direct activation by MPC088 (mean ± SD). *Left*, *middle* and *right* bars show results obtained, respectively, with 30 μM *trans*-dominant (n=3), 60 μM *trans*-dominant (n=7), and 60 μM *cis*-dominant MPC088 (n=4).

4.5.3 Effect of picrotoxin on MPC088 activity

To confirm that the observed activity of MPC088 on retinal ganglion cells was indeed mediated by $GABA_AR$s, we examined the effect of PTX, a $GABA_AR$ channel blocker, on the potentiating and direct activation properties of *trans*-dominant MPC088 on ganglion cells. As observed in the experiment of Fig. 4.5.3A and 4 others of similar

design, PTX at 100 μM decreased the response to co-applied 2 μM GABA and 10 μM *trans*-dominant MPC088 by 94 ± 1% (n = 5). 100 μM PTX also reduced the response to 60 μM *trans*-dominant MPC088 alone by 95 ± 2% (n = 4; Fig. 4.5.3B). This virtually complete elimination, by PTX, of the ganglion cell response to MP088 + GABA or MPC088 alone strongly suggests that $GABA_A$Rs mediate the potentiation and direct activation effects of *trans*-MPC088.

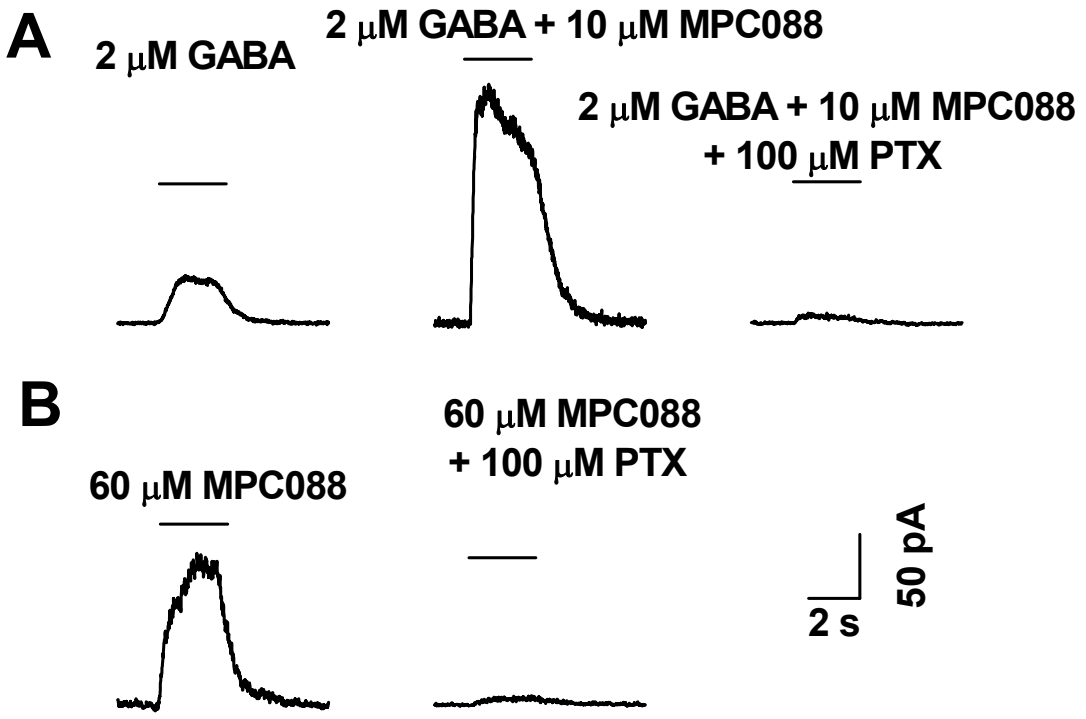

Fig. 4.5.3: Inhibitory effect of PTX on the action of *trans*-dominant MPC088 on the RGC. Representative data obtained from a single cell. (A) Responses to 2 μM GABA, and to (2 μM GABA + 10 μM *trans*-dominant MPC088) without (*left*) and with (*right*) co-applied 100 μM PTX. (B) Responses to 60 μM *trans*-dominant MPC088 without (*left*) and with (*right*) 100 μM PTX.

4.5.4 Effect of real-time UV illumination on MPC088 activity

Having demonstrated the differential behavior of *trans*- and *cis*-dominant MPC088, we explored the effects of real-time UV illumination on the cell during *trans*-

MPC088 perfusion. In the first experiment, we examined responses elicited by 40-s co-application of 2 μM GABA and 10 μM *trans*-dominant MPC088, in the presence of UV light pulses of various durations (1-3 s). Here, UV light produced a slow upswing in the response, distinct from the reducing effect of UV–triggered photo-isomerization observed on oocytes. In control experiments where cells were presented with medium containing GABA alone or no pharmacological agents, we observed a similar outward current during the period of UV presentation, indicating it as an intrinsic response of retinal ganglion cells to 365 nm UV light. This UV-induced intrinsic response obtained in the presence of GABA alone is illustrated in Fig. 4.5.4; that obtained with co-applied MPC088 is evident in Fig. 4.5.5B (note the upswing in the current upon UV illumination).

Fig. 4.5.4: Intrinsic response of RGCs to UV illumination. Representative data obtained in the presence of 2 μM GABA. UV illumination induced a slow outward membrane current at the holding potential of 0 mV. Membrane current recovered to the pre-UV level after termination of UV exposure.

Further, this UV-generated response appeared non-saturable, as indicated by the continuous slow increase in the response throughout the prolonged period of UV illumination (>10 s) observed in several experiments (data not shown). The slow development and non-saturability resemble the characteristics of the increase in membrane current induced by UVA (340-380 nm) light in mammalian cell lines, as reported by Mendez and Penner [112]. In this study, they investigated the UV-induced current ubiquitous to mammalian cell lines. They found that this current is non-selective for cations, can include a contribution from Ca^{2+}, and is inhibited by trivalent cations,

e.g., Gd^{3+} and La^{3+}. To test whether Gd^{3+} inhibited the UV-elicited response of RGCs, we supplemented the perfusing Ringer with 100 μM $GdCl_3$ and recorded the response in the presence of UV. The results showed that $GdCl_3$ exhibited little if any effect on the UV-generated membrane current. Since brief repetitive UV illuminations did not significantly alter responses to subsequently applied GABA or MPC088, and because the focus of our study was on the effect of UV specifically on MPC088 elicited responses, we did not further investigate this UV-triggered response of RGCs. An additional reason for not pursuing this issue was that for the ultimate goal of clinical application in vision restoration, more structural modifications will be made on MPC088-like compounds to yield red-shifted peak absorption wavelength. For such red-shifted compounds, the cell's native response to UV may not present a problem due to the longer stimulating wavelength.

The lack of de-potentiation by UV with continuously perfusing MPC088 leaves open the possibility that the UV-generated *cis*-isoform was quickly diluted and displaced by constant supply of *trans*-dominant compound before a change in response could

occur. Therefore, we designed experiments to examine MPC088 activity in static bathing, similar to that observed in oocyte experiments (e.g., Fig. 4.3.10). However, the large size of the dish regularly used for RGC recording precluded rapid switching of perfusing medium (Ringer to test solution), and thus presented a hurdle to establishing differing static environment of test agents. To address this issue, we replaced our regular recording dishes (30 mm in diameter) with custom-made dishes modified to have a considerably smaller inner diameter (6 mm) and thus a suitably small chamber (volume ~60 μL). With the system's perfusion rate of 17 μL per second and on a first-order approximation for the solution exchange kinetics, it should require ~15 s for a near-complete replacement of the chamber solution upon switch of the perfusing channel.

A typical experiment using these small-volume dishes is presented in Fig. 4.5.5. In this experiment, the cell was initially superfused with regular Ringer solution, followed by a ~20 s period of perfusion with test solution containing *trans*-dominant MPC088 and GABA, after which the cell remained statically bathed in the test agents.

UV illumination was presented during the static bathing, at different phases of development of the MPC088-enhanced GABA current, e.g., during the desensitizing phase and the fully desensitized plateau phase. The period of static bathing was followed by perfusion with fresh MPC088-supplemented GABA solution and, finally, with standard Ringer. The results showed that response to co-applied 2 μM GABA and 7 μM *trans*-dominant MPC088 underwent pronounced desensitization. Presentation of UV during either the desensitizing or the plateau phase failed to produce a significant further reduction in response amplitude. However, upon the resumption of perfusion with fresh test mixture, the response obtained with UV exposure presented during static bathing exhibited a marked increase (3.0 ± 1.0 fold; n = 3; Fig. 4.5.5B, red box) in amplitude, by contrast with that obtained without UV illumination (1.3 ± 0.1 fold; n = 3; Fig. 4.5.5A, red box).

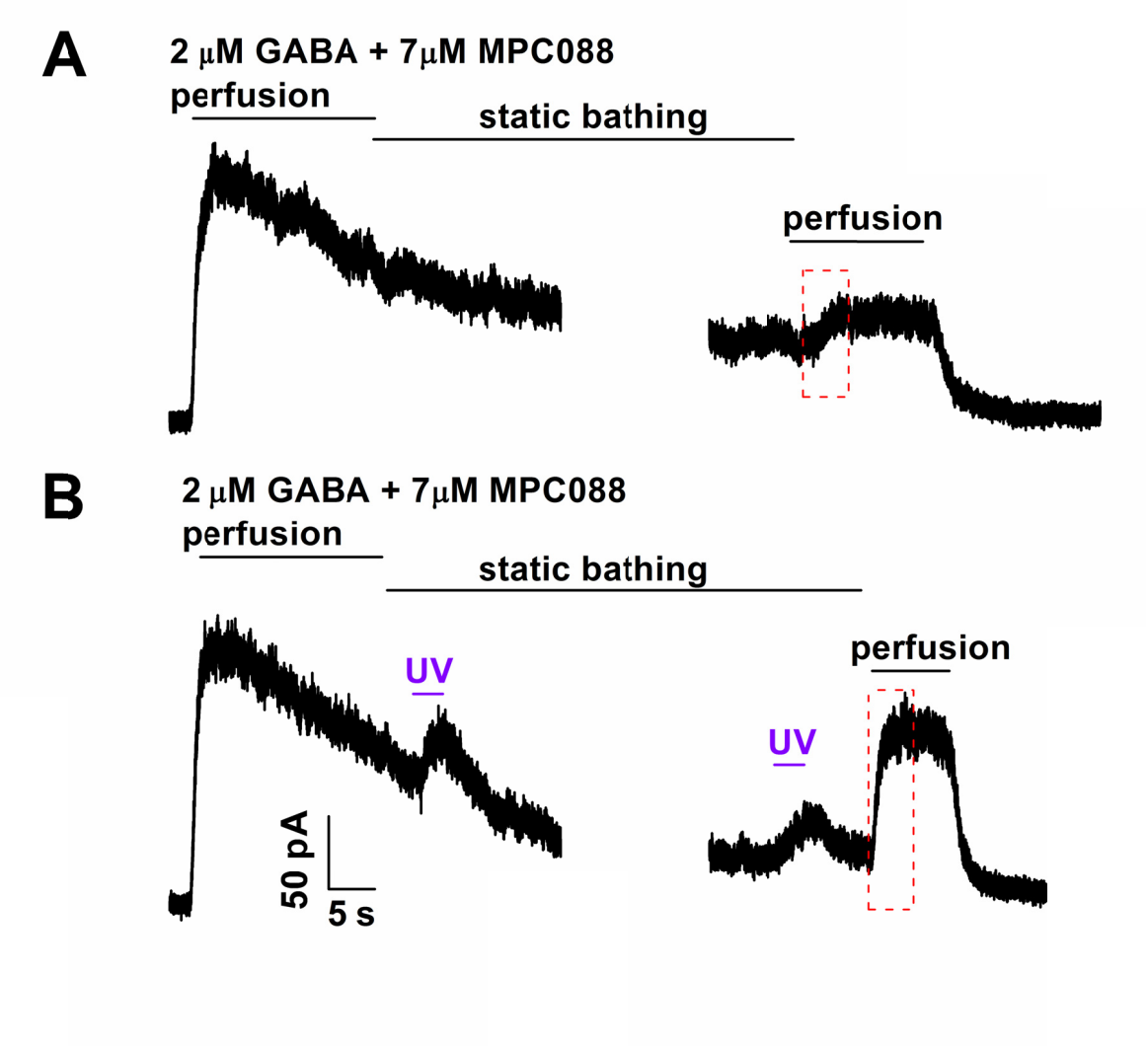

Fig. 4.5.5: Effect of UV illumination during static bathing of MPC088-containing test solution. Representative data in A and B obtained from a single RGC, in temporal order, with perfusion, static bathing and subsequent perfusion of 2 μM GABA + 7 μM *trans*-dominant MPC088. (A) Responses obtained in the absence of UV. Left and right responses separated by ~5 s of static bathing. The response recorded at the transition from static bathing to perfusion is identified by the dotted rectangle. (B) Responses obtained with UV illumination introduced during the static bathing period.

We considered two possible interpretations of these observations just described. On the first of these, (i) the initially perfused *trans*-dominant MPC088 was converted to *cis*-isoform by UV, (ii) this conversion to *cis* drove the $GABA_AR$s out of the desensitized state, but (iii) the low activity of the *cis*-bound re-sensitized state yielded little or no change in amplitude. Therefore, the receptors were readily responsive to *trans*-isomers upon resumption of fresh MPC088 perfusion, consistent with the observed increase in membrane current. By contrast, without UV exposure, most of the *trans*-MPC088 bound receptors were desensitized at the time of transition from static bathing to perfusion, and thus did not exhibit a substantial change in membrane current. The second possibility is that UV illumination perturbed $GABA_AR$s in a manner that yielded a transient enhancement in their activity, as represented by the increased response to subsequently applied *trans*-dominant MPC088. To test this second possibility, we examined the action of GABA on UV-illuminated cells. The results showed that UV exposure did not alter the desensitized GABA response upon resumption of perfusion (Fig. 4.5.6). This finding argues against the notion of a UV-

triggered hyper-activity of the receptors and favors the possibility that real-time UV illumination photo-converts *trans*-isoform MPC088 to *cis* and promotes recovery of the $GABA_AR$s from the desensitized state.

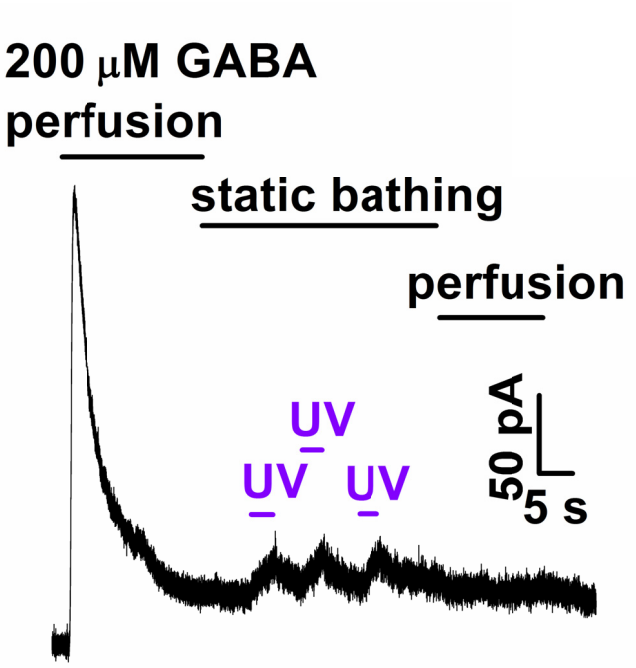

Fig. 4.5.6: Effect of UV illumination on subsequent GABA response. Representative data obtained, in temporal order, with perfusion, static bathing and subsequent perfusion of 200 μM GABA. UV illumination presented during static bathing period.

In summary, this section shows the differential $GABA_A$-specific activity of *trans*-dominant and UV pre-illuminated *cis*-dominant MPC088 on dissociated RGCs. Further, real-time UV illumination delivered during static bathing of the RGC with MPC088, by converting *trans*-MPC088 to the *cis*-isomer, appears to induce the recovery of $GABA_A$Rs from the desensitized state initially generated by exposure to the *trans*-isomer.

CHAPTER 5

DISCUSSION

5.1 Activity of propofol on $GABA_A$ receptors of retinal bipolar cells

5.1.1 Evidence for $GABA_A$ potentiation

The results provide direct evidence for a potentiating effect of propofol, a well-studied allosteric $GABA_AR$ modulator, on the GABA-elicited response of retinal bipolar cells. Four types of evidence lead us to conclude that this action of propofol is mediated largely or entirely by the $GABA_ARs$ of the bipolar cell. First, propofol potentiates the GABA response obtained in the presence of the $GABA_C$ antagonist TPMPA (Fig. 4.1.3B). Second, this response is virtually entirely eliminated by the $GABA_A$ antagonist bicuculline (Fig. 4.1.3C). Third, propofol also potentiates the response to THIP, a compound that on retinal bipolar cells activates only $GABA_ARs$ (Fig. 4.1.3D). Fourth, propofol does not enhance the response to 5Me-I4AA, a $GABA_C$-selective agonist (Fig. 4.1.2).

The results presented in (Fig. 4.1.3) indicate that, under the present experimental conditions using 10 μM GABA as a nominal agonist concentration, 100 μM TPMPA suppresses, on average, 83% of the GABA response. Thus, the RBC $GABA_A$Rs contribute only a minor fraction (~17%) of the overall GABA-elicited response. This observation is consistent with results obtained by Euler and Wässle [62], who isolated $GABA_A$–mediated responses with 3-aminopropyl-(methyl)phosphinic acid (3-APMPA), a $GABA_C$ antagonist, and examined responses elicited by GABA *vs*. co-applied (GABA and 3-APMPA) in rod bipolar cells in the rat retinal slice preparation.

5.1.2 Preservation of single-channel conductance

In previously studied systems, the effect of propofol on the GABA response function has been observed to reflect an increased sensitivity of the receptor to agonist rather than to an increase in the maximal, saturating membrane current [113]. On this basis, the potentiating effect of propofol has been attributed primarily to an action of the compound in increasing the probability of channel opening as opposed to an increase in

the conductance of individual channels [113]. Consistent with this finding and interpretation, our results obtained with 10 μM GABA and 30 μM GABA indicated a decreased potentiation factor associated with an increased GABA concentration. In principle, determining whether propofol increases $GABA_A$ single-channel conductance in the bipolar cell could come from single-channel recording of propofol's effect when co-applied with GABA. However, we found such a measurement to be difficult in the present system. In the present Fig. 4.1.4 experiments, we analyzed response noise to derive values for single-channel conductance in a response regime well below saturation. Under these conditions, propofol at 150 μM, a concentration with substantial potentiating activity, produced little, if any, change in the single-channel conductance of the (presumably $GABA_A$) receptors that mediate the propofol-dependent increase. We thus conclude that, as in other cell types, the mechanism of propofol potentiation of bipolar cell $GABA_A$Rs is unlikely to involve an increase in single-channel conductance.

5.1.3 Complex effects on $GABA_A$ receptors

Propofol at higher concentrations, in addition to causing a potentiation of the GABA-elicited response, induced a pronounced subsequent decrease from peak amplitude (i.e., development of a sag in the response). Repeated applications of the propofol-containing test mixture progressively increased the magnitude of this sag and a rebound of current on the cessation of propofol application (Fig. 4.1.5-6). Further, in the presence of propofol at fixed concentration, responses elicited by 30 μM GABA exhibited a more pronounced response sag than that exhibited by 10 μM GABA, indicating a substantial contribution of $GABA_AR$ desensitization, a well-established property of $GABA_ARs$, to the observed sag. However, the desensitization alone cannot fully explain the rebound current present immediately upon cessation of propofol perfusion, which raised the possibility of a receptor-blocking action of propofol. A simple possible basis of this rebound is the rapid dissociation of a blocker (propofol) from GABA-bound receptors that are already in the active state. Such a blocking activity of propofol is also consistent with the results obtained with propofol or (G + T) in the

perfusing medium (Fig. 4.1.7A-C, respectively). In the former case, the evident elimination of the rebound component is consistent with the maintained presence of propofol during response deactivation; in the latter case, removal of the putative blocker (propofol) with maintained presence of GABA readily explains the observed increase in size of the rebound component. Previous studies have reported an inhibitory effect of high concentrations of propofol at $GABA_A$ receptors [94, 96] and have shown that etomidate, a compound whose binding site overlaps with (albeit is distinct from) the propofol binding site, can at high concentration exhibit channel-blocking activity [91, 103, 104].

5.1.4 Dependence of activity on repeated applications

The above discussion of the Fig. 4.1.5-6 data has pointed out the progressive increase in propofol activity with repeated brief (2-s) applications of (G + T + P) despite relatively long (~15-25 s) periods of Ringer perfusion between applications. The progressive nature of this increase indicates an effective memory of the potentiation

process, that is, an effect of preceding (G + T + P) applications that lingers over the ~15- to 25-s washout period. By contrast, Fig. 4.1.7C-D indicate a recovery of the (G + T) response to the unpotentiated level on a subsecond time scale after propofol cessation, evidenced by the deactivation time constant of ~400 ms. This contrast in the time scales of potentiation memory and return to the unpotentiated state suggests the occurrence of a propofol-binding event that is inert (does not in itself generate the potentiated state) but that, on further presentation of propofol, directly or indirectly leads to receptor potentiation. As the propofol-binding cavity likely resides in the upper region of the transmembrane domain of $GABA_AR$s [93], one possibility is that the lipid layer surrounding the transmembrane domain affords a buffer zone that retains the lipophilic propofol molecules and slows their diffusion to the binding cavity. On this possibility, the dependence of propofol potentiation on its repeated presentation reflects the lipid-dependent slowing of propofol binding to $GABA_AR$s, and the potentiation observed with further propofol delivery corresponds to a condition of near-saturation of the buffering process.

A second, quite different, possibility is that a site on the $GABA_AR$ itself, on occupation by propofol, produces a “primed” but unpotentiated state of the receptor. On this latter possibility, initial brief applications of (G + T + P) or initial exposures to propofol in the perfusing medium generate a propofol-bound, primed receptor state that exhibits a pronounced, rapidly developing potentiated response on subsequent exposure to (G + T + P). For example, if the propofol-sensitive $GABA_ARs$ of the bipolar cells contain two propofol binding sites, the primed (but unpotentiated) and potentiated receptor states might correspond respectively, to propofol binding at one versus both sites. That is, the potentiated receptor state could correspond with propofol binding at both high-affinity “priming” site and low-affinity “potentiating” site, and transition of the receptor from the potentiated to unpotentiated (but primed) state could reflect propofol dissociation only from the low-affinity site.

5.1.5 Significance of propofol study on retinal bipolar cells

This study advanced our understanding of the activity of propofol on rat RBCs and suggested the feasibility of employing a propofol-based allosteric $GABA_A$ ligand to modulate the activity of native retinal neurons. An interesting question not addressed by our study is whether propofol potentiation of RBC $GABA_A$ receptors contributes to the effects of propofol on the *b*-wave of the full-field ERG and the p1 component of the multifocal ERG reported previously [83, 84, 114]. Propofol is known to exert effects on other receptor/channel types, including glycine receptors and sodium channels. Inasmuch as retinal neurons have receptors identical or similar to these additional targets [115-121], the effect of propofol on the ERG may in substantial part reflect modulation of these and/or other "non-$GABA_A$" mechanisms. Future studies testing the effect of propofol in combination with other agents that suppress specific ERG components [122-124] may help to identify the possibly multiple mechanisms of action of propofol in the retina. Reciprocally, clarification of these mechanisms could enable

the use of propofol as a pharmacologic tool for investigating signaling pathways within the retina.

5.2 Photo-control of recombinant $GABA_A$ receptors

5.2.1 Potent and reversible photo-regulation by free MPC088

Our data demonstrate that MPC088, a photoisomerizable derivative of propofol, exerts a highly potent and light-sensitive regulation of $\alpha_1\beta_2\gamma_2$ $GABA_AR$ activity, by means of both modulation (potentiation) and direct activation of the receptors (Fig. 4.3.10-12). The fact that light of differing wavelength can reversibly and in a quasi-stable manner inter-convert the relatively active and inactive isomers of MPC088 distinguishes the compound from previously reported photosensitive caged $GABA_AR$ ligands in which light activates the receptor by irreversibly eliminating a protective (caging) structure from the ligand [125-127]. In addition to conferring pronounced light-sensitivity to the receptor, MPC088 in its active (*trans*) form exhibits a potency of both modulatory and direct activating effects that is ~25 times as great as those of propofol

itself (Fig. 4.3.4-5). Previous studies have identified several mutations on the β subunit of $GABA_AR$s that substantially affected propofol activity, e.g., M286W, N265M, and Y444W [88-90]. Our data, however, show that the activity of MPC088 is much less influenced by these mutations (Fig. 4.3.7), suggesting an interaction of MPC088 with the binding cavity that is likely different from that of propofol. Additional data indicate that the propofol moiety is required for activity, but it remains to be determined whether the high potency of MPC088 and its reduced sensitivity to alteration of the propofol binding region are due, in addition, to specific receptor-binding interactions with the butyryl, azobenzene and/or ethylenediamine moieties of the compound.

5.2.2 Photo-regulation by covalently tethered MPC100

We have also examined the properties of MPC100, a tetherable derivative of MPC088 that, via its terminating maleimide group, covalently binds to the cysteine-substituted γ-79C mutant form of the $\alpha_1\beta_2\gamma_2$ $GABA_AR$.

The tethered compound exhibits persistent, light-regulated potentiating and activating effects on $GABA_ARs$ (Figs. 4.4.2, 4.4.4 and 4.4.6), further demonstrating the feasibility of anchoring an MPC088-based structure to the receptor protein. Furthermore, the UV-triggered de-potentiation exhibited by free MPC100 on WT $GABA_ARs$ exhibits a dependence on UV light intensity that differs from the UV-dependence exhibited by MPC100 tethered on γ-79C mutant (Fig. 4.4.8). In addition, on γ-79C mutant receptors that were pre-tethered by a biotin-maleimide compound, the MPC100-potentiated GABA response did not exhibit a strong dependence on UV intensity, consistent with the notion that occupation of the benzodiazepine binding site allosterically increases the binding affinity of propofol and therefore prolongs ligand dissociation [78, 111]. Together, these findings suggest that the response de-potentiation is rate limited, in part, by the dissociation of the propofol moiety in the *trans*-isoform from the binding cavity, and that the difference in de-potentiation rate between free and tethered compound reflects their differential dissociation rate.

5.2.3 Significance of MPC100 and future tether strategy

The tetherable MPC100 may have application in approaches that involve neuronal expression of a genetically engineered $\alpha_1\beta_2\gamma_2$ $GABA_AR$ to which the photoswitch could be anchored, as in previous studies of potassium channels and L-glutamate receptors [47, 48, 59]. Furthermore, by contrast with previous structures designed for photo-control of transmembrane ion channels [47, 48, 52, 59], a relatively long linear chain (PEG24) separates the regulating structure (MPC088 moiety) from the tethering moiety (maleimide). Beyond demonstrating that a long and flexible hydrophilic linker (and resultant high conformational entropy) can preserve substantial physiological activity of the distal MPC088 moiety, the properties exhibited by MPC100 suggest the potential workability of other, similarly remote locations on the $GABA_AR$ itself, or at a site on an affinity reagent designed for binding to the extracellular domain of the native $GABA_AR$, that could be engineered as a tethering site. As a general route to controlling neuronal activity with a modulating ligand, covalent binding of an introduced reactive (e.g., maleimide-terminated) ligand to an engineered receptor site offers the advantage,

in principle, of defining the precise receptor subtype [72] on which the ligand will act. However this approach presents possible challenges relating to the need for inducing expression of the engineered receptor in the target cell type, and for avoiding problematic binding of the reactive ligand to unintended sites (e.g., other cysteine-containing surface proteins) on both the target cells and others. For the ultimate clinical goal of vision restoration, the induced expression of non-native cysteine-containing receptors in retinal neurons has multiple drawbacks, and we are instead pursuing an approach that involves the anchoring of light-regulating structures to native $GABA_AR$s via an antibody-based affinity reagent. In this design, MPC088-based structures are tethered onto the antibody that binds, specifically, to a site on the extracellular domain of $GABA_AR$s. Research to develop such antibody structures is in progress in our laboratory.

5.3 Application of MPC088 on retinal ganglion cells

5.3.1 Isomer-dependent activity of MPC088

$GABA_A$Rs of retinal ganglion cells are important mediators of inhibitory visual signaling in retina [128-131] and are sensitive to propofol modulation [132]. As in the heterologously expressed system studied here, $GABA_A$Rs on native rat RGCs are potentiated and directly activated specifically by the *trans* isomer of MPC088 (Fig. 4.5.1-2). The intrinsic response of ganglion cells to UV irradiation, and the extensive receptor desensitization exhibited during static bathing of GABA and MPC088, presented difficulties for our original experimental aim to determine the effect of real-time UV illumination on *trans*-dominant MPC088 applied to the ganglion cell. Yet the preliminary data did indicate that *trans*-to-*cis* photoisomerization of the compound under UV produced the recovery of receptors from the desensitized state (Fig. 4.5.5). These observations further suggest that in diseases that involve degeneration of the retina's rod and cone photoreceptors, structures related to MPC088 may have application as a

vision restoration therapy, by establishing a photosensitivity of inner retinal neurons that effectively bypasses the dysfunctional rods and cones.

5.3.2 Tuning photoisomerization characteristics of MPC088-based structures for vision-related applications

The ultimate clinical goal of the MPC088-related work described in this thesis, that of restoring visual perception to blind patients, will require the addressing of multiple key issues. These include the modification of the MPC088 structure to accomplish a red-shifting of the photoisomerizing wavelength, and the boosting of light sensitivity. The absorption spectra of the photo-sensitive compounds we have synthesized so far, including the most promising MPC088, all exhibited a maximum absorption peak in the UV range (338 nm), therefore a shift in the absorption peak to longer wavelength, ideally in the visible range (~500 nm) is desirable for the clinical application. To this end, our chemistry colleagues are attempting to substitute the ortho-positions of the azobenzene moiety with electron-donating groups, which, based on the

findings of Sadovski *et al*. [133], are expected to substantially red-shift the photoisomerization peak.

In a functional retinal photoreceptor, phototransduction, the process of converting light signals to electrochemical signals that can be transmitted to secondary retinal cells, consists of a multi-stage biochemical amplification system [134, 135]. At the first stage, each photo-activated rhodopsin activates multiple molecules of transducin (~100-fold), and at the second stage, each PDE enzymatically cleaves multiple cGMPs (~1000-fold), leading to closure of multiple cation channels. These amplifications naturally yield a very high sensitivity of the signal transduction to photon absorption, permitting the generation of a measurable response to a single photon. To function at physiologically workable (non-damaging) light levels, our nano-scale, receptor-anchored photosensors must have sufficiently high photon absorption efficiency. In light of the enhanced local electromagnetic fields produced by strong interaction between light and metal nanoparticles, we have proposed to interface our MPC088-like propofol-azobenzene conjugates with metal nanoparticles as an approach

to enhance their photosensitivity by a plasmon resonance mechanism. Such an enhanced local light intensity would facilitate the photoisomerization of the azobenzene group and thereby increase the efficiency of receptor modulation.

It is well established that plasmons, the coherent oscillations of the surface electrons of metal nanostructures (e.g., nanoparticles, nanorods), when excited by the specific wavelengths, create intense electromagnetic fields in close proximity (~nm) to the structure surface [136]. This enhanced near-field wave can influence the spectrometric and fluorescent properties of organic molecules (e.g., photochromes) that are positioned in close proximity or adsorbed to the nanoparticle, which gives rise to physical phenomena such as surface-enhanced Raman scattering (SERS) [137, 138] and enhanced fluorescence [139-141]. The localized intense electromagnetic field can be tuned by controlling the particle material, shape and size of the particle, and the refractive index near the particle surface. For a spherically shaped nanoparticle, increased diameter and higher local refractive index result in longer resonance wavelength. Silver nanoparticles typically exhibit a shorter peak resonance wavelength

(~400 nm at 10 nm diameter) than gold nanoparticles of equal size. Close association of these nanoparticles has been experimentally found to produce greatly intensified plasmon fields in the inter-particle regions, also termed “hot spots” [142-144]. Several pioneering studies on plasmon-assisted azo group-involving chemistry processes have been reported [145-147]. Most of these studies have employed silver nanoparticles, due to the proximity of their plasmon wavelength to the peak absorption wavelength of azo groups. By doping azo-containing polymer films with silver nanoparticles, Zhou *et al.* achieved up to 50% enhancement of the light-induced re-orientation rate of azo groups [145]. More recently, Stamplecoskie *et al*. demonstrated that an enhanced plasmon field around silver nanoparticles markedly facilitates triacrylate polymerization, likely by promoting the decomposition of AIBN, an azo-containing free radical initiator of polymerization [146]. The investigators reasoned that the resultant 8-10 nm polymer structure encapsulating the nanoparticles effectively mapped the plasmon field of their silver nanoparticles. Of particular interest to our study of azobenzene-containing MPC088 and related compounds is the study reported by Shin *et al*., in which they

described the photoisomerization behavior of azobenzene-alkanethiol conjugated to small gold nanoparticles of 2 nm in diameter [147]. They found that both the *trans* to *cis* photoisomerization rate and the *cis* to *trans* thermal relaxation rate of azobenzene became accelerated (~3 times faster for the former and ~2 times faster for the latter) when the azobenzene was tethered on nanoparticle surface.

Recently, our chemistry colleagues successfully synthesized MPD099, a MPC088-like compound linked via a 12-PEG chain to a moiety (lipoic acid) that can serve to conjugate the compound with a metallic nanoparticle. Like MPC088, MPD099 in *trans*-configuration exhibited a marked potentiating effect on $\alpha_1\beta_2\gamma_2$ $GABA_A$Rs, where 1 μM *trans*-dominant MPD099 produced a ~30-fold potentiation of the 3 μM GABA response. A significant degree of potentiating strength (~25%) remained when 1 μM MPD099 was conjugated to ~5-nm gold nanoparticles at a valency of 1:100, i.e., 100 MPD099 molecules per particle. Here the choice of gold as the nanoparticle metal was based on its higher stability against oxidization, by comparison with silver. Preliminary spectrophotometric data revealed that *trans* to *cis* photoisomerizing wavelength was not

altered by nanoparticle conjugation, that is, both conjugated and non-conjugated MPD099 exhibited an absorption peak at ~330 nm. However, we did not observe an accelerated photoisomerization rate, which, possibly due to the gap between the photoswitching wavelength (330 nm) and the plasmon resonance wavelength of the gold nanoparticle (550 nm). We anticipate that future work in this line of study could involve reducing the nanoparticle size and substituting gold with silver to achieve shorter resonance wavelength or, when available, using red-shifted MPC088-based photoswitches.

5.4 Potential applications in other neural systems

The wide distribution of $\alpha_1\beta_2\gamma_2$ $GABA_A$ receptors in tissues of the central nervous system (CNS) and the clinical importance of propofol encourage the investigation of MPC088 as a pharmacological tool in studies of other CNS neural circuits in addition to retina. Toward this end our colleagues at UCLA, Dr. Thomas S. Otis and Dr. Shlomo S. Dellal in the Department of Neurobiology, have demonstrated

that, in the presence of MPC088, light reversibly modulates GABA currents in cerebellar Purkinje neurons (PNs) and that the compound can be used to reversibly control spiking output of PNs. Given that PNs are intrinsically active at constant rates [148, 149], they are useful for examining light modulation because their spike rate provides a continuous readout of excitability.

In providing the ability to control circuit excitability with spatial and temporal precision, photo-switchable modulators of neural activity open new possibilities for exploring the links between neuronal activity and behavior. For example, MPC088 and related diffusible compounds could allow regional induction of anesthesia through the use of implanted optical fibers or a head-fixed preparation. This approach could be used to explore which brain regions are most important for anesthesia and sedation. Clinical contexts in which a photo-switchable $GABA_AR$ modulator might be useful include diseases of hyperexcitability, such as epilepsy [77, 101, 150-152]. Propofol is known to be an effective therapeutic for intractable epilepsy, although side effects are a concern [77, 79, 102]. Photo-switchable propofol analogs, in combination with local optical

stimulation [23] and appropriate electrical monitoring, might enable both a reduction of side effects in treating epilepsies, and perhaps allow optically-regulated utilization of the modulator specifically during bouts of hyperexcitability. Furthermore, even with a diffusible modulator, focally directed illumination could perhaps allow spatially restricted actions of the anti-epileptic drug around seizure foci.

CITED LITERATURE

1. Kolb, H., *Simple Anatomy of the Retina*, in *Webvision: The Organization of the Retina and Visual System*, H. Kolb, E. Fernandez, and R. Nelson. 1995. http://webvision.med.utah.edu/book/part-i-foundations/simple-anatomy-of-the-retina/.

2. Wong, I.Y., et al., *Promises of stem cell therapy for retinal degenerative diseases.* Graefes Arch Clin Exp Ophthalmol, 2011. **249**(10): p. 1439-48.

3. Busskamp, V., et al., *Genetic reactivation of cone photoreceptors restores visual responses in retinitis pigmentosa.* Science, 2010. **329**(5990): p. 413-7.

4. Heckenlively, J.R., *RP cone-rod degeneration.* Trans Am Ophthalmol Soc, 1987. **85**: p. 438-70.

5. Jackson, G.R., C. Owsley, and C.A. Curcio, *Photoreceptor degeneration and dysfunction in aging and age-related maculopathy.* Ageing Res Rev, 2002. **1**(3): p. 381-96.

6. Curcio, C.A., C. Owsley, and G.R. Jackson, *Spare the rods, save the cones in aging and age-related maculopathy.* Invest Ophthalmol Vis Sci, 2000. **41**(8): p. 2015-8.

7. Marc, R.E., et al., *Neural remodeling in retinal degeneration.* Prog Retin Eye Res, 2003. **22**(5): p. 607-55.

8. Olson, J.H., J.C. Erie, and S.J. Bakri, *Nutritional supplementation and age-related macular degeneration.* Semin Ophthalmol, 2011. **26**(3): p. 131-6.

9. Coleman, H. and E. Chew, *Nutritional supplementation in age-related macular degeneration.* Curr Opin Ophthalmol, 2007. **18**(3): p. 220-3.

10. McGill, T.J., et al., *Transplantation of human central nervous system stem cells - neuroprotection in retinal degeneration.* Eur J Neurosci, 2012. **35**(3): p. 468-77.

11. Sahni, J.N., et al., *Therapeutic challenges to retinitis pigmentosa: from neuroprotection to gene therapy.* Curr Genomics, 2011. **12**(4): p. 276-84.

12. West, E.L., et al., *Manipulation of the recipient retinal environment by ectopic expression of neurotrophic growth factors can improve transplanted photoreceptor integration and survival.* Cell Transplant, 2012. **21**(5): p. 871-887.

13. Schwartz, S.D., et al., *Embryonic stem cell trials for macular degeneration: a preliminary report.* Lancet, 2012. **379**(9817): p. 713-20.

14. Singh, M.S. and R.E. MacLaren, *Stem cells as a therapeutic tool for the blind: biology and future prospects.* Proc Biol Sci, 2011. **278**(1721): p. 3009-16.

15. Komeima, K., B.S. Rogers, and P.A. Campochiaro, *Antioxidants slow photoreceptor cell death in mouse models of retinitis pigmentosa.* J Cell Physiol, 2007. **213**(3): p. 809-15.

16. Sanz, M.M., et al., *Significant photoreceptor rescue by treatment with a combination of antioxidants in an animal model for retinal degeneration.* Neuroscience, 2007. **145**(3): p. 1120-9.

17. Huang, Y., V. Enzmann, and S.T. Ildstad, *Stem cell-based therapeutic applications in retinal degenerative diseases.* Stem Cell Rev, 2011. **7**(2): p. 434-45.

18. Weiland, J.D., A.K. Cho, and M.S. Humayun, *Retinal prostheses: current clinical results and future needs.* Ophthalmology, 2011. **118**(11): p. 2227-37.

19. Matthaei, M., et al., *Progress in the development of vision prostheses.* Ophthalmologica, 2011. **225**(4): p. 187-92.

20. Stingl, K., et al., *[Subretinal visual implants].* Klin Monbl Augenheilkd, 2010. **227**(12): p. 940-5.

21. Doroudchi, M.M., et al., *Towards optogenetic sensory replacement.* Conf Proc IEEE Eng Med Biol Soc, 2011. **2011**: p. 3139-41.

22. Tomita, H., et al., *Visual properties of transgenic rats harboring the channelrhodopsin-2 gene regulated by the thy-1.2 promoter.* PLoS One, 2009. **4**(11): p. e7679.

23. Lagali, P.S., et al., *Light-activated channels targeted to ON bipolar cells restore visual function in retinal degeneration.* Nat Neurosci, 2008. **11**(6): p. 667-75.

24. Gorostiza, P. and E.Y. Isacoff, *Optical switches for remote and noninvasive control of cell signaling.* Science, 2008. **322**(5900): p. 395-9.

25. Szobota, S. and E.Y. Isacoff, *Optical control of neuronal activity.* Annu Rev Biophys, 2010. **39**: p. 329-48.

26. Caporale, N., et al., *LiGluR restores visual responses in rodent models of inherited blindness.* Mol Ther, 2011. **19**(7): p. 1212-9.

27. Dowling, J., *Current and future prospects for optoelectronic retinal prostheses.* Eye (Lond), 2009. **23**(10): p. 1999-2005.

28. Brindley, G.S. and W.S. Lewin, *The sensations produced by electrical stimulation of the visual cortex.* J Physiol, 1968. **196**(2): p. 479-93.

29. Brindley, G.S. and W.S. Lewin, *The visual sensations produced by electrical stimulation of the medial occipital cortex.* J Physiol, 1968. **194**(2): p. 54-55.

30. Tehovnik, E.J., et al., *Microstimulation of visual cortex to restore vision.* Prog Brain Res, 2009. **175**: p. 347-75.

31. Troyk, P.R., et al., *Intracortical visual prosthesis research - approach and progress.* Conf Proc IEEE Eng Med Biol Soc, 2005. **7**: p. 7376-9.

32. Normann, R.A., et al., *Toward the development of a cortically based visual neuroprosthesis.* J Neural Eng, 2009. **6**(3): p. 035001.

33. Rizzo, J.F., 3rd, *Update on retinal prosthetic research: the Boston Retinal Implant Project.* J Neuroophthalmol, 2011. **31**(2): p. 160-8.

34. Zrenner, E., et al., *Subretinal electronic chips allow blind patients to read letters and combine them to words.* Proc Biol Sci, 2011. **278**(1711): p. 1489-97.

35. Loudin, J.D., et al., *Optoelectronic retinal prosthesis: system design and performance.* J Neural Eng, 2007. **4**(1): p. S72-84.

36. Fenno, L., O. Yizhar, and K. Deisseroth, *The development and application of optogenetics.* Annu Rev Neurosci, 2011. **34**: p. 389-412.

37. Yizhar, O., et al., *Optogenetics in neural systems.* Neuron, 2011. **71**(1): p. 9-34.

38. Haupts, U., et al., *General concept for ion translocation by halobacterial retinal proteins: the isomerization/switch/transfer (IST) model.* Biochemistry, 1997. **36**(1): p. 2-7.

39. Deisseroth, K., et al., *Next-generation optical technologies for illuminating genetically targeted brain circuits.* J Neurosci, 2006. **26**(41): p. 10380-6.

40. Zhang, F., et al., *Channelrhodopsin-2 and optical control of excitable cells.* Nat Methods, 2006. **3**(10): p. 785-92.

41. Boyden, E.S., et al., *Millisecond-timescale, genetically targeted optical control of neural activity.* Nat Neurosci, 2005. **8**(9): p. 1263-8.

42. Zhang, F., et al., *Multimodal fast optical interrogation of neural circuitry.* Nature, 2007. **446**(7136): p. 633-9.

43. Tsubota, T., et al., *Optogenetic manipulation of cerebellar Purkinje cell activity in vivo.* PLoS One, 2011. **6**(8): p. e22400.

44. Doroudchi, M.M., et al., *Virally delivered channelrhodopsin-2 safely and effectively restores visual function in multiple mouse models of blindness.* Mol Ther, 2011. **19**(7): p. 1220-9.

45. Bartels, E., N.H. Wassermann, and B.F. Erlanger, *Photochromic activators of the acetylcholine receptor.* Proc Natl Acad Sci U S A, 1971. **68**(8): p. 1820-3.

46. Lester, H.A., et al., *A covalently bound photoisomerizable agonist: comparison with reversibly bound agonists at Electrophorus electroplaques.* J Gen Physiol, 1980. **75**(2): p. 207-32.

47. Banghart, M., et al., *Light-activated ion channels for remote control of neuronal firing.* Nat Neurosci, 2004. **7**(12): p. 1381-6.

48. Volgraf, M., et al., *Allosteric control of an ionotropic glutamate receptor with an optical switch.* Nat Chem Biol, 2006. **2**(1): p. 47-52.

49. Fortin, D.L., et al., *Photochemical control of endogenous ion channels and cellular excitability.* Nat Methods, 2008. **5**(4): p. 331-8.

50. Janovjak, H., et al., *A light-gated, potassium-selective glutamate receptor for the optical inhibition of neuronal firing.* Nat Neurosci, 2010. **13**(8): p. 1027-32.

51. Farrar, S.J., et al., *Stoichiometry of a ligand-gated ion channel determined by fluorescence energy transfer.* J Biol Chem, 1999. **274**(15): p. 10100-4.

52. Feigenspan, A., H. Wässle, and J. Bormann, *Pharmacology of GABA receptor Cl- channels in rat retinal bipolar cells.* Nature, 1993. **361**(6408): p. 159-62.

53. Qian, H. and J.E. Dowling, *$GABA_A$ and $GABA_C$ receptors on hybrid bass retinal bipolar cells.* J Neurophysiol, 1995. **74**(5): p. 1920-8.

54. Palmer, M.J., *Functional segregation of synaptic $GABA_A$ and $GABA_C$ receptors in goldfish bipolar cell terminals.* J Physiol, 2006. **577**(Pt 1): p. 45-53.

55. Lukasiewicz, P.D., *Synaptic mechanisms that shape visual signaling at the inner retina.* Prog Brain Res, 2005. **147**: p. 205-18.

56. Fletcher, E.L., P. Koulen, and H. Wässle, *$GABA_A$ and $GABA_C$ receptors on mammalian rod bipolar cells.* J Comp Neurol, 1998. **396**(3): p. 351-65.

57. Euler, T. and H. Wässle, *Different contributions of $GABA_A$ and $GABA_C$ receptors to rod and cone bipolar cells in a rat retinal slice preparation.* J Neurophysiol, 1998. **79**(3): p. 1384-95.

58. Frech, M.J. and K.H. Backus, *Characterization of inhibitory postsynaptic currents in rod bipolar cells of the mouse retina.* Vis Neurosci, 2004. **21**(4): p. 645-52.

59. Greferath, U., et al., *Localization of $GABA_A$ receptors in the rat retina.* Vis Neurosci, 1993. **10**(3): p. 551-61.

60. Grigorenko, E.V. and H.H. Yeh, *Expression profiling of $GABA_A$ receptor β-subunits in the rat retina.* Vis Neurosci, 1994. **11**(2): p. 379-87.

61. Enz, R., et al., *Expression of GABA receptor ρ1 and ρ2 subunits in the retina and brain of the rat.* Eur J Neurosci, 1995. **7**(7): p. 1495-501.

62. Yeh, H.H., E.V. Grigorenko, and M.L. Veruki, *Correlation between a bicuculline-resistant response to GABA and $GABA_A$ receptor ρ1 subunit expression in single rat retinal bipolar cells.* Vis Neurosci, 1996. **13**(2): p. 283-92.

63. Hughes, T.E., et al., *Immunohistochemical localization of $GABA_A$ receptors in the retina of the new world primate Saimiri sciureus.* Vis Neurosci, 1989. **2**(6): p. 565-81.

64. Grunert, U., et al., *Parasol ($P\alpha$) ganglion-cells of the primate fovea: immunocytochemical staining with antibodies against $GABA_A$-receptors.* Vision Res, 1993. **33**(1): p. 1-14.

65. Greferath, U., et al., *Localization of $GABA_A$ receptors in the rabbit retina.* Cell Tissue Res, 1994. **276**(2): p. 295-307.

66. Gutiérrez, A., Z.U. Khan, and A.L. De Blas, *Immunocytochemical localization of the α6 subunit of the γ-aminobutyric acid A receptor in the rat nervous system.* J Comp Neurol, 1996. **365**(3): p. 504-10.

67. Lukasiewicz, P.D., *$GABA_C$ receptors in the vertebrate retina.* Mol Neurobiol, 1996. **12**(3): p. 181-94.

68. Lukasiewicz, P.D. and C.R. Shields, *Different combinations of $GABA_A$ and $GABA_C$ receptors confer distinct temporal properties to retinal synaptic responses.* J Neurophysiol, 1998. **79**(6): p. 3157-67.

69. Tian, N., T.N. Hwang, and D.R. Copenhagen, *Analysis of excitatory and inhibitory spontaneous synaptic activity in mouse retinal ganglion cells.* J Neurophysiol, 1998. **80**(3): p. 1327-40.

70. Protti, D.A., H.M. Gerschenfeld, and I. Llano, *GABAergic and glycinergic IPSCs in ganglion cells of rat retinal slices.* J Neurosci, 1997. **17**(16): p. 6075-85.

71. Trapani, G., et al., *Propofol in anesthesia. Mechanism of action, structure-activity relationships, and drug delivery.* Curr Med Chem, 2000. **7**(2): p. 249-71.

72. Olsen, R.W. and W. Sieghart, *$GABA_A$ receptors: subtypes provide diversity of function and pharmacology.* Neuropharmacology, 2009. **56**(1): p. 141-8.

73. Amin, J. and D.S. Weiss, *$GABA_A$ receptor needs two homologous domains of the β-subunit for activation by GABA but not by pentobarbital.* Nature, 1993. **366**(6455): p. 565-9.

74. Berezhnoy, D., et al., *On the benzodiazepine binding pocket in $GABA_A$ receptors.* J Biol Chem, 2004. **279**(5): p. 3160-8.

75. Sigel, E. and B.P. Luscher, *A closer look at the high affinity benzodiazepine binding site on $GABA_A$ receptors.* Curr Top Med Chem, 2011. **11**(2): p. 241-6.

76. Sigel, E. and A. Buhr, *The benzodiazepine binding site of $GABA_A$ receptors.* Trends Pharmacol Sci, 1997. **18**(11): p. 425-9.

77. Orser, B.A., et al., *Propofol modulates activation and desensitization of $GABA_A$ receptors in cultured murine hippocampal neurons.* J Neurosci, 1994. **14**(12): p. 7747-60.

78. Reynolds, J.N. and R. Maitra, *Propofol and flurazepam act synergistically to potentiate $GABA_A$ receptor activation in human recombinant receptors.* Eur J Pharmacol, 1996. **314**(1-2): p. 151-6.

79. Bali, M. and M.H. Akabas, *Defining the propofol binding site location on the $GABA_A$ receptor.* Mol Pharmacol, 2004. **65**(1): p. 68-76.

80. Bai, D., et al., *The general anesthetic propofol slows deactivation and desensitization of $GABA_A$ receptors.* J Neurosci, 1999. **19**(24): p. 10635-46.

81. Sanna, E., et al., *Actions of the general anesthetic propofol on recombinant human $GABA_A$ receptors: influence of receptor subunits.* J Pharmacol Exp Ther, 1995. **274**(1): p. 353-60.

82. Sanna, E., F. Garau, and R.A. Harris, *Novel properties of homomeric $\beta 1$ γ-aminobutyric acid type A receptors: actions of the anesthetics propofol and pentobarbital.* Mol Pharmacol, 1995. **47**(2): p. 213-7.

83. Kommonen, B., E. Hyvatti, and W.W. Dawson, *Propofol modulates inner retina function in Beagles.* Vet Ophthalmol, 2007. **10**(2): p. 76-80.

84. Ng, Y.F., et al., *The characteristics of multifocal electroretinogram in isolated perfused porcine eye: cellular contributions to the in vitro porcine mfERG.* Doc Ophthalmol, 2008. **117**(3): p. 205-14.

85. Krasowski, M.D., et al., *4D-QSAR analysis of a set of propofol analogues: mapping binding sites for an anesthetic phenol on the $GABA_A$ receptor.* J Med Chem, 2002. **45**(15): p. 3210-21.

86. Cooke, A., et al., *Water-soluble propofol analogues with intravenous anaesthetic activity.* Bioorg Med Chem Lett, 2001. **11**(7): p. 927-30.

87. Krasowski, M.D., et al., *General anesthetic potencies of a series of propofol analogs correlate with potency for potentiation of γ-aminobutyric acid (GABA) current at the $GABA_A$ receptor but not with lipid solubility.* J Pharmacol Exp Ther, 2001. **297**(1): p. 338-51.

88. Krasowski, M.D., et al., *Methionine 286 in transmembrane domain 3 of the $GABA_A$ receptor β subunit controls a binding cavity for propofol and other alkylphenol general anesthetics.* Neuropharmacology, 2001. **41**(8): p. 952-64.

89. Richardson, J.E., et al., *A conserved tyrosine in the β2 subunit M4 segment is a determinant of γ-aminobutyric acid type A receptor sensitivity to propofol.* Anesthesiology, 2007. **107**(3): p. 412-8.

90. Siegwart, R., R. Jurd, and U. Rudolph, *Molecular determinants for the action of general anesthetics at recombinant $\alpha_2\beta_3\gamma_2$ γ-aminobutyric acid A receptors.* J Neurochem, 2002. **80**(1): p. 140-8.

91. Li, G.D., et al., *Identification of a $GABA_A$ receptor anesthetic binding site at subunit interfaces by photolabeling with an etomidate analog.* J Neurosci, 2006. **26**(45): p. 11599-605.

92. Li, G.D., et al., *Numerous classes of general anesthetics inhibit etomidate binding to γ-aminobutyric acid type A ($GABA_A$) receptors.* J Biol Chem, 2010. **285**(12): p. 8615-20.

93. Nury, H., et al., *X-ray structures of general anaesthetics bound to a pentameric ligand-gated ion channel.* Nature, 2011. **469**(7330): p. 428-31.

94. Wagner, C.A., et al., *The use of Xenopus laevis oocytes for the functional characterization of heterologously expressed membrane proteins.* Cell Physiol Biochem, 2000. **10**(1-2): p. 1-12.

95. Ramsey, D.J., H. Ripps, and H. Qian, *Streptozotocin-induced diabetes modulates GABA receptor activity of rat retinal neurons.* Exp Eye Res, 2007. **85**(3): p. 413-22.

96. Qian, H., et al., *GABA receptors of bipolar cells from the skate retina: actions of zinc on GABA-mediated membrane currents.* J Neurophysiol, 1997. **78**(5): p. 2402-12.

97. Prinz, H., *Hill coefficients, dose-response curves and allosteric mechanisms.* J Chem Biol, 2010. **3**(1): p. 37–44

98. Alvarez, O., C. Gonzalez, and R. Latorre, *Counting channels: a tutorial guide on ion channel fluctuation analysis.* Adv Physiol Educ, 2002. **26**(1-4): p. 327-41.

99. Zimmerman, G., L. Chow, and U. Paik, *The photochemical isomerization of azobenzene.* Journal of the American Chemical Society 1958. **80**(14): p. 3528-31.

100. Madsen, C., et al., *5-Substituted imidazole-4-acetic acid analogues: synthesis, modeling, and pharmacological characterization of a series of novel γ-aminobutyric acid$_C$ receptor agonists.* J Med Chem, 2007. **50**(17): p. 4147-61.

101. Krogsgaard-Larsen, P., B. Frolund, and T. Liljefors, *GABA$_A$ agonists and partial agonists: THIP (Gaboxadol) as a non-opioid analgesic and a novel type of hypnotic.* Adv Pharmacol, 2006. **54**: p. 53-71.

102. Stewart, D., et al., *Tryptophan mutations at azi-etomidate photo-incorporation sites on α1 or β2 subunits enhance GABA$_A$ receptor gating and reduce etomidate modulation.* Mol Pharmacol, 2008. **74**(6): p. 1687-95.

103. Hong, Z. and D.S. Wang, *Potentiation, activation and blockade of GABA$_A$ receptors by etomidate in the rat sacral dorsal commissural neurons.* Neuroscience, 2005. **132**(4): p. 1045-53.

104. Campagna-Slater, V. and D.F. Weaver, *Anaesthetic binding sites for etomidate and propofol on a GABA$_A$ receptor model.* Neurosci Lett, 2007. **418**(1): p. 28-33.

105. Chang, C.S., R. Olcese, and R.W. Olsen, *A single M1 residue in the β2 subunit alters channel gating of GABA$_A$ receptor in anesthetic modulation and direct activation.* J Biol Chem, 2003. **278**(44): p. 42821-8.

106. Ueno, S., et al., *Bicuculline and gabazine are allosteric inhibitors of channel opening of the GABA$_A$ receptor.* J Neurosci, 1997. **17**(2): p. 625-34.

107. Muroi, Y., et al., *Distinct structural changes in the $GABA_A$ receptor elicited by pentobarbital and GABA.* Biophys J, 2009. **96**(2): p. 499-509.

108. Kucken, A.M., et al., *Identification of benzodiazepine binding site residues in the γ2 subunit of the γ-aminobutyric $acid_A$ receptor.* Mol Pharmacol, 2000. **57**(5): p. 932-9.

109. Kucken, A.M., et al., *Structural requirements for imidazobenzodiazepine binding to $GABA_A$ receptors.* Mol Pharmacol, 2003. **63**(2): p. 289-96.

110. Teissere, J.A. and C. Czajkowski, *A β-strand in the γ2 subunit lines the benzodiazepine binding site of the $GABA_A$ receptor: structural rearrangements detected during channel gating.* J Neurosci, 2001. **21**(14): p. 4977-86.

111. Luo, A. and K. Sugiyama, *Propofol combined with diazepam synergistically potentiates the GABA-activated chloride current in rat sensory neurons.* Chin Med J (Engl), 2000. **113**(9): p. 840-3.

112. Mendez, F. and R. Penner, *Near-visible ultraviolet light induces a novel ubiquitous calcium-permeable cation current in mammalian cell lines.* J Physiol, 1998. **507 (Pt 2)**: p. 365-77.

113. Kitamura, A., et al., *Halothane and propofol modulation of γ-aminobutyric $acid_A$ receptor single-channel currents.* Anesth Analg, 2004. **99**(2): p. 409-15, table of contents.

114. Tanskanen, P., et al., *Propofol influences the electroretinogram to a lesser degree than thiopentone.* Acta Anaesthesiol Scand, 1996. **40**(4): p. 480-5.

115. Chen, X., S. Shu, and D.A. Bayliss, *Suppression of ih contributes to propofol-induced inhibition of mouse cortical pyramidal neurons.* J Neurophysiol, 2005. **94**(6): p. 3872-83.

116. Chen, X., S. Shu, and D.A. Bayliss, *HCN1 channel subunits are a molecular substrate for hypnotic actions of ketamine.* J Neurosci, 2009. **29**(3): p. 600-9.

117. Krampfl, K., et al., *Effects of propofol on recombinant AMPA receptor channels.* Eur J Pharmacol, 2005. **511**(1): p. 1-7.

118. Ying, S.W., et al., *Propofol block of I(h) contributes to the suppression of neuronal excitability and rhythmic burst firing in thalamocortical neurons.* Eur J Neurosci, 2006. **23**(2): p. 465-80.

119. Haeseler, G., et al., *High-affinity blockade of voltage-operated skeletal muscle and neuronal sodium channels by halogenated propofol analogues.* Br J Pharmacol, 2008. **155**(2): p. 265-75.

120. Dong, X.P. and T.L. Xu, *The actions of propofol on γ-aminobutyric acid$_A$ and glycine receptors in acutely dissociated spinal dorsal horn neurons of the rat.* Anesth Analg, 2002. **95**(4): p. 907-14, table of contents.

121. Cacheaux, L.P., et al., *Impairment of hyperpolarization-activated, cyclic nucleotide-gated channel function by the intravenous general anesthetic propofol.* J Pharmacol Exp Ther, 2005. **315**(2): p. 517-25.

122. Bush, R.A. and P.A. Sieving, *A proximal retinal component in the primate photopic ERG a-wave.* Invest Ophthalmol Vis Sci, 1994. **35**(2): p. 635-45.

123. Robson, J.G. and L.J. Frishman, *Response linearity and kinetics of the cat retina: the bipolar cell component of the dark-adapted electroretinogram.* Vis Neurosci, 1995. **12**(5): p. 837-50.

124. Dong, C.J. and W.A. Hare, *Contribution to the kinetics and amplitude of the electroretinogram b-wave by third-order retinal neurons in the rabbit retina.* Vision Res, 2000. **40**(6): p. 579-89.

125. Zayat, L., et al., *A new inorganic photolabile protecting group for highly efficient visible light GABA uncaging.* Chembiochem, 2007. **8**(17): p. 2035-8.

126. Rial Verde, E.M., et al., *Photorelease of GABA with vsible light using an inorganic caging group.* Front Neural Circuits, 2008. **2**: p. 2.

127. Yang, X., et al., *Optical control of focal epilepsy in vivo with caged γ-aminobutyric acid.* Ann Neurol, 2012. **71**(1): p. 68-75.

128. Ishida, A.T. and B.N. Cohen, *GABA-activated whole-cell currents in isolated retinal ganglion cells.* J Neurophysiol, 1988. **60**(2): p. 381-96.

129. Grunert, U., *Distribution of GABA and glycine receptors on bipolar and ganglion cells in the mammalian retina.* Microsc Res Tech, 2000. **50**(2): p. 130-40.

130. Wassle, H., et al., *Glycine and GABA receptors in the mammalian retina.* Vision Res, 1998. **38**(10): p. 1411-30.

131. Koulen, P., et al., *Selective clustering of $GABA_A$ and glycine receptors in the mammalian retina.* J Neurosci, 1996. **16**(6): p. 2127-40.

132. Xie, A., et al., *Propofol potentiates GABA-elicited responses of bipolar and ganglion cells in rat retina*. Abstract number 1865. Annual meeting of the Association for Research in Vision and Ophthalmology (ARVO). Ft. Lauderdale, Florida, May 2-6, 2010.

133. Sadovski, O., et al., *Spectral tuning of azobenzene photoswitches for biological applications.* Angew Chem Int Ed Engl, 2009. **48**(8): p. 1484-6.

134. Pugh, E.N., Jr. and T.D. Lamb, *Amplification and kinetics of the activation steps in phototransduction.* Biochim Biophys Acta, 1993. **1141**(2-3): p. 111-49.

135. Leskov, I.B., et al., *The gain of rod phototransduction: reconciliation of biochemical and electrophysiological measurements.* Neuron, 2000. **27**(3): p. 525-37.

136. Klar, T., et al., *Surface-plasmon resonances in single metallic nanoparticles.* Physical Review Letters, 1998. **80**(19): p. 4249-4252.

137. Vo-Dinh, T., *Surface-enhanced Raman spectroscopy using metallic nanostructures.* Trac-Trends in Analytical Chemistry, 1998. **17**(8-9): p. 557-582.

138. Wu, D.Y., et al., *Electrochemical surface-enhanced Raman spectroscopy of nanostructures.* Chemical Society Reviews, 2008. **37**(5): p. 1025-1041.

139. Lobmaier, C., et al., *Direct monitoring of molecular recognition processes using fluorescence enhancement at colloid-coated microplates.* Journal of Molecular Recognition, 2001. **14**(4): p. 215-222.

140. Aslan, K., P. Holley, and C.D. Geddes, *Metal-enhanced fluorescence from silver nanoparticle-deposited polycarbonate substrates.* Journal of Materials Chemistry, 2006. **16**(27): p. 2846-2852.

141. Anger, P., P. Bharadwaj, and L. Novotny, *Enhancement and quenching of single-molecule fluorescence.* Physical Review Letters, 2006. **96**(11).

142. Kottmann, J.P. and O.J.F. Martin, *Plasmon resonant coupling in metallic nanowires.* Optics Express, 2001. **8**(12): p. 655-663.

143. Talley, C.E., et al., *Surface-enhanced Raman scattering from individual Au nanoparticles and nanoparticle dimer substrates.* Nano Lett, 2005. **5**(8): p. 1569-1574.

144. Quinten, M., *Local fields close to the surface of nanoparticles and aggregates of nanoparticles.* Applied Physics B-Lasers and Optics, 2001. **73**(3): p. 245-255.

145. Zhou, J.L., et al., *Effect of silver nanoparticles on photo-induced reorientation of azo groups in polymer films.* Thin Solid Films, 2007. **515**(18): p. 7242-7246.

146. Stamplecoskie, K.G., et al., *Plasmon-mediated photopolymerization maps plasmon fields for silver nanoparticles.* Journal of the American Chemical Society, 2011. **133**(24): p. 9160-9163.

147. Shin, K.H. and E.J. Shin, *Photoresponsive azobenzene-modified gold nanoparticle.* Bulletin of the Korean Chemical Society, 2008. **29**(6): p. 1259-1262.

148. Hausser, M. and B.A. Clark, *Tonic synaptic inhibition modulates neuronal output pattern and spatiotemporal synaptic integration.* Neuron, 1997. **19**(3): p. 665-78.

149. Smith, S.L. and T.S. Otis, *Persistent changes in spontaneous firing of Purkinje neurons triggered by the nitric oxide signaling cascade.* J Neurosci, 2003. **23**(2): p. 367-72.

150. Palma, E., et al., *Abnormal $GABA_A$ receptors from the human epileptic hippocampal subiculum microtransplanted to Xenopus oocytes.* Proc Natl Acad Sci U S A, 2005. **102**(7): p. 2514-8.

151. Goodkin, H.P., et al., *Subunit-specific trafficking of $GABA_A$ receptors during status epilepticus.* J Neurosci, 2008. **28**(10): p. 2527-38.

152. Macdonald, R.L., J.Q. Kang, and M.J. Gallagher, *Mutations in $GABA_A$ receptor subunits associated with genetic epilepsies.* J Physiol, 2010. **588**(Pt 11): p. 1861-9.

VITA

NAME Lan Yue

EDUCATION

2002 – 2006 B.S., Electronic Engineering and Information Science,
University of Science and Technology of China, Hefei, Anhui, China

2006 - 2012 Ph.D., Bioengineering, University of Illinois at Chicago,
Chicago, Illinois

TEACHING EXPERIENCE

2006 – 2007 *Biomedical Instrumentation,* Department of Bioengineering,
University of Illinois at Chicago, Chicago, Illinois

HONORS

ARVO Foundation for Eye Research/Retina Research Foundation Travel Grant, Association for Research in Vision and Ophthalmology, Ft. Lauderdale, Florida, 2011

Graduate College Student Presenter Award, University of Illinois at Chicago, Chicago, Illinois, 2009-2011

Graduate Student Council Travel Award, University of Illinois at Chicago, Chicago, Illinois, 2009 & 2011

PROFESSIONAL MEMBERSHIP

Association for Research in Vision and Ophthalmology (ARVO)
Society for Neuroscience (SfN)

ABSTRACTS

Yue L., Pawlowski M., Bruzik K.S., Qian H. & Pepperberg D.R.: Direct activation of $GABA_A$ receptors of retinal ganglion cells by a propofol-based photoisomerizable compound. Abstract number 279. Annual meeting of the Association for Research in Vision and Ophthalmology (ARVO), Ft. Lauderdale, FL, 2012.

Yue L., Pawlowski M., Gussin H.A., Feng F., Bruzik K.S., Qian H. & Pepperberg D.R.: Influence of altered $GABA_A$ propofol-binding cavity on the activity of a propofol-based, photo-controlled $GABA_A$ agonist. Abstract number 42.13. Annual meeting of the Society for Neuroscience, Washington DC, 2011.

Yue L., Pawlowski M., Feng F., Bruzik K.S., Qian H. & Pepperberg D.R.: Photo regulated activity of a tethered propofol derivative at $GABA_A$ receptors. Abstract number 1166. Annual meeting of the Association for Research in Vision and Ophthalmology (ARVO), Ft. Lauderdale, FL, 2011.

Yue L., Pawlowski M., Feng F., Bruzik K.S., Qian H. & Pepperberg D.R.: Light-modulated activation of $GABA_A$ receptors by a propofol-azobenzene conjugate. Abstract number 338.21. Annual meeting of the Society for Neuroscience, San Diego, CA, 2010.

Pepperberg D.R., Yue L., Pawlowski M., Hurst S.J., Bruzik K.S. & Rajh T.: Plasmonic nano-antennas to enhance light sensitivity of retinal molecular devices designed for vision restoration. Grantee presentation at conference on An Interdisciplinary Vision of AMD, Arnold and Mabel Beckman Initiative for Macular Research, Irvine, California, 2011.

Yue L., Pawlowski M., Feng F., Bruzik K.S., Qian H. & Pepperberg D.R.: Light-regulated, propofol-based potentiators of $GABA_A$ receptors. Abstract number 3301. Annual meeting of the Association for Research in Vision and Ophthalmology (ARVO), Ft. Lauderdale, FL, 2010.

Xie A., Yue L., Feng F., Pepperberg D.R. & Qian H.: Propofol potentiates GABA-elicited responses of bipolar and ganglion cells in rat retina. Abstract number 1865. Annual meeting of the Association for Research in Vision and Opthalmology (ARVO), Ft. Lauderdale, FL, 2010.

Yue L., Xie A., Bruzik K.S., Qian H. & Pepperberg D.R.: Potentiating effect of propofol on $GABA_A$ receptor-mediated responses of retinal bipolar cells. Abstract number 1015. Annual meeting of the Association for Research in Vision and Opthalmology (ARVO), Ft. Lauderdale, FL, 2009.

Xie A., Yue L., Feng F., Mir F., Yan J., Welsh L.M., Wang J., Frishman L.J., Kaplan J.H., Standaert R.F., Le Breton G.C., Qian H. & Pepperberg D.R.: 2-aminoethyl methylphosphonate analog of GABA: antagonist activity at $GABA_C$ receptors. Abstract number 608.10. Annual meeting of the Society for Neuroscience, Washington DC, 2008.

PUBLICATIONS

Yue L., Xie A., Bruzik K.S., Bente F., Qian H. & Pepperberg D.R.: Potentiating action of propofol at $GABA_A$ receptors of retinal bipolar cells. Invest. Ophthalmol. Vis. Sci., 52: 2497-2509, 2011

Xie A., Yan J., Yue L., Feng F., Mir F., Abdel-Halim H., Chebib M., Le Breton G.C., Standaert R.F., Qian H. & Pepperberg D.R.: 2-aminoethyl methylphosphonate (2-AEMP), a potent and rapidly acting antagonist of $GABA_A$-ρ1 receptors. Mol. Pharmacol., 80: 965-78, 2011

Yue L., Pawlowski M., Dellal S.S., Xie A., Feng F., Otis T.S., Bruzik S.B., Qian H. & Pepperberg D.R.: Robust photo-regulation of $GABA_A$ receptors by allosteric modulation with a propofol analog. (Submitted)